Natural Resources Canada | Ressources naturelles Canada

GEOLOGICAL SURVEY OF CANADA
OPEN FILE 8317

Precious- and base-metal deposits of the southern Abitibi greenstone belt, Superior Province, Ontario and Quebec: 14th Biennial Society for Geology Applied to Mineral Deposits meeting field trip guidebook

P. Mercier-Langevin, J. Goutier, and B. Dubé (ed.)

2017

GEOLOGICAL SURVEY OF CANADA
OPEN FILE 8317

Precious- and base-metal deposits of the southern Abitibi greenstone belt, Superior Province, Ontario and Quebec: 14th Biennial Society for Geology Applied to Mineral Deposits meeting field trip guidebook

P. Mercier-Langevin[1], J. Goutier[2], and B. Dubé[1] (ed.)

[1] Geological Survey of Canada, 490 rue de la Couronne, Québec, Quebec G1K 9A9
[2] Ministère de l'Énergie et des Ressources naturelles, 70 Avenue Québec, Rouyn-Noranda, Quebec J9X 6R1

2017

Permanent link: https://doi.org/10.4095/306250

This publication is available for free download through GEOSCAN (http://geoscan.nrcan.gc.ca/).

Recommended citation

Mercier-Langevin, P., Goutier, J., and Dubé, B. (ed.), 2017. Precious- and base-metal deposits of the southern Abitibi greenstone belt, Superior Province, Ontario and Quebec: 14th Biennial Society for Geology Applied to Mineral Deposits meeting field trip guidebook; Geological Survey of Canada, Open File 8317, 86 p. https://doi.org/10.4095/306250

Publications in this series have not been edited; they are released as submitted by the author.

14th Biennial Meeting

Québec City, Canada

August 20-23, 2017

MINERAL RESOURCES TO DISCOVER

EXCURSION GUIDEBOOK FT-06

Precious- and base-metal deposits of the southern Abitibi greenstone belt, Superior Province, Ontario and Quebec: 14th Biennial Society for Geology Applied to Mineral Deposits meeting field trip guidebook

Mercier-Langevin, P., Goutier, J., and Dubé, B. (ed.)

SGA QUÉBEC 2017 FIELD TRIPS COMMITTEE

Chair
Michel Houlé

Co-chair
Anne-Aurélie Sappin

Guidebook Publication
Anne-Aurélie Sappin
Michel Houlé
Claude Dion
André Tremblay

SGA QUÉBEC 2017 / FT-06 Abitibi guidebook

Cover photo: Native gold in a quartz ±carbonate vein hosted in strongly iron-carbonatized mafic volcanic rocks from the Lac Fortune area west of Rouyn-Noranda

Photo: *P. Mercier-Langevin (Geological Survey of Canada)*

Precious- and base-metal deposits of the southern Abitibi greenstone belt, Superior Province, Ontario and Quebec: 14th Biennial Society for Geology Applied to Mineral Deposits meeting field trip guidebook

P. Mercier-Langevin, J. Goutier and B. Dubé (ed.)

2017

SOCIETY FOR GEOLOGY APPLIED TO MINERAL DEPOSITS (SGA) FIELD TRIP GUIDEBOOK FT-06

Precious- and base-metal deposits of the southern Abitibi greenstone belt, Superior Province, Ontario and Quebec: 14th Biennial Society for Geology Applied to Mineral Deposits meeting field trip guidebook

Organized by: P. Mercier-Langevin[1], J. Goutier[2], B. Dubé[1], K.H. Poulsen[3], M.G. Houlé[1], S. de Souza[4], P, Pilote[5], S. Préfontaine[6], and V. Bécu[1]

Field trip leaders: P. Mercier-Langevin[1], J. Goutier[2], B. Dubé[1], K.H. Poulsen[3], M.G. Houlé[1], S. de Souza[4], and P. Pilote[5]

[1] Natural Resources Canada, Geological Survey of Canada, 490, rue de la Couronne, Québec, Quebec G1K 9A9
[2] Ministère de l'Énergie et des Ressources naturelles, 70 avenue Québec, Rouyn-Noranda, Quebec J9X 6R1
[3] Consultant, 34 Walford Way, Ottawa, Ontario K2E 6B6
[4] Département des sciences de la Terre et de l'atmosphère, 201 avenue Président Kennedy, Montréal, Quebec H2X 3Y7
[5] Ministère de l'Énergie et des Ressources naturelles, 201 avenue Président Kennedy, Montréal, Quebec H2X 3Y7
[6] Earth Resources and Geoscience Mapping Section, Ontario Geological Survey, 933 Ramsey Lake Road, Sudbury, Ontario P3E 6B5

Field Trip held August 24-30, 2017

Recommended Citation:

For the entire guidebook:

Mercier-Langevin, P., Goutier, J., and Dubé, B. (ed.), 2017. Precious- and base-metal deposits of the southern Abitibi greenstone belt, Superior Province, Ontario and Quebec 14th Biennial Society for Geology Applied to Mineral Deposits meeting field trip guidebook; Geological Survey of Canada, Open File 8317, 86 p. https://doi.org/10.4095/306250

Table of Contents

Foreword

The southern Abitibi greenstone belt is amongst the best endowed regions of the world in terms of total precious and base metals. It is also a well-exposed segment of the Archean crust. For over a hundred years now, this geological region that straddles the Ontario and Québec border has been the cornerstone of the mining industry in Canada. It is still a major mining and exploration area that also serves as a base for exploration and mining in northern regions of central and eastern Canada. Because of an overall good state of preservation, a nice glacial polish, and easy access, the southern Abitibi has also been an amazing area for research and teaching, something that remains true even after 100 years of groundbreaking work.

The objective of the "Base and precious metal deposits of the southern Abitibi greenstone belt, Superior province, Canada" field trip (SGA FT-06) is to give participants an overview of the geology and metallogeny of this exceptionally well-endowed region, with an emphasis on the geologic setting of the main ore deposit types in the belt. This field trip provides an overview of the southern Abitibi, including mine visits of some of the largest gold deposits of the belt. Supplementary information will be provided through evening lectures and discussions. This field trip follows and builds on a long series of similar field trips in the southern Abitibi that were organized and led by our predecessors, and many field trips that were organized by the leaders of this excursion. One such field trip was the SEG Foundation Student Field Trip 13 held in September 2014. From this SEG field trip was produced a *Reviews in Economic Geology* (Volume 19 – in press). To avoid duplication, we intentionally kept this guidebook as simple and brief as possible, referring to the *Reviews* volume as necessary.

Patrick Mercier-Langevin
Jean Goutier
Benoît Dubé

Program

Day 0 **- Thursday August 24th – Drive to Rouyn-Noranda**

AM: Departure from Québec City Convention Center at 7:30 AM.
PM: Arrival at Rouyn-Noranda, DeVille hotel, at ~18:00-19:00.
Evening lecture: (~21h00-21h30) Introduction to the geology and metallogeny of the Southern Abitibi greenstone belt.

Day 1 **- Friday August 25th – The evolution of the Southern Abitibi greenstone belt and the Cadillac-Larder Lake break**

AM: Departure at 7:30, visit of key outcrops along the Larder Lake-Cadillac fault zone from Kirkland Lake to Rouyn-Noranda, starting in Kirkland Lake
PM: Visit of key outcrops along the Larder Lake-Cadillac fault zone
Evening lecture: (~20h30-21h30) Introduction to the geology of the Kidd-Munro assemblage and ultramafic rocks of the Abitibi greenstone belt.

Day 2 **- Saturday August 26th – Ultramafic rocks of the Kidd Munro Assemblage and the Potter mine VMS deposit**

AM: Departure at 7:30, visit of key outcrops in the Pyke Hill area (ultramafic complex)
PM: Lunch at Potter mine site. Visit of outcrops and observation of drill core.
Evening lecture: (~20h30-21h30) Overview of the Blake River Group geology and its VMS deposits

Day 3 **- Sunday August 27th – Geology of the Blake River Group and VMS deposits of the Noranda district**

AM: Departure at 8:00, stops at selected outcrops in the Noranda central camp and Blake River Group
PM: Stops at selected outcrops in the Noranda mining camp and Blake River Group, stop at the Horne West Zone stripped outcrop, and stop at the Falco Resources core facility to look at Horne Zone 5 drill core.
Evening lecture: (~20h30-21h30) Introduction to the geology of the Doyon-Bousquet-LaRonde mining camp

Day 4 **- Monday August 28th – Au-rich VMS deposits of the Doyon-Bousquet-LaRonde mining camp – The LaRonde Penna mine**

AM: Departure from hotel at 6:15. Arrival at LaRonde Penna mine at 7:00. Introduction and undergound mine tour.
PM: Lunch generously provided by Agnico Eagle Mines ltd. LaRonde Division. Visit of key outcrops and drill core observations in the afternoon.
Evening lecture: (~20h30-21h30) Introduction to the geology of the Canadian Malartic mine and Malartic district.

Day 5 **- Tuesday August 29th – The Canadian Malartic gold deposit and geology of the Malartic district**

AM: Departure from hotel at 7:00. Arrival at Canadian Malartic mine at 8:00. Introduction, open pit tour, and drill core observation.
PM: Stops at the Malartic Lakeshore prospect stripped outcrops and at Spinifex Ridge outcrops.
Evening: Final group dinner and closing discussions.

Day 6 **- Wednesday August 30th – Return trip**

AM: Return trip to Québec City, departure from DeVille hotel at 7:00. Stop at Rouyn-Noranda airport at 7:20. Stop at Montréal Trudeau airport at ~13:30-14:00.
PM: Arrival at Québec City Convention Center at ~17:30-18:30.

Safety and Access

Field trip participants should be aware that any geological fieldwork, including field trips, can present some safety hazards. Foreseeable hazards of a general nature include inclement weather, slips, and falls on uneven terrain, falling or rolling rock, insect bites or stings, animal encounters and flying rock from hammering.

Furthermore, this trip may involve walking over rough and often slippery rocks, likely in rainy conditions, so a considerable degree of agility is required to be able to safely participate in this excursion.

The leaders have prepared thoroughly the field trip and will take all reasonable care to provide the safety of the participants on its field trips. Similarly, each visited site and host companies have specific set of rules that will need to be followed at all times. However, field trip participants are responsible for acting in a manner that is safe for themselves and their co-participants. This responsibility includes using the appropriate personal protective equipment (PPE) such as rain gear, sunscreen, insect repellent, safety glasses, work gloves, hardhat, and sturdy steel-toed boots when necessary or when recommended by field trip leader or mine staff, or upon personal identification of a hazard requiring PPE use.

If you feel exhausted or ill do not force yourself. In all cases, let one of the field trip leaders know about any discomfort. If you take medication, carry it with you at all times.

Transportation will be done by coach bus at all times. We will be staying at the DeVille Complexe Hotelier in downtown Rouyn-Noranda, with most necessary services at walking distance.

Acknowledgements

The leaders and organizers of this field trip are most sincerely grateful to the companies that gave access to their property, and especially to their employees who made each visit possible and as rewarding as can be. We are more particularly grateful to G. Long (Kinross Gold), G. Riverin (Yorbeau Resources), D. Gamble (consultant), E. Harrison (Millstream), C. Bernier and C. Pilote (Falco Resources), D. Fortin, D. Pitre, A. Laberge, and L. Burke (Agnico Eagle Mines Ltd.), G. Poirier, D. Gervais, M.-C. Brunet-Ladrie, and F. Bouchard (Mine Canadian Malartic). Thanks to A.-A. Sappin for constructive comments on an earlier version of this document.

We also want to acknowledge the generous support of the sponsors of this field trip: Natural Resources Canada (Geological Survey of Canada), the Society for Geology Applied to Mineral Deposits (SGA), the Society of Economic Geologists (SEG), and the Ministère de l'Énergie et des Ressources naturelles du Québec (MERN).

Sponsors for FT-06

Ressources naturelles Canada
Natural Resources Canada

Célébrons 175 ans
Celebrating 175 yrs

SOCIETY for GEOLOGY APPLIED to MINERAL DEPOSITS

SOCIETY OF ECONOMIC GEOLOGISTS
FOUNDED 1920
www.segweb.org

Énergie et Ressources naturelles
Québec

Chapter 1: Introduction

Patrick Mercier-Langevin
Natural Resources Canada – Geological Survey of Canada

Jean Goutier
Ministère de l'Énergie et des Ressources naturelles du Québec

Benoît Dubé
Natural Resources Canada – Geological Survey of Canada

1.1 Introduction

The Abitibi greenstone belt is part of the Superior Province (Fig. 1.1), the largest coherent Archean craton in the world. Archean cratons are generally well endowed in precious and base metals, the Superior being particularly well endowed in gold, copper, and zinc (Mercier-Langevin et al. 2012, 2014; and references therein). Exceptionnal within the Superior Province is the Abitibi greenstone belt that is the single largest Archean greenstone belt of the world. Even more remarkable is the amazing and almost unique concentration of metals in a narrow corridor that is the southerm Abitibi belt (Fig. 1.2), where the earliest discoveries were made in the early 20th century, and where mining has been continuous since then.

Figure 1.1. Location of the Abitibi greenstone belt within the Superior Province. From Monecke et al. (2017).

This field trip, part of the 14th SGA biennial meeting (SGA Québec 2017 "Resources to Discover"), complements a series of symposia and sessions that clearly had a strong Archean flavour such as symposium SY01 "Gold through time and space", symposium SY02 "Magmatic sulfide and oxide ore deposits in mafic and ultramafic rocks - a symposium in memoriam of the work and life of Prof. Hazel Prichard", and session S03 "Key controls on the quality (size and/or grade) of metal deposits in volcanic and sedimentary basins". This five day-long field trip will take participants to Kirkland Lake, Rouyn-Noranda, Duparquet, Doyon-Bousquet-LaRonde, and Malartic, each of these districts hosting world class deposits (gold and/or base metals). Exceptionnal exposures of komattites will also be visited.

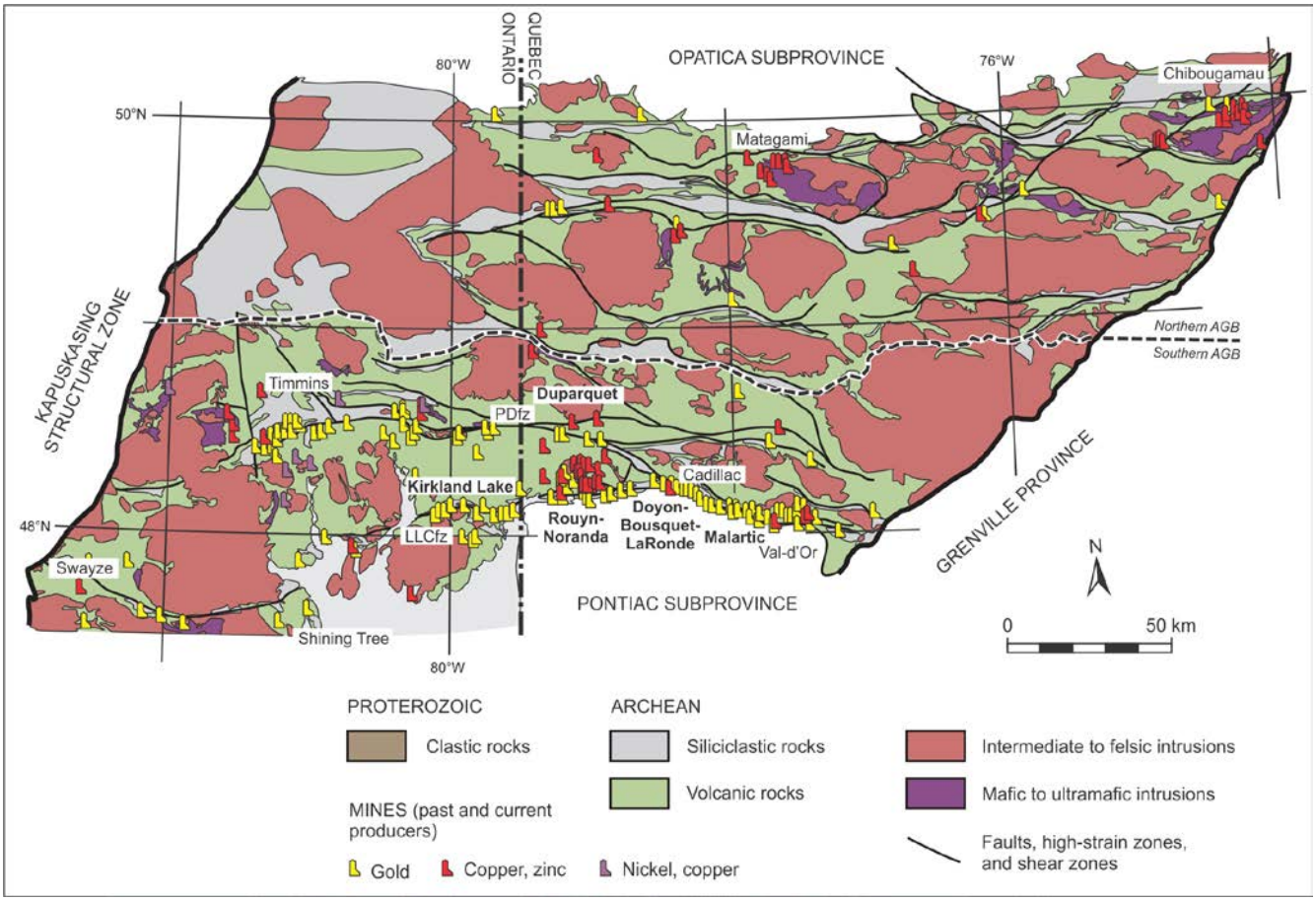

Figure 1.2. Geologic map of the Abitibi greenstone belt (AGB) showing the distribution of supracrustal rocks and intervening domes of intrusive rocks. The map also shows the boundary between the southern and northern parts of the Abitibi greenstone belt. LLCfz = Larder Lake-Cadillac fault zone, PDfz = Porcupine-Destor fault zone. From Monecke et al. (2017).

1.2 Geology

The Abitibi greenstone belt was formed over a period that spans approximately 150 m.y. It has been subdivided into eight assemblages (or episodes depending on the authors) of major submarine volcanic activity (see Monecke et al. 2017 for details about the geology of the belt). The belt consists of E-trending successions of folded volcanic and sedimentary rocks and intervening domes of intrusive rocks (Fig. 1.3). Submarine volcanism mostly occurred between 2795 and 2695 Ma and was followed by sedimentation in large deep basins and then by large-scale thin-skin folding and thrusting. This deformation and associated crustal thickening is associated with the development of smaller, molasses-like sedimentary basins in which "orogenic conglomerates" and finer-grained sediments were deposited between ≤2679 and ≤2669 Ma, defining the "Timiskaming" basins (see Monecke et al. 2017 for source of data). Protracted deformation is responsible for the deformation and burial of these "young" basins and the development of thick-skin deformation and major crustal faults that now control the location of most major greenstone-hosted gold districts and deposits of the Southern Abitibi belt.

1.3 Ore deposits

Gold represents the main commodity in the southern Abitibi belt. Greenstone-hosted quartz-carbonate vein-type

systems (or orogenic gold, or mesothermal gold) dominate (Robert et al. 2005; Dubé and Gosselin 2007). These vein systems (often associated with disseminations and variable abundance of sulfides and tourmaline) are clearly associated with the Porcupine-Destor and Larder Lake-Cadillac fault zones (Figs. 1.2 and 1.3). The overall endowment of these two faults is somewhat comparable, with slightly more gold along the Larder Lake-Cadillac fault zone with a larger number of major camps as well (Fig. 1.4). The largest camp however is associated with the Porcupine-Destor fault zone, i.e. the Timmins-Porcupine district (Figs. 1.2 and 1.4). The overall endowment of the southern Abitibi belt relative to the northern part of the belt is huge (Fig. 1.4). There are however new discoveries being done in the northern part of the belt, including the Detour Lake gold mine, which is currently the largest gold resource in Canada with mineral reserves and resources of 21.5 Moz Au (Detour Gold, December 31, 2016). The startup of this low-grade, large tonnage operation spurred a new wave of exploration in northern Abitibi. There are other types of gold deposits, including some of pre-main deformation origin (e.g., Fig. 1.5), but these are overshadowed by the quartz-carbonate vein-type deposits in terms of total gold tonnage at belt scale.

Many of the volcanic assemblages or episodes are favorable periods for VMS formation. However, the 2704-2695 Ma Blake River Group is the richest one in terms of total tonnage and total VMS-Au (Table 1.1; see Mercier-Langevin et al. 2011a for details on the geology and metallogeny of the Blake River Group).

Komatiite-associated Ni-Cu-(PGE) deposits remain scarce in the Abitibi greenstone belt despite the presence of significant amounts of ultramafic units (Houlé et al. 2017). Deposits like Dumont, which is not mined, still represent major accumulations of metals that, if mined, could radically change the figures regarding Ni-Cu-PGE systems in the Abitibi.

Many other deposit types are present in the Abitibi, including molybdenum deposits, “Chibougamau-type” Cu-Au vein systems, V-Cr deposits, pegmatite-hosted Li deposits, etc., making the belt a great exploration target even though it is considered as a “mature” area.

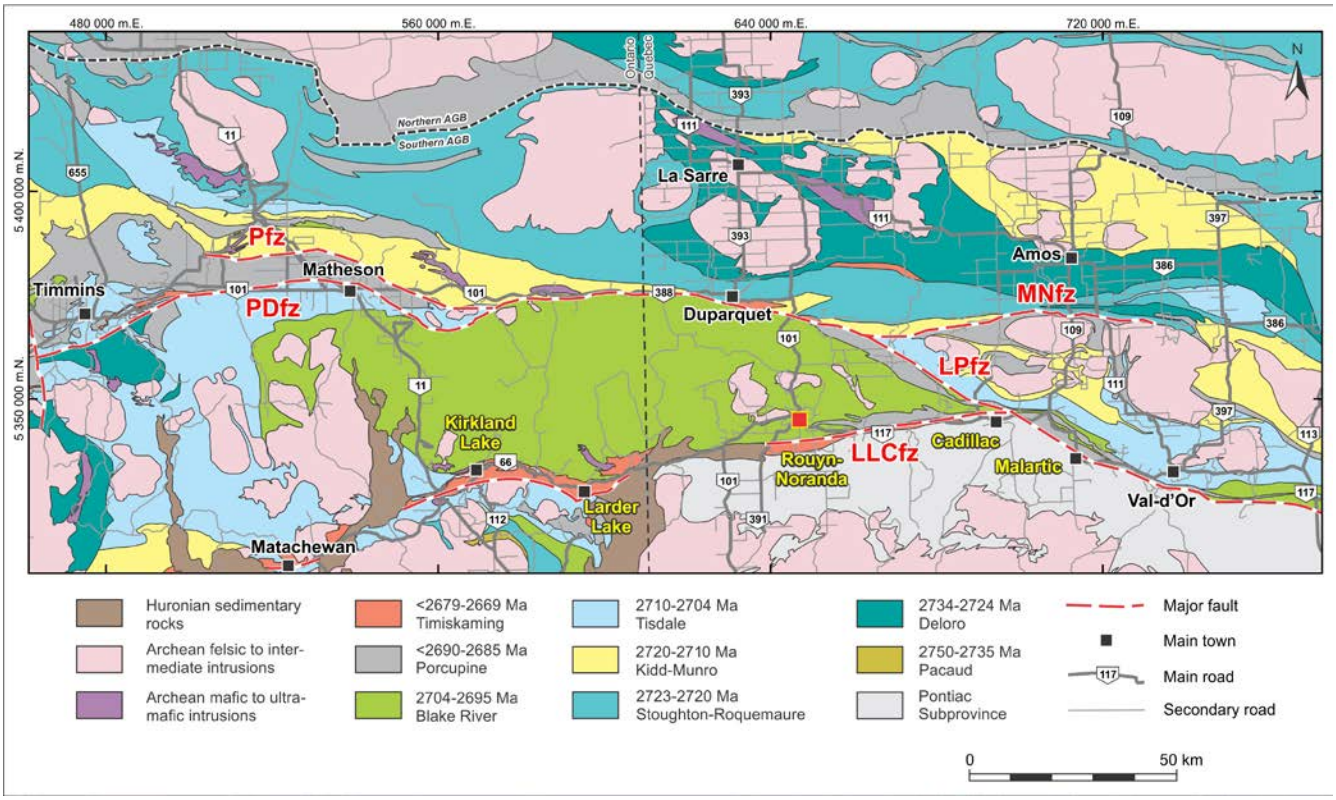

Figure 1.3. Geologic map of the southern Abitibi greenstone belt showing the distribution of volcanic and sedimentary rocks LLCfz = Larder Lake-Cadillac fault zone, LPfz = La Pause fault zone, MNfz = Manneville North fault zone, PDfz = Porcupine-Destor fault zone, Pfz = Pipestone fault zone. From Monecke et al. (2017).

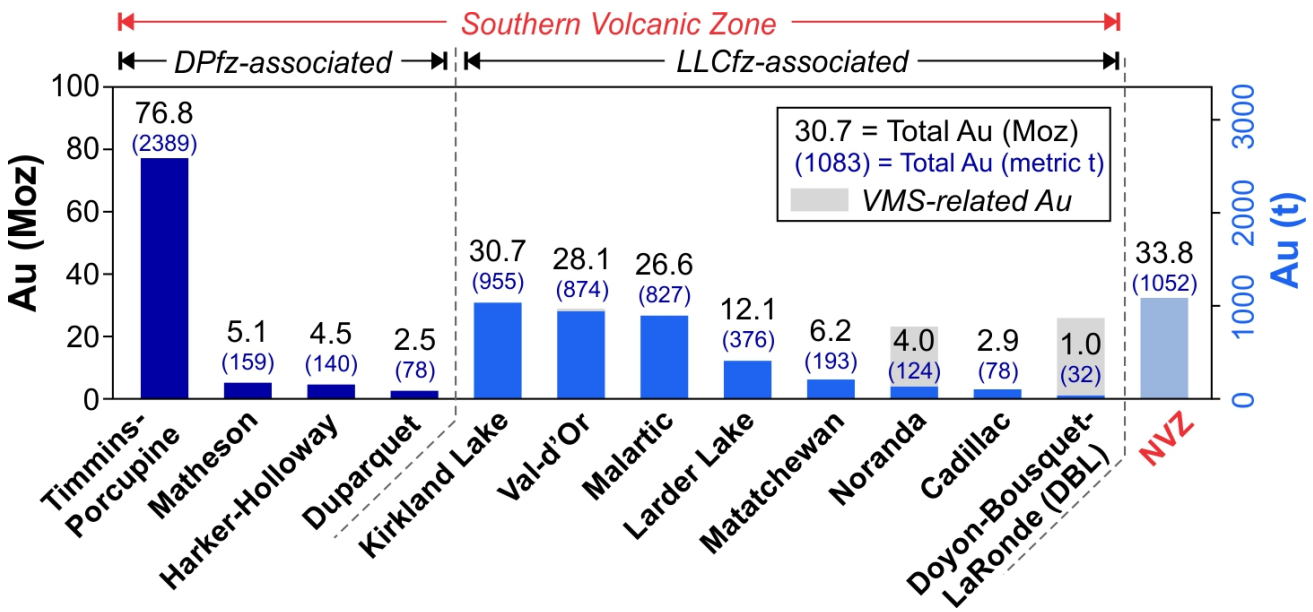

Figure 1.4. Global gold endowment of the principal gold districts distributed along the Destor-Porcupine and Larder Lake-Cadillac fault zones in the southern Abitibi greenstone belt (Au-rich VMS deposits are not included). Data from Gosselin and Dubé (2005, 2015). Dubé and Gosselin (2007, and unpublished data). Modified from Monecke et al. (2017). DPfz = Destor-Porcupine fault zone, LLCfz = Larder Lake-Cadillac fault zone, NVZ=Northern Volcanic Zone.

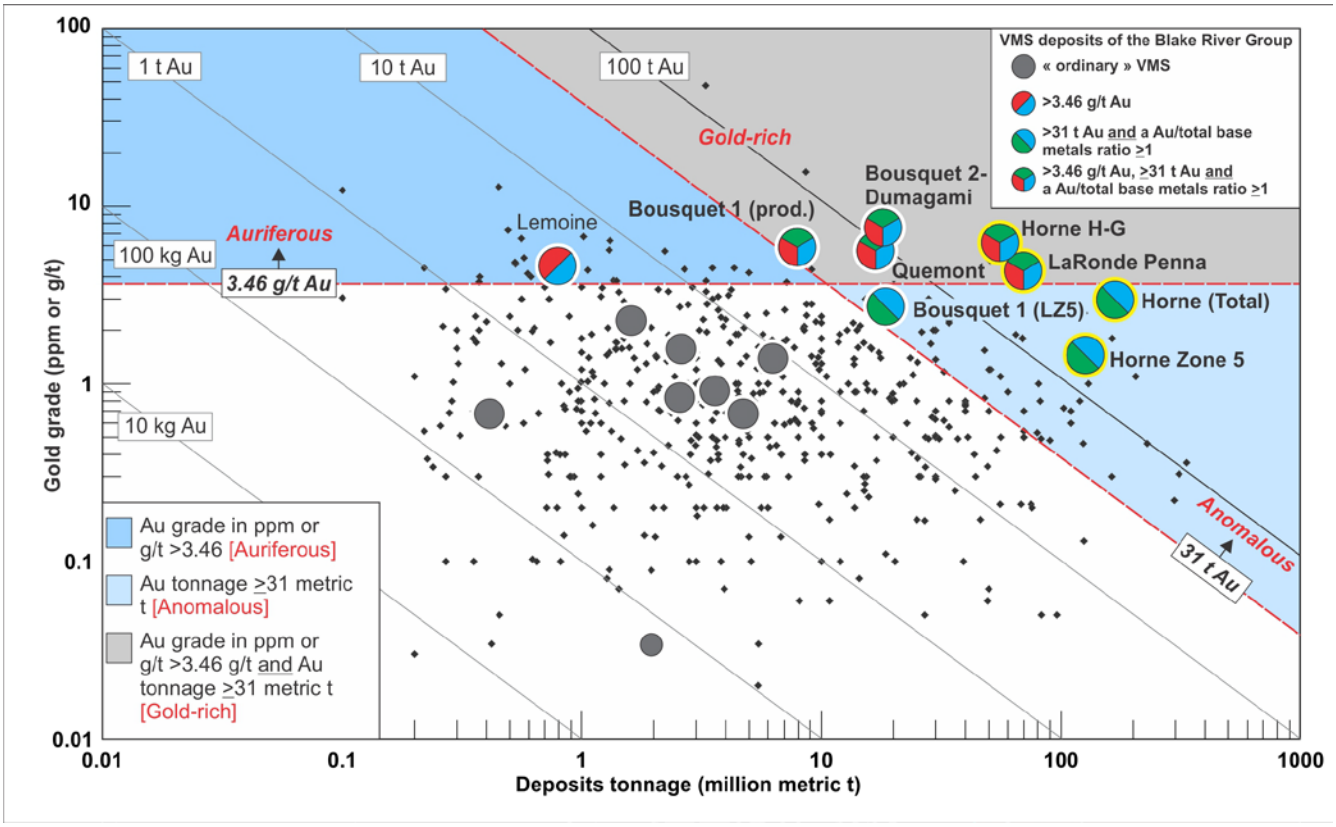

Figure 1.5. Bivariate plot of gold grade versus tonnage for VMS deposits. Modified from Mercier-Langevin et al. (2011b). Au-rich, auriferous and anomalous VMS deposits of the Abitibi greenstone belt are highlighted, along with some of the Noranda central camp Cu-Zn deposits as well for comparison.

1.4 Itinerary

Five days of field and mine visits constitute this field trip. On day 1 we will do a "traverse" along the Larder Lake-Cadillac Fault Zone or break from the Town of Kirkland Lake to east of Rouyn-Noranda (Fig. 1.6 and Chapter 2). On day 2 we will spend almost the entire day in Ontario at the Potter mine site looking at the Pyke hill komatiites and at the mafic-ultramafic-associated Potter Cu-Zn-Co VMS deposit host rocks and ore lenses (Fig. 1.6 and Chapter 3). We will stop in Duparquet to look at the Timiskaming conglomerates on our way back to Noranda (Fig. 1.6 and Chapter 4). On day 3 we will make a series of quick stops in key areas of the Noranda central VMS camp (Fig. 1.6 and Chapter 5) and then look at one stripped outcrop near the Horne mine and at drill core from the Horne 5 deposit (Chapter 6). Day 4 will be spent entirely at the LaRonde Penna mine east of Rouyn-Noranda (Fig. 1.6 and Chapter 7), learning about Au-rich VMS deposits. The final day (5) is divided in three parts: part 1 will take us to the low grade, large tonnage Canadian Malartic Mine in Malartic (Fig. 1.6 and Chapter 8); part 2 will take us north of Malartic at the Malartic Lake Shore showing where early stage auriferous quartz veins are exposed (Fig. 1.6 and Chapter 9); and part 3 will take us to Spinifex Ridge where komatiitic flow are exceptionally well exposed (Fig. 1.6 and Chapter 10).

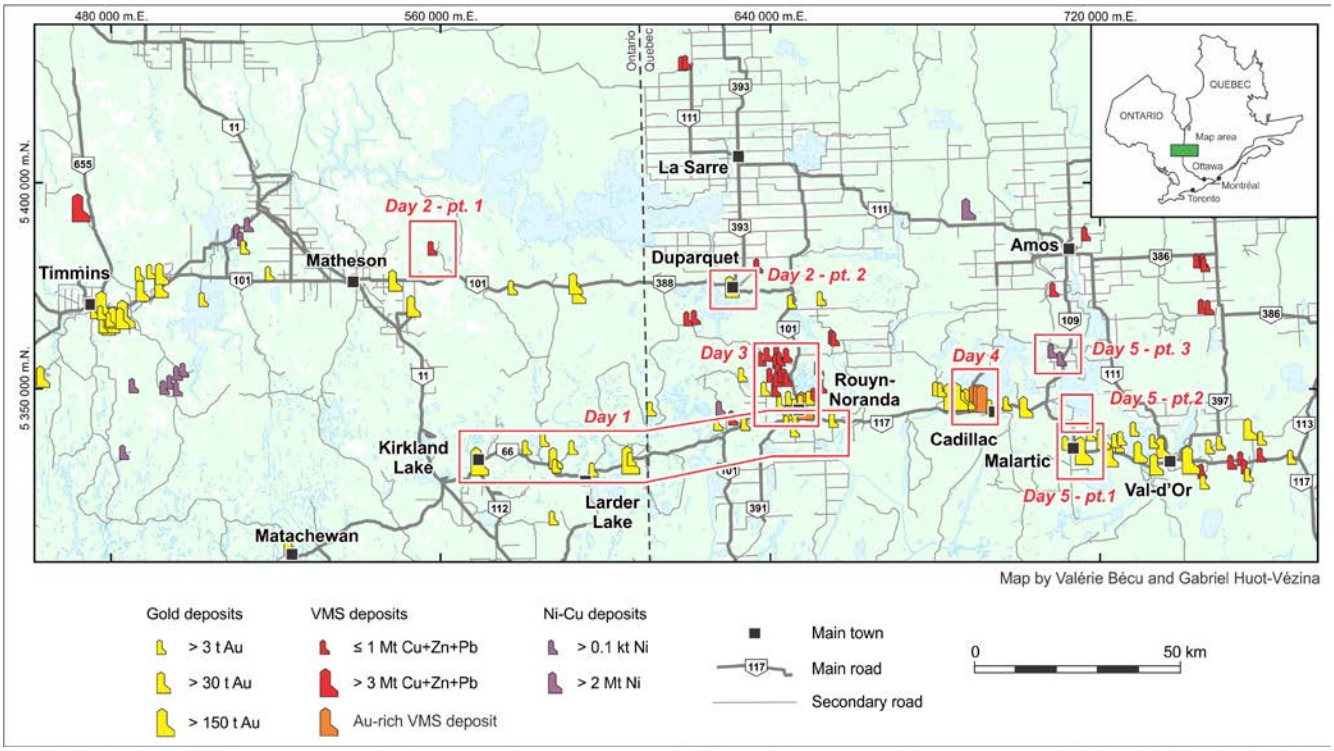

Figure 1.6. FT-06 field trip itinerary with the approximate location of the main areas that will be studied. Modified from Monecke et al. (2017).

1.5 References

Dubé B, Gosselin P (2007) Greenstone-hosted quartz-carbonate vein deposits, *in* Goodfellow WD (ed) Mineral deposits of Canada: A synthesis of major deposit-types, district metallogeny, the evolution of geological provinces, and exploration methods: Mineral Deposits Division, Geological Association of Canada, Special Publication 5: 49–73

Gosselin P, Dubé B (2005) Gold deposits of Canada: distribution, geological parameters and gold content. Geological Survey of Canada, Open File 4896, 1 CD-ROM.

Gosselin P, Dubé B (2005) Gold deposits of Canada: distribution, geological parameters and gold content. Geological Survey of Canada, Open File 7930, 27 p

Houlé M, Lesher CM, Préfontaine S (2017) Chapitre 4. Physical volcanology of komatiites and Ni-Cu-(PGE) deposits of the southern Abitibi greenstone belt: Reviews in Economic Geology 19, in press.

Mercier-Langevin P, Goutier J, Ross PS, McNicoll V, Monecke T, Dion C, Dubé B, Thurston P, Bécu V, Gibson H, Hannington M, Galley A (2011a) The Blake River Group of the Abitibi greenstone belt and its unique VMS and gold-rich VMS endowment. GAC-MAC-SEG-SGA Joint Annual Meeting 2011, Ottawa,

Field Trip 02B guidebook; Geological Survey of Canada, Open File report 6869, 61 p.

Mercier-Langevin P, Hannington MD, Dubé B, Bécu V (2011b) The gold content of volcanogenic massive sulfide deposits: Min Dep 46: 509–539Mercier-Langevin P, Houlé MG, Dubé B, Monecke T, Hannington MD, Gibson HL, Goutier J (2012) A special issue on Archean magmatism, volcanism and ore deposits: Part 1. Komatiite-associated Ni-Cu-(PGE) sulfide and greenstone-hosted Au deposits – Preface: Econ Geol 107: 745-753

Mercier-Langevin P, Gibson HL, Hannington MD, Goutier J, Monecke T, Dubé B, Houlé MG (2014) A special issue on Archean magmatism, volcanism and ore deposits: Part 2. Volcanogenic massive sulfide deposits – Preface: Econ Geol 109: 1-9

Monecke T, Mercier-Langevin P, Dubé B (2017) Chapter 1. Geology of the Abitibi greenstone belt: Reviews in Economic Geology 19, in press.

Robert F, Poulsen KH, Cassidy KF, Hodgson CJ (2005) Gold metallogeny of the Superior and Yilgarn cratons: Economic Geology 100th Anniversary Volume, p. 1001–1033

Table 1.1. Blake River Group VMS deposits tonnage and grade (modified from Mercier-Langevin et al., 2011b)

Deposit Number [1]		*Camp* [2]	Deposit name [3]	Tonnage Mt	Cu %	Zn %	Au g/t	Ag g/t	Sources (see Mercier-Langevin et al. 2011b for references)
1		West	Magusi	1.68	3.3	5.13	1.84	65.9	Ress. indicated and inferred, First Metals, 2009 (website)
2	1	West	**Fabie (New Insco)**	0.46	2.53		0.02	1.23	Prod. 2008, Moorhead et al. (2009); prod. 1976-77, 0.09 Mt at 2.8% Cu
3	2	West	**Aldermac (3, 4, 5)**	1.87	1.65		0.02	1.23	Prod. 1933-1943, Cattalani et al. (1995)
3		West	Aldermac (7 and 8)	1.04	1.5	4.13	0.3	31.2	Jones (1990)
4		NCC	West Ansil	1.13	3.35	0.29	0.82	7.45	Indicated and inferred resources, Alexis Minerals (website)
5	3	NCC	**Ansil**	1.6	7.06	1.77	2.21	26.3	Prod. 1989-1993, Rive (1991, 1992); Verpaelst (1993, 1994)
6	4	NCC	**Vauze**	0.36	3.1	2.2	0.69	30.78	Prod. 1961-1965, Ministère des Richesses naturelles, 1963 to 1967
7	5	NCC	**Norbec**	4.6	2.61	3.88	0.65	43.8	Prod. 1964-1976, Cattalani et al. (1994)
8		NCC	Zone D						Satellite lens of Norbec, Cattalani et al. (1994)
9	6	NCC	**East Waite**	1.496	4.1	3.25	1.8	31.00	Prod. 1952-1961, Gibson et Watkinson (1990)
10	7	NCC	**Old Waite**	1.12	4.7	2.98	1.1	22.00	Prod. 1928-1930; 1937-1948, Gibson et Watkinson (1990)
11		SCC	Bedford Hill	0.229	1.45				McMurchy (1961). Stringer-type mineralization
12	8	SCC	**Amulet F**	0.27	3.4	8.6	0.3	46.3	Prod. 1930-1937; 1944-1962, Gibson and Watkinson (1990)
13	9	SCC	**Amulet C**	0.56	2.2	8.5	0.6	86.7	Prod. 1930-1953, Gibson and Watkinson (1990)
14	10	SCC	**Amulet Lower A**	4.69	5.1	5.2	1.43	44.1	Prod. 1937-1962, Gibson and Watkinson (1990)
14		SCC	Amulet Upper A	0.18	2.3	6.1	2.00	46.00	Prod. 1937-1962, Gibson and Watkinson (1990)
14		SCC	Amulet A-11	0.44	3.6	2.4	0.7	22.00	Prod. 1956-1962, Gibson and Watkinson (1990)
14		SCC	Bluff						Prod. Included in Amulet Lower A, Gibson and Watkinson (1990)
14		SCC	Lake Dufault (zinc)	0.073	0.17	8.65	0.69	45.26	Knuckey et al. (1982)
15		SCC	D-266		4.00	5.9	1.524	49.94	Knuckey et al. (1982). (0.056 Mt included in Millenbach)
16	11	SCC	**Millenbach**	3.48	3.42	4.28	0.91	46.25	Prod. 1971-1981, see references below [4]
16		SCC	# 14		3.75	6.6	0.818	63.49	Knuckey et al. (1982) (0.151 Mt included in Millenbach)
17		SCC	# 23		2.15	6.49	0.508	53.33	Knuckey et al. (1982) (0.032 Mt included in Millenbach)
18		SCC	D-68		3.82	5.02	1.975	61.79	Knuckey et al. (1982) (0.041 Mt included in Millenbach)
19	12	SCC	**Corbet**	2.65	2.92	1.57	0.84	17.48	Prod. 1979-1986, MacIntosh, J.A. (1980); Rive (1981 to 1987)
20	13	South	**Quemont**	13.82	1.32	2.44	5.49	30.9	Prod. 1949-1971, Bancroft (1987)
20		South	Quemont	0.087	0.33	9.26	4.42	46.3	Prod. 2001, Verglas project, Perreault et al. (2002)
21	14	South	**Horne**	53.7	2.2	0.17	6.06	13.0	Prod. 1927-1976, Cattalini et al. (1993)
21		South	lenses (A to E; K)						Prod. included in Horne
21		South	lens F and zone tunnel						Prod. included in Horne, prod. 1994, 0.04 Mt 1.1 % Cu, 3.4 g/t Au [5]
21		South	lens G						Prod. included in Horne
21		*South*	lens H						Upper H et Lower H (main lenses of Horne deposit)
21		South	Horne Zone 5	113.40	0.18	0.82	1.54	16.09	Prod. 1967-1976, 0.2 Mt (0.73 % Cu, 7.1 Au g/t), Falco Resources
22	15	South	**D'Eldona**	0.08	0.2	5.27	5.27	27.36	Prod. 1951-1952, Farnsworth (1953, 1954)
23	15	South	**Delbridge**	0.37	0.61	9.66	2.8	109.5	Prod. 1969-1971, Van de Walle (1971a, 1971b); MacIntosh (1973)
24		East	South Dufault	0.216	1.08				Spiegle (1990)
25	16	East	**West MacDonald**	0.936	0.00	3.03	0.05	1.37	Prod.1955-1959, see references below [6]
25	16	East	**Gallen**	2.6	0.12	4.94	1.12	33.57	Prod.1981-1985; 1997-2000, see references below [7]
26	17	NE	**Mobrun**	1.63	0.84	2.45	2.41	27.39	Prod. 1986-1992, Rive (1987 to 1992); Verpaelst (1993)
27	17	NE	**Bouchard-Hébert**	9.61	0.78	4.74	1.41	43.28	Prod. 1995-2005, see references below [8]
28	18	DBL	**Westwood**	3.74			8.72		Reserves and resources [9]
29	19	DBL	**Bousquet 2**	10.31	0.53		7.95		Prod. 1990-2002, Mercier-Langevin (2017) [10]
30	20	DBL	**Dumagami**	7.33	0.7	0.07	6.84	19.5	Prod. 1988-1999, Mercier-Langevin (2017) [10]
31	21	DBL	**Bousquet 1**	7.45			5.70		Prod. 1978-1996, Mercier-Langevin et al. (2017)
31		DBL	LZ5	18.04			2.80		Reserves and resources, Zone 5 of Bousquet 1 deposit
32	22	DBL	**LaRonde Penna**	69.91	0.28	1.96	4.17	39.70	Resources and prod. 2000- , Mercier-Langevin (2017)
			Total tonnage	**341.17**					

[1] First column refers to deposits numbers in figure 1-4b of Mercier-Langevin et al. (2011b), second column is for deposits that were, or that are still in operation

[2] See figure 1-4b for camps location. DBL = Doyon-Bousquet-LaRonde camp, NCC = northern central camp, NE = northeast camp, SCC = southern central camp.

[3] Deposit names in bold = Past or current producers

[4] Millenbach: Van de Walle (1971b); MacIntosh (1973 to 1980); Rive (1981, 1982)

[5] Gaudreau and Goutier (1995)

[6] West MacDonald : Farnsworth, D.A. (1957, 1958); Courtemanche, G., and Duchesne, G. (1959); Inspecteurs des Mines (1960, 1961)

[7] Gallen: Rive (1982 to 1986); Gaudreau et al. (1998 to 2001); Perreault et al. (2002)

[8] Bouchard-Hébert: Gaudreau (1996); Lacroix et al. (1997); Gaudreau et al. (1998 to 2001); Perreault et al. (2002 to 2006)

[9] The Westwood mine comprises numerous ore zones, including intrusion-related Qz-sulfide veins and VMS-style mineralization (Westwood Corridor), only the reserves and resources associated with the VMS-style ore (Westwood corridor) are reported here

[10] The Dumagami and Bousquet 2 mines exploited the same orebody that was divided in two by a property boundary (totalling 17.64 Mt at 7.49 g/t Au)

Chapter 2: (Day 1) The evolution of the southern Abitibi greenstone belt and the Larder Lake-Cadillac break

K. Howard Poulsen
Consultant

2.1 Introduction

A geological review and full description of key field localities along the Larder Lake-Cadillac Break are given in the 2017 *Reviews in Economic Geology* Volume 19 (Poulsen, 2017). For the SGA trip we will attempt to stop at all localities described in that document except number 8 which can be rather time-consuming. The field trip begins in the Kirkland Lake district (Fig. 2.1) and moves eastward through Larder Lake (Fig. 2.2) to Rouyn-Noranda (Fig. 2.3).

2.2 Stop descriptions

Locality 1 – Larder Lake – Cadillac Break at Vigrass Lake

Komatiite-sediment contact, mafic dike, carbonate alteration and veins, fault-slip surfaces.

Locality 2 – Timiskaming Group Rocks near Chaput-Hughes

Polymictic conglomerate, cross-bedded sandstone, feldspar porphyry intrusion, carbonate alteration.

Locality 3 – Timiskaming rocks at former Lakeshore Mine Site (Don-Lou stop)

Alkalic tuff, syenite, feldspar porphyry.

Locality 4 – Kirkland Lake Fault at Wright-Hargreaves Discovery Outcrop

Feldspar porphyry, carbonate-sericite alteration, quartz veins.

Locality 5 – Timiskaming Group Rocks at Morris-Kirkland Mine

Wacke-mudstone facies, intersecting cleavages, foliated sericite alteration.

Locality 6 – Larder Lake-Cadillac Break at Cheminis Mine

Albitite dike, “flow ore”, folded southern sedimentary rocks and dikes.

Locality 7 – “Green Carbonate” rock (listwanite) at Virginiatown

Ankerite-magnesite-fuchsite-quartz rock derived from carbonatization of ultramafic komatiite – host of the “green carbonate ore” at Kerr Addison.

Locality 9 – Larder Lake – Cadillac Break at Astoria Mine

Footwall contact between carbonatized komatiite and Timiskaming sedimentary rocks; high-strain hanging-wall contacts between komatiite and conglomerate deformed contact between Blake River pillow basalt and basal Timiskaming Group.

Locality 10 – Larder Lake – Cadillac Break near McWatters Mine

Pillowed metabasalt of Blake River Group; Timiskaming wacke-mudstone facies; deformed Timiskaming conglomerate and sandstone; basal conglomerate at Timiskaming Group unconformity.

2.3 References

Poulsen KH (2017) The Larder Lake-Cadillac break and its gold deposits: Reviews in Economic Geology 19, in press.

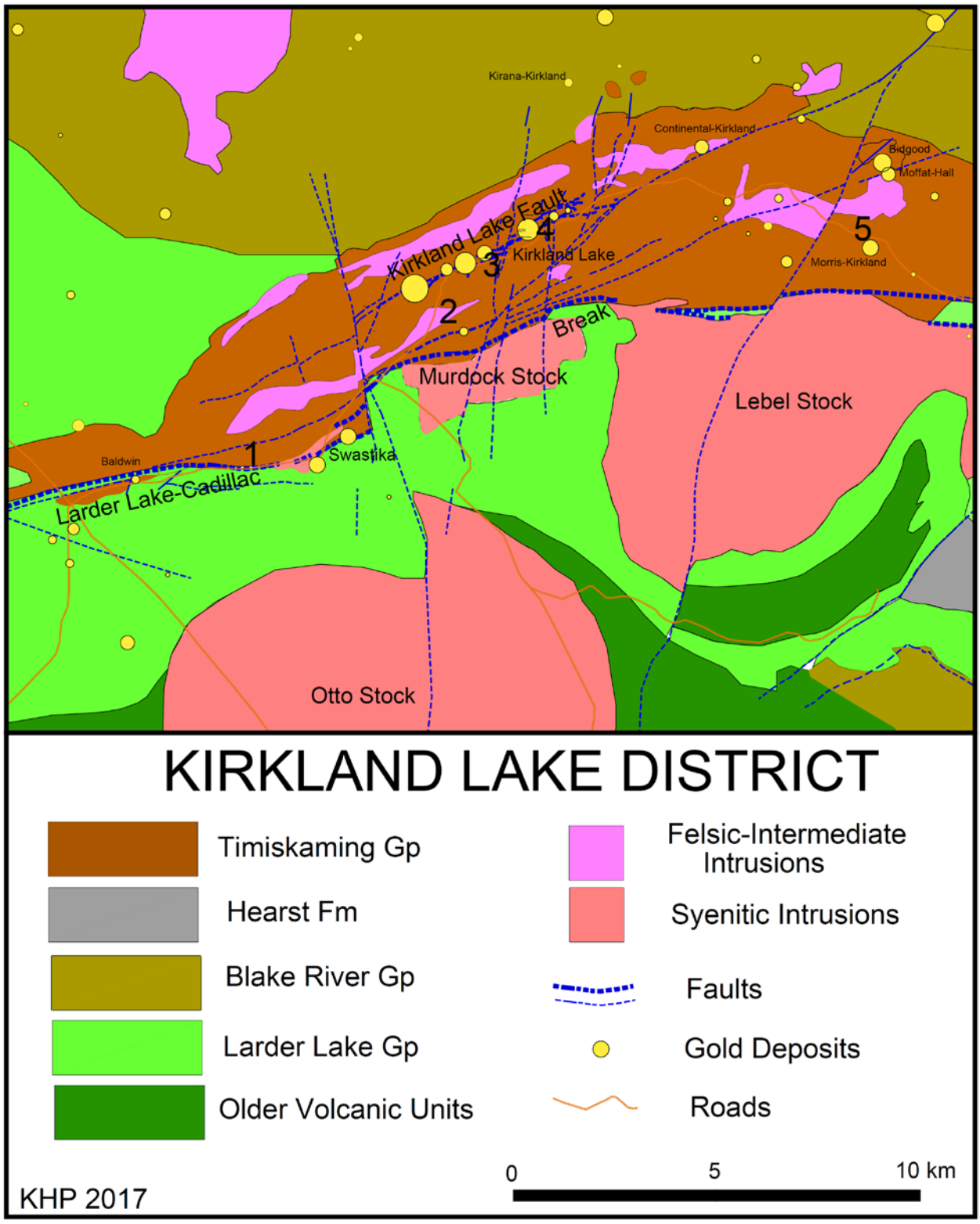

Figure 2.1. Kirkland Lake field localities. Gp = Group, Fm = Formation

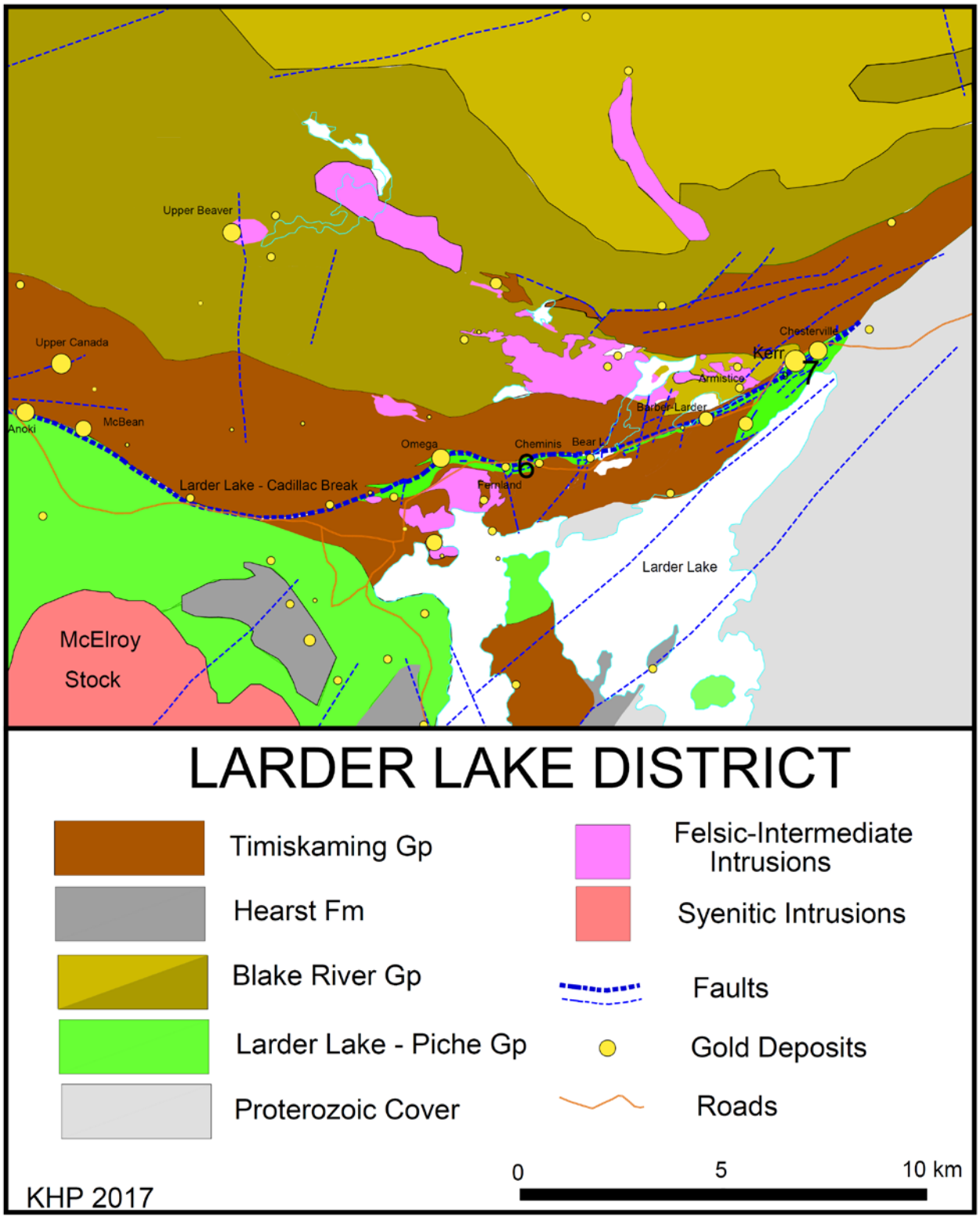

Figure 2.2. Larder Lake field localities. Gp = Group, Fm = Formation.

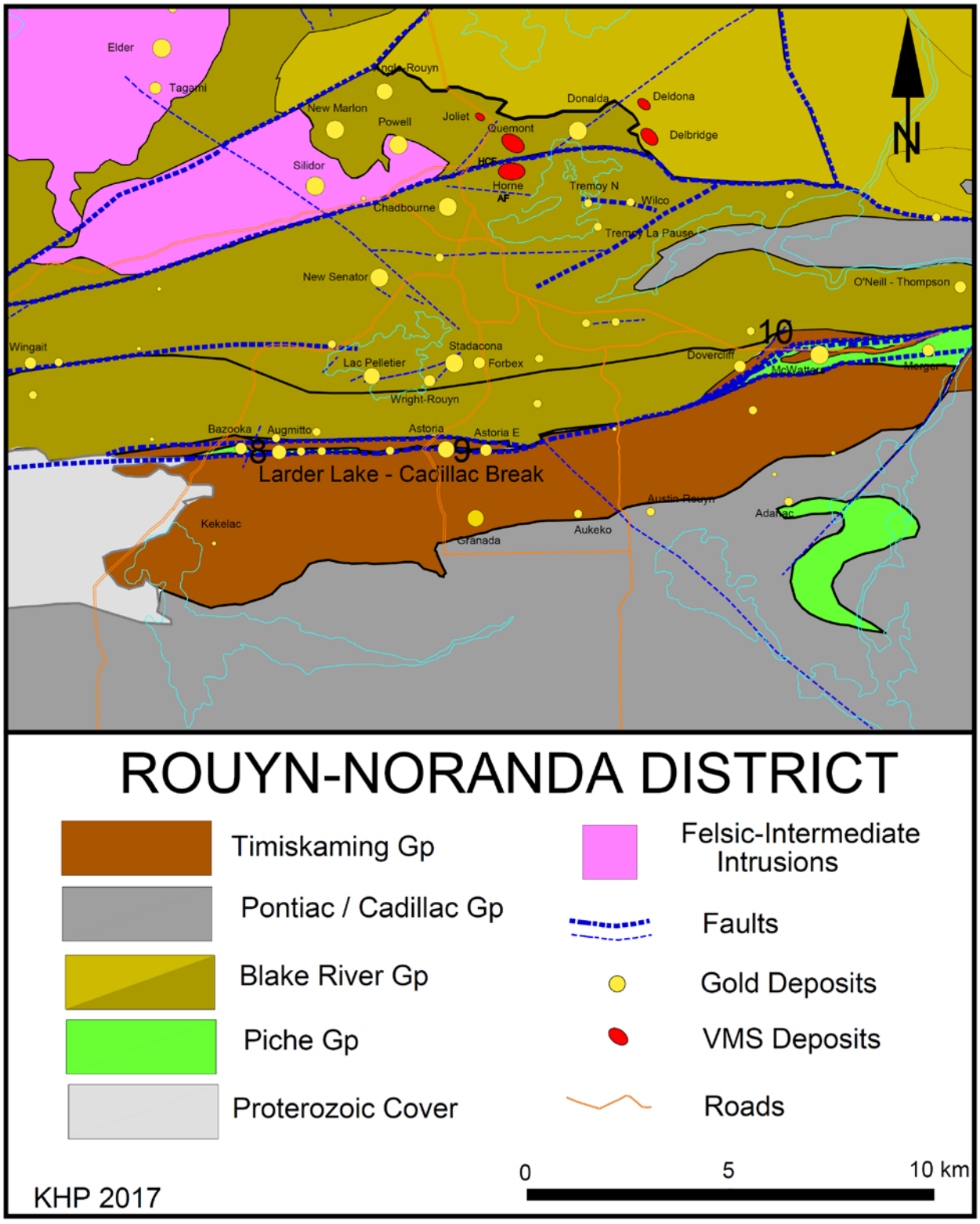

Figure 2.3. Rouyn-Noranda field localities. Gp = Group, Fm = Formation.

Chapter 3: (Day 2 – Part 1) Geology and mineralization in the Potter Mine Area, Munro Township

Michel G. Houlé
Natural Resources Canada – Geological Survey of Canada

Sonia Préfontaine
Ontario Geological Survey

3.1 Geological context of Munro Township

Munro Township, located approximately 80 km east of Timmins, in the western part of the Abitibi greenstone belt (AGB), covers part of the eastern extension of the Kidd–Munro assemblage (2720 to 2710 Ma: Ayer et al. 2005a; Ayer et al. 2005b; Berger et al. 2009; Berger 2011). The northern part of the township is composed dominantly of komatiitic and mafic tholeiitic metavolcanic rocks with lesser tholeiitic felsic metavolcanic rocks (FIII of Lesher et al. 1986). Layered ultramafic and mafic sills and dikes of the Center Hill Complex (Ayer et al. 2005a; Ayer et al. 2005b) intruded the Kidd–Munro age metavolcanic. Younger clastic metasedimentary rocks of Porcupine age (2690 to 2685 Ma: Ayer et al. 2005a; Ayer et al. 2005b) are in fault contact (i.e., Pipestone fault) with the older Kidd–Munro age metavolcanic rock in the southwest portion of Munro Township (Fig. 3.1). The komatiitic and tholeiitic metavolcanic rocks host many base metal, nickel, asbestos and gold deposits and showings. These include the Potter and Potterdoal Cu-Zn volcanogenic massive sulfide deposits, the komatiite-associated Mickel Ni-Cu-(PGE) showing, the Hedman and Munro asbestos mines (peridotite- and dunite-associated chrysotile deposits), the Croesus gold mine (tholeiitic basalt flows), and numerous other small gold showings.

The metavolcanic rocks in Munro Township are structurally complex, with evidence for several folding and faulting events. However, the main structure consists of a large northwest-trending syncline with an axial trace in the central part of the township (Péloquin et al. 2005). Four major faults transect Munro Township subparallel to the stratigraphy (Fig. 3.1): 1) the Pipestone fault at the contact between the Kidd–Munro and Porcupine assemblages; 2) the Munro fault zone centred in the southern part of the township; 3) the Centre Hill fault immediately south of the Centre Hill Complex; and 4) the Warden Hill fault in the area of the Munro Lake sill in the north part of the township.

On the southern limb of the major syncline, a minor northwest-trending anticline–syncline pair of limited extent also occurs within the western part of Munro Township and in Beatty Township, suggesting more complex fold patterns in the southern limb (Péloquin et al. 2005). Based on Péloquin et al. (2005), the southern limb stratigraphy is composed of (from base to top): a sequence of interlayered spherulitic/variolitic felsic and mafic flows (pillowed and massive facies), a sequence of subaqueous basalt flows (massive, pillowed and flow breccias facies) and a tholeiitic Beatty rhyolite (massive, lobe and breccia flow facies), intercalated within a subaqueous basaltic sequence (pillowed, massive, pillow breccias and hyaloclastites facies) that has a high magnetic signature. The magnetic basalts are intruded by the layered mafic to ultramafic tholeiitic Munro sill. It is overlain by a thick sequence of komatiitic lava flows. The komatiitic sequence is composed of variable proportions of massive and olivine spinifex-textured peridotitic komatiite flows intercalated with massive and pyroxene spinifex-textured basaltic komatiite flows. More differentiated flows also occur locally and are composed of massive peridotitic komatiite flows that exhibit upper gabbroic zones overlain by thin olivine spinifex-textured zones. At the base of this komatiite succession, the Mickel Ni-Cu-(PGE) showing occurs within the differentiated komatiitic Dee's flow at the boundary between Munro and Beatty townships. The mafic metavolcanic rocks have been subdivided into 2 units, based on their magnetic signature, but are characterized by similar volcanic facies (abundant pillowed flows with lesser massive flows and flow breccias).

On the northern limb of the major syncline, facing reversals are associated with the McCool syncline and the Potter anticline. The volcanic succession trends northwest and exposure on the southern limb of the McCool syncline is dominated by ultramafic with lesser mafic volcanic rocks, whereas the northern limb of the McCool syncline is composed of a mix of ultramafic and mafic volcanic rocks and ultramafic to mafic intrusions (Fig. 3.1). The southern limb includes the well-preserved exposures of the Pyke Hill and "Lava Lake" komatiite flows, the Cu-Zn past-producing Potter Mine and the Centre Hill layered intrusive complex. The northern limb includes the tholeiitic Theo's flow and the differentiated komatiitic Fred's flow (Arndt 1977).

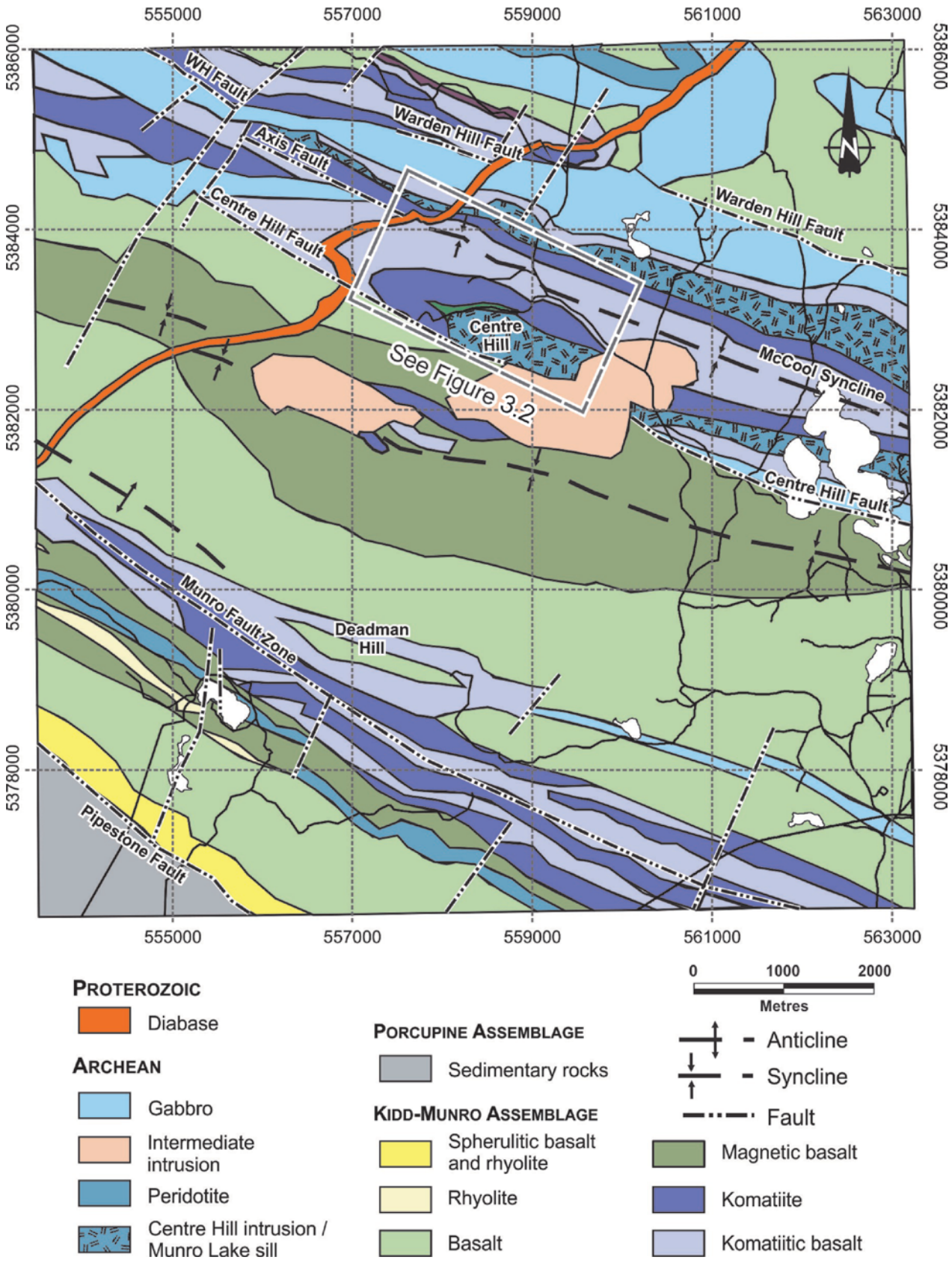

Figure 3.1. Geology of Munro Township, showing the location of the Potter mine (boxed area) in the northern part of the Munro Township (*modified from* Péloquin et al. 2005).

3.2 Geological context of the Potter mine

Komatiitic and tholeiitic metavolcanic rocks, with subordinate metasedimentary rocks, dominate the volcanic succession at Potter (2716 Ma: Berger et al. 2011; Préfontaine et al. 2012; Préfontaine 2013). It is bounded, to the south, by the younger layered mafic to ultramafic Centre Hill Intrusive Complex. The metavolcanic strata were subdivided by Gibson (1998) and Gamble (2000) into three informal lithostratigraphic and chemostratigraphic units which, from oldest to youngest, include: 1) a Lower Komatiitic unit; 2) a Middle Tholeiitic unit; and 3) an Upper Komatiitic unit (Fig. 3.2).

The volcanic succession at the Potter mine, including the Centre Hill Intrusive Complex, are affected by several minor faults and are folded about the NW trending, upright Potter anticline based detailed mapping and re-logging of drill core by Oliver et al. (1999) on the Potter succession and deposit (Fig. 3.2). Subsequently, Houlé et al. (2002) reinforced the anticline interpretation by identifying facing reversals in the Upper Komatiitic unit that coincide with the anticlinal axis. However, due to the scarcity of top indicators, the precise location of the Potter anticlinal axis is difficult to determine within the volcaniclastic succession. Several minor faults are expressed by less than 1m wide shear zones and the contact between the metavolcanic rocks and the Centre Hill Intrusive Complex is often sheared. The volcanic succession, as well as the Centre Hill Intrusive Complex, is truncated to the south by the Centre Hill Fault.

The metamorphic grade is greenschist facies with metamorphic mineral assemblage of talc-serpentine-chlorite-amphibole-quartz for the ultamafic rocks and albite-quartz-chlorite-epidote-amphibole for basaltic rocks (Préfontaine 2013).

3.2.1 The Lower Komatiitic unit

The Lower Komatiitic unit is poorly exposed at surface and is cut by the ultramafic to mafic Centre Hill intrusive Complex (Fig. 3.2). The unit is best observed in drill core and occur essentially east of the mine shaft around Pyke Hill, where it consists of thin, differentiated (cumulate and spinifex) to undifferentiated (cumulate/olivine-phyric) komatiitic flows (Gibson 1998; Gamble 2000; Gibson and Gamble 2000; Houlé et al. 2002, 2008, 2010) similar to those observed at Pyke Hill.

3.2.2 The Middle Tholeiitic unit

The Middle Tholeiitic unit is dominantly composed of basaltic volcaniclastic rocks, such as tuff breccias and lapillistone and minor tuff, with lesser intercalated graphitic, carbonaceous argillite chert, massive sulfide and massive to autobrecciated mafic to ultramafic intrusions and possible ultramafic flows. All of these units are cross-cut by several mafic, mafic to ultramafic and ultramafic synvolcanic intrusions.

3.2.2.1 Volcanic and volcaniclastic units

The volcanic and volcaniclastic units are the dominant lithofacies within the Middle Tholeiitic unit and are continuous over the entire property (Fig. 3.2). East of the Potter mine, and south of Pyke Hill, the Middle Tholeiitic unit consist of massive to pillowed variolitic basaltic flows that contain minor base metal sulfide mineralization (Gamble 2000; Fig. 3.2). To the west, and along strike of the pillowed flows, the Middle Tholeiitic unit has been subdivided by Gibson and Gamble (2000) into two main lithofacies: tuff breccia and lapillistone lithofacies.

The tuff breccia lithofacies is exposed at the surface for over 700m stike length between the Potter mine headframe and Pyke Hill. It is truncated to the south by the Centre Hill Intrusive Complex (Figs. 3.2 and 3.3A). It consists of juvenile, globular, irregular “moulded” lapilli that include agglutinate, fluidal bombs, cored bombs, blocks and armoured lapilli with rare, less than 1%, accidental fragments of carbonaceous mudstone, argillaceous mudstone, siliceous siltstone and massive pyrrhotite (Gibson and Gamble 2000). The tuff breccia is free of a finer (< 2 mm) clastic matrix, but does contain from 5 to 15%calcite, albite and amphibole as an open space filling matrix cement (Préfontaine 2013).

The lapillistone lithofacies occurs mainly west of the Potter mine headframe. It overlies the tuff breccia lithofacies and it is exposed over a strike length of approximately 1 km where it is folded about the NW trending Potter anticline. It attains a maximum thickness at surface of approximately 200m (Figs. 3.2 and 3.3B). The lapillistone lithofacies consist of decimetre to metre thick, poorly to well defined, massive lapillistone beds, is defined by an abrupt change in grain size, and locally exhibit normal or reverse grading. The beds are moderately to well sorted and consist of densely packed, fragment-supported lapilli interbedded with graphitic, carbonaceous argillite and siliceous siltstone. Hundred to 95% of the clasts are angular to subrounded lapilli with up to 5% accessory clasts of amygdaloidal, porphyritic, globular to angular, plate-like lapilli (<1 to 5 mm) and occasional armoured lapilli with minor accessory fragments of olivine-porphyritic basalt, amygdaloidal aphyric basalt, plagioclase microlitic basalt, graphitic argillite, spinifex bearing ultramafic, and massive pyrrhotite (Gibson and Gamble 2000; Tardif et al. 2000; Préfontaine 2013). Similar to the tuff breccia lithofacies, the lapillistone lithofacies lacks a finer clastic matrix, but does contain between 5 and 20% calcite, albite, chlorite, pyroxene, amphibole and pyrrhotite as open-space filling matrix cement. However, the lapillistone locally have a matrix of massive graphitic argillite or carbonaceous siltstone which was not observed in the tuff breccia. The occurrence of relict palagonite textures (pseudomorphed by chlorite) and perlitic cracks indicates that the lapilli of both lithofacies were originally vitric and originally composed of volcanic glass with microphenocryts of pyroxene and plagioclase (Gibson 1998; Gibson and Gamble 2000).

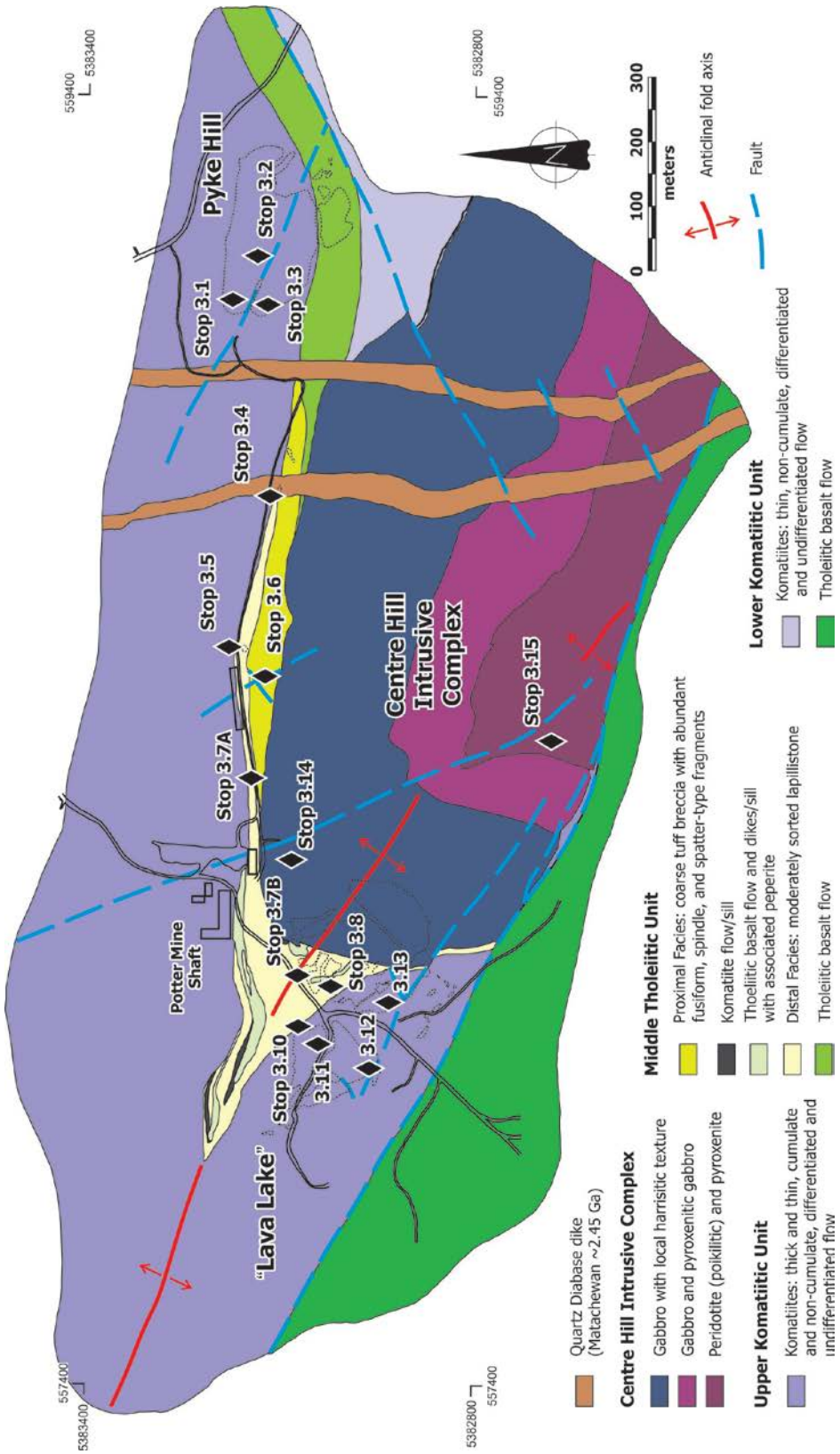

Figure 3.2. Geology of the Potter Mine property showing locations of field trip stops 3.1 to 3.5 (*modified from* Oliver et al. 1999; Gamble 2000; and Houlé et al. 2002).

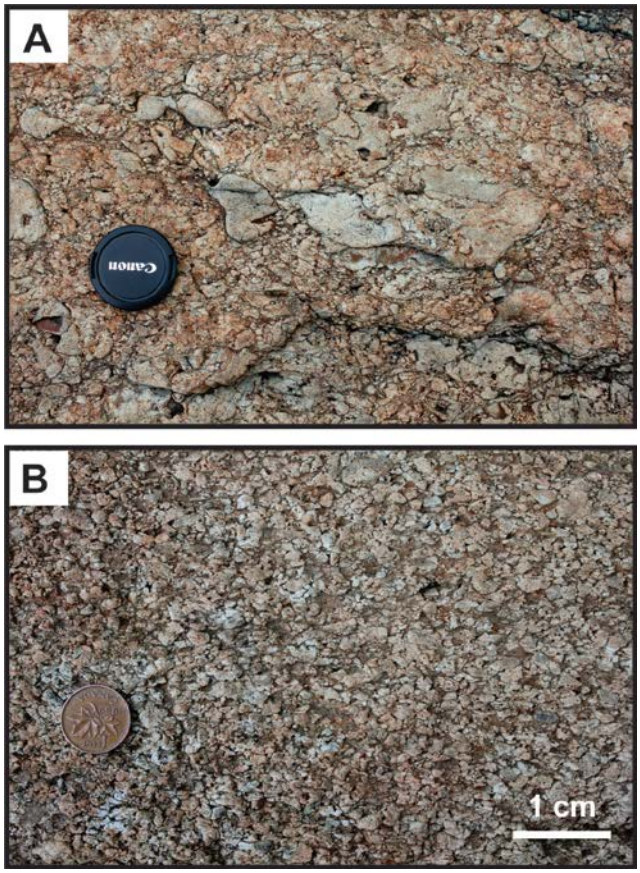

Figure 3.3. Field photos of the basaltic volcaniclastic rocks and the massive sulfides at the Potter Cu-Zn deposit in Munro Township, Ontario. **a** Proximal basaltic tuff breccia unit. Coin is 58 mm in diameter. **b** Distal basaltic lapillistone unit. Coin is 18 mm in diameter.

3.2.2.2 Sedimentary units

Graphitic and carbonaceous argillite, as well as thin-bedded tuffs and chert, occur throughout the volcaniclastic succession. Although limited, the argillites are to a large extent concentrated in the deposit area and are often spatially associated with areas of more significant sulfide mineralization. The argillite is massive to thinly-bedded and is locally intercalated with beds of disseminated to massive sulfide. Locally, in areas containing semi-massive to massive sulfide mineralization, wispy fragments of argillite define layers. In areas, argillite constitutes the matrix of the lapillistone or is interbedded with the lapillistone. Commonly, the argillites have millimetre to centimetre size, spherical to disc-shape massive pyrrhotite ± chalcopyrite ± magnetite concretions, which presumably formed during diagenesis. Fragments of massive pyrrhotite within the lapillistone lithofacies may be derived from the concretions. Less commonly, the argillite forms a matrix to a matrix-supported, polymictic debris flow that contains angular to subrounded, pebble to cobble size fragments of lapillistone, tuffs, chert, massive sulfides, sulfide concretions and mafic intrusion. The argillite is intruded by mafic, mafic to ultramafic and ultramafic sills and contains fractures filled by calcite or sulfides. Tuff and chert beds often occur near the stratigraphic top of the volcaniclastic succession. The chert is thinly bedded to laminated and often interbedded with layers of thinly bedded tuff that contains fine disseminated sulfide mineralization.

3.2.2.3 Synvolcanic intrusions

Sills and dikes of mafic, mafic to ultramafic and ultramafic composition intrude both lithofacies, although the lapillistone lithofacies contains more intrusions. The coherent ultramafic rocks in the lapillistone lithofacies occur primarily as intrusions, some with spinifex texture, but the presence of komatiitic lava flows cannot be completely excluded.

Field observations and geochemistry indicates that the coherent and autobrecciated sills and dikes that intrude the volcaniclastic succession are divisible into three compositional types: mafic to ultramafic (Type 1), mafic (Type 2) and komatiitic (Type 3) (Gibson 1998; Gibson and Gamble 2000; Préfontaine 2013).

Both, Type 1 and 2 intrusions are massive, fine-grained to aphanitic, locally pyroxene porphyritic, rarely amygdaloidal, and range in thickness from a decimetre to several metres. Intrusive contacts with the volcaniclastic and the sedimentary lithofacies are sharp, autobrecciated or peperitic (Gibson 1998; Gibson and Gamble 2000). However, based on the geochemistry, Type 1 mafic to ultramafic intrusions have a composition that is similar to the volcaniclastic rocks, whereas Type 2 mafic intrusions have a composition more typical of basalts. Type 2 intrusions have contacts dominantly sharp, straight to irregular, with quenched margins that display a perlitic texture. Autobrecciation textures defined by blocky, clast-supported to almost jigsaw-fit clasts are common. Peperitic contacts occur with volcaniclastic, sedimentary and massive sulfide lithofacies. Type 3 ultramafic intrusions are generally thicker and range from metres to tens of metres in thickness; some may be extrusive. The ultramafic rocks are aphanitic to fine-grained, massive, locally poikilitic and contain oikocrysts that range from a few millimetres to approximately one centimetre in size. Contacts between the ultramafic intrusion and the volcaniclastic lithofacies are autobrecciated with blocky fragments forming an almost jigsaw fit breccia and, where in contact with the mafic to ultramafic and mafic intrusions, the contacts are generally sharp, straight to irregular, and locally difficult to trace, suggesting that the ultramafic intruded still-cooling, mafic to ultramafic and mafic intrusions.

3.2.3 The Upper Komatiitic unit

The Upper Komatiitic unit, with a thickness of approximately 400m, is well exposed on surface and consists of komatiitic flows, including those at the well-known Pyke Hill (Pyke et al. 1973) and “Lava Lake” localities (Arndt 1986; Fig. 3.2) which represent some of the best preserved and best exposed sequences of thin

differentiated (spinifex-cumulate) non-cumulate, thin

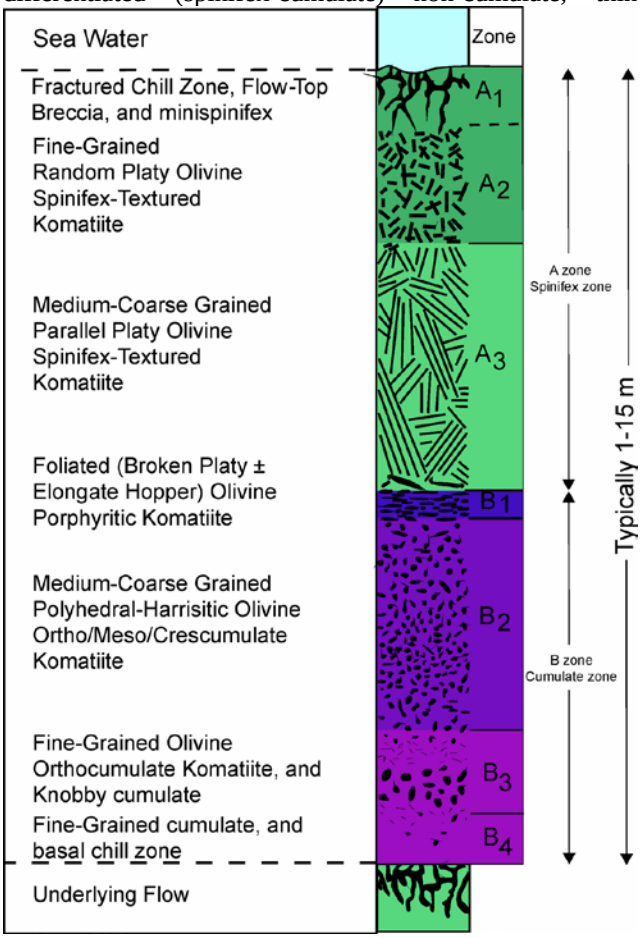

Figure 3.4. Sketch of a typical thin differentiated (spinifex-cumulate textured) komatiite flow in Munro Township, Ontario, showing volcaniclastic, aphyric, random olivine spinifex, platy olivine spinifex and cumulate lithofacies (modified from Pyke et al. 1973).

in the world. It includes thin to thick, differentiated (cumulate and spinifex) and massive flows that are characterized by a lower cumulate zone and an upper spinifex-textured zone with chilled and polygonal fractured flow top (Figs. 3.4 and 3.5). On the other hand, the poorly differentiated, non-cumulate flows have a lobate sheet and flattened pillow morphology. The immediate hanging wall to the Middle Tholeiitic unit volcaniclastic lithofacies is a more magnesian medium-grained, adcumulate to mesocumulate massive to weakly layered flow.

Peridotitic komatiite flows of the Upper Komatiitic unit are overlain by basaltic komatiitic flows. The basaltic komatiite flows are poorly exposed and occur as pillowed or massive flows with minor differentiated flows exhibiting a massive lower olivine-phyric to cumulate zone and an upper pyroxene spinifex-textured zone (Houlé et al. 2008, 2010).

3.2.4 Centre Hill Complex

The Centre Hill Intrusive Complex is a layered, massive non-cumulate, and thick high-Mg komatiite flows differentiated mafic to ultramafic intrusion that has a strike length of approximately 1km and a thickness of about 500m (Fig. 3.2). It is interpreted to be a shallowly emplaced intrusion, characterised by alternating layers of peridotite and clinopyroxenite overlain by an upper gabbroic portion (MacRae 1963, 1969; Johnstone 1987; Thériault and Fowler 1996).

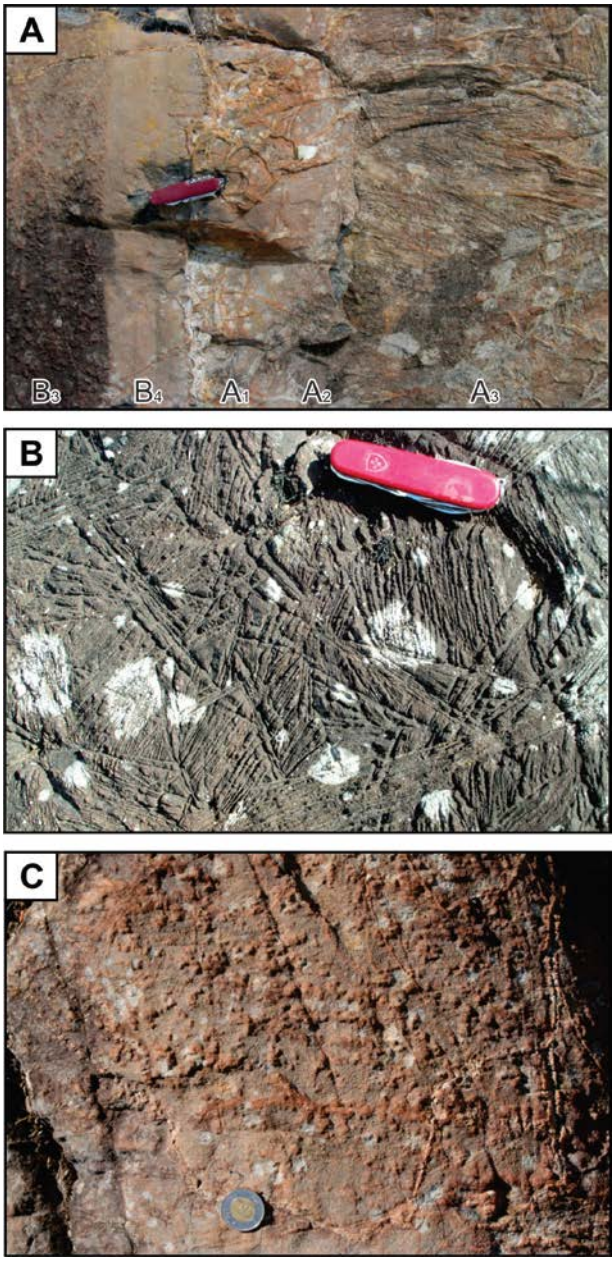

Figure 3.5. Field photos from Pyke Hill in Munro Township, Ontario. **a** Komatiite flow that exhibits the platy (A3) spinifex zone and the glassy flow-top and flow top breccia overlain by the fine-grained olivine cumulate and the knobby olivine cumulate zones of the next komatiite flow. Stratigraphic top to the left. Knife is 10 cm long. **b** Medium-grained randomly oriented olivine spinifex texture (A2). Knife is 10 cm long. **c** Knobby olivine cumulate zone. Stratigraphic top to the top of the photo. Coin is 28 mm in diameter.

Early interpretations (Coad 1976) suggested that the Centre Hill Intrusive Complex was a synvolcanic intrusion emplaced into its own volcanic pile due to its broad compositional similarity to the mafic intrusions and the volcaniclastic succession (Gibson and Gamble 2000); however, a U-Pb zircon age of 2706.8±1.2 Ma clearly indicates it is 9 to 11 Ma younger than the succession it intrudes (Ayer et al. 2005b).

3.3 VMS mineralization at the Potter mine

3.3.1 Mineralization styles

The Potter Cu-Zn mine has produced 477 572 tonnes at 1.63 wt% Cu and 1.5 wt% Zn from 1967 to 1972 and recent resource estimations have shown an additional indicated resource of approximately 3 Mt at 1.45 wt% Cu, 1.19 wt% Zn, 390 ppm Co and an inferred resource of approximately 2 Mt at 1.08 wt% Cu, 1.05 wt% Zn and 301ppm Co (Gamble and Bettiol 2008).

The volcaniclastic lithofacies of the Middle Tholeiitic unit host the base metal sulfide mineralization at the Potter mine (Gibson 1998; Gamble 2000; Gibson and Gamble 2000; Houlé et al. 2008, 2010). The base metal mineralization occurs as eleven, tabular, stacked massive to semi-massive sulfide mineable lenses that are vertical to steeply north dipping and are enveloped within zones of semi-massive to disseminated sulfides within the host volcaniclastic lithofacies (Gibson and Gamble 2000; Gamble and Bettiol 2008). The mineralization is characterized by an assemblage of sulfides dominated by pyrrhotite with lesser sphalerite and chalcopyrite. Two main styles of base metal mineralization are recognized to date by Gibson (1998): 1) subseafloor replacement; and 2) seafloor mineralization.

Subseafloor mineralization appears to be the most volumetrically significant mineralization type. The disseminated to semi-massive sulfides occurs within the open-space matrix to the volcaniclastic rocks, in some cases, replace an earlier carbonate cement matrix (Figs. 3.6A, B). Where intensely mineralized, the matrix consists entirely of sulfides and the lapilli are pervasively chloritized and are partially replaced by sulfides. This type of mineralization was interpreted to be a product of subseafloor replacement of the volcaniclastic strata (Gibson 1998; Gibson and Gamble 2000).

The seafloor mineralization consists of massive sulfides lenses intercalated with argillite and carbonaceous mudstone within the volcaniclastic rocks (Fig. 3.6C to F). This style of mineralization was interpreted by Gibson (1998) to have formed on the sea floor during volcanic hiatuses marked by the deposition of argillaceous sediments. Several of the ore lenses contain both styles of mineralization. Furthermore, base metal mineralization also occurs as fragments or veins within basaltic to ultramafic, mafic and ultramafic intrusions, which may represent a third mineralization style.

3.3.2 Hydrothermal alteration

Hydrothermal alteration associated with the Potter deposit can be separated into 4 mineral assemblages which are found primarily in the open-space matrix of the volcaniclastic lithofacies and by the alteration of the lapilli. These are, with decreasing distance form massive sulfides: 1) actinolite-chlorite-albite; 2) chlorite-clinopyroxene; 3) albite-calcite; and 4) chlorite.

The actinolite-chlorite-albite assemblage, which has a mineralogy that is similar to a background greenschist metamorphic assemblage, records a mass increase and is interpreted as being the result of regional metamorphism. The chlorite-clinopyroxene assemblage also contains albite. Clinopyroxene in the chlorite-clinopyroxene assemblage is interpreted to be the results from the metamorphic recrystallization of a Ca-enriched alteration zone. The albite-calcite assemblage is characterized by widespread replacement of the matrix by variable amounts of albite, calcite and minor chlorite, with a partial chloritization of the fragments. Locally, albite is the dominant matrix mineral with lesser chlorite and minor calcite and locally, calcite is the domiant matrix mineral with lesser chlorite and minor albite. Finally, the chlorite assemblage is limited to the immediate margins of the massive sulfide lenses. Replacement of the matrix and the lapilli are partial to complete and locally the matrix as well as the lapilli are replaced by sulphides.

The chlorite assemblage shows a direct spatial association with massive sulfide mineralization and is interpreted to be result from the interaction between glass-rich lapilli and a higher temperature (250-350°C), hydrothermal fluid, presumably evolved seawater that moved, in this case, laterally through the volcaniclastic lithofacies to produce the chlorite assemblage and to form the sulfide lenses.

Other mineral assemblages do not show spatial or compositional variations in whole rock modal mineralogy or in mass change that are typical of chlorite and sericite discordant alteration associated with the bimodal-mafic VMS deposit. The difference is assemblages are developed in an open space matrix. These matrix mineral assemblages formed from progressively heated seawater that was drawn into and moved laterally within the porous and permeable volcaniclastic within the lower temperature (150-200°C), upper part of the Potter VMS hydrothermal system resulting in a semi-conformable, stratabound background alteration. Systematic, spatial variations in the mineral chemistry of the primary hydrothermal matrix and subsequent metamorphic minerals, their modal mineralogy, and associated mass change indicate the influence of a thermal gradient within this seawater dominated system that increased in temperature toward the Potter deposit, and indicates that these assemblages formed pre- and/or syn-mineralization.

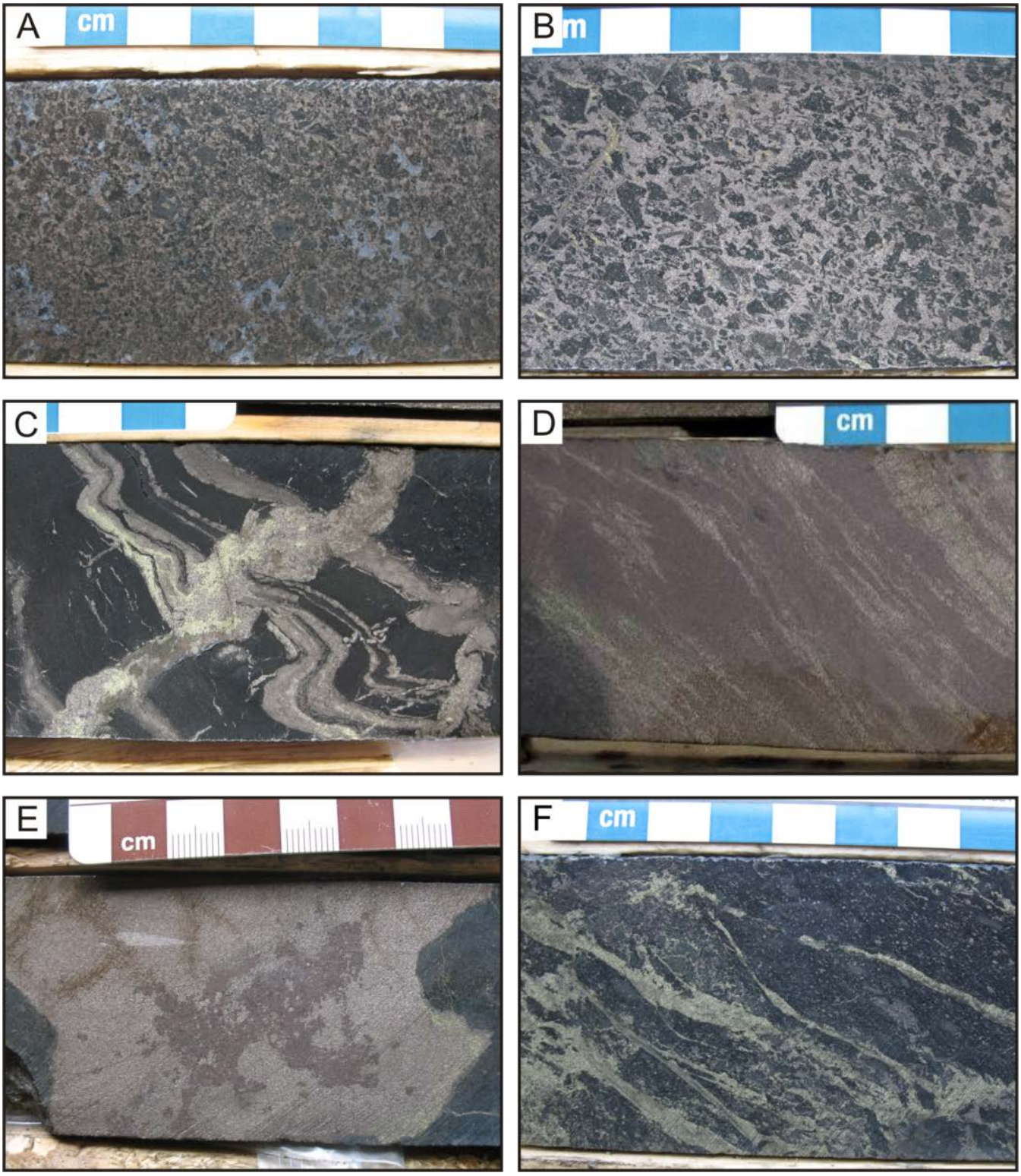

Figure 3.6. Examples of the mineralization styles at the Potter Cu-Zn deposit. **a** Subseafloor replacement of calcite matrix (in white) by pyrrhotite. **b** Subseafloor replacement where pyrrhotite in the matrix of the lapillistone partially replaces the lapilli margins. **c** Interlayered argillite and massive sulfides as well as cross-cutting remobilized sulfide veins. **d**. Banded sphalerite and pyrrhotite massive sulphide. **e** Block or vein of massive sulfide (pyrrhotite and sphalerite) within an ultramafic intrusion. **f** Chalcopyrite veins within the lapillistone.

3.4 Field trip stop descriptions

Thin well-differentiated flows at Pyke Hill:
Pyke Hill (*see* Figs. 3.2 and 3.7 for location of Stop 3.1 to 3.3) is located approximately 1 km east-southeast of the Potter mine, and represents one of the best preserved and best exposed sequences of thin differentiated (spinifex-textured) and massive peridotitic komatiite flows in the world. It represents a series of compound flows. At least 60 flows have been identified over an exposure width of approximately 125 m (Pyke et al. 1973). Individual flows range in thickness from 0.5 to 15 m, averaging approximately 3 m (Pyke et al. 1973). The relative proportions of spinifex-textured "A" zones and cumulate-textured "B" zones vary within individual flows, owing to irregularities along the contact between the zones in response to different rates of cooling. The ratio of Zone A to Zone B averages approximately 2:1 to 1.5:1 at Pyke Hill (Pyke et al. 1973), confirming that this area contains primarily non-cumulate rather than cumulate flows. However, preliminary data indicate that the proportion of A:B zones decreases with increasing thickness. This is consistent with increases in flow thickness allowing for increases in the amount of olivine accumulation—a trend also observed in Western Australia (e.g., Lesher 1989).

1) **Thin differentiated komatiite flows:**
(UTM Z17 NAD83 – 559077mE, 5383181mN)

This stop at Pyke Hill comprises, from base to top, very thin (~0.75 to 2.5 m) well-differentiated sheet flows, thick (~4 to 12 m) well-differentiated sheet flows and thin (~3 to 4.5 m) well-differentiated sheet flows. The uppermost section is characterized by thin sheet flows that have conspicuous textural differentiation and represent the komatiite flow archetype described by Pyke et al. (1973), which includes a spinifex-textured "A" zone in the upper part, and a cumulus-textured "B" zone in the lower part of the flow. The A zone unit may be further subdivided into the A1 (fractured upper chill zone / flow-top breccia / microspinifex), A2 (randomly oriented spinifex) and A3 (coarse platy spinifex) zones. The B zone may be further subdivided into the B1 (aligned skeletal "hopper" olivine), B2 (medium- to coarse-grained cumulate), B3 (knobby cumulate) and B4 (fine-grained cumulate and basal chill) zones.

2) **Spinifex-textured sills:**
(UTM Z17 NAD83 – 5591137mE, 5383142mN)

Thin (centimetre-scale) semi-conformable olivine spinifex-bearing sills intrude the cumulate zones of some komatiite flows at Pyke Hill, producing a complex pattern. Euhedral cumulate olivine crystals of the flows immediately adjacent to the contact are coarser than elsewhere. Thin section examination shows that the coarser olivines are composed of olivine crystals that have been overgrown during the intrusion of the sills. We interpret this evidence to mean that komatiite flow cumulate materials were somewhat permeable at the time the sills were introduced. In addition, some cumulate olivine crystals of the flows have dendritic overgrowths where the dendrites have grown into the sills away from the cooling contacts. This demonstrates that there was a sufficient thermal gradient between the host cumulate and the magma within the sill to promote dendritic growth, and suggests that the host cumulate had undergone cooling prior to introduction of the sills. Hence, the sills were intruded into relatively hot unconsolidated cumulate material, which further indicates komatiite growth by inflation (Préfontaine 2003; Houlé et al. 2009).

3) **Komatiite flow morphologies:**
(UTM Z17 NAD83 – 559075mE, 5383138mN)

The southern part of Pyke Hill consists of, from base to top, thick (~6.5-16 m) differentiated sheet flows, thin (~2.5-4.5 m) differentiated sheet flows, thick (~5.5-13.5 m) differentiated sheet flows overlain by thin (~0.75-2 m) differentiated sheet flows. Most of the komatiite flows, especially thicker ones, are not as texturally or structurally organized as those of area of Stop 3.1. Furthermore, within the uppermost section, komatiite flows also occur as thin lobate sheet flows and flattened pillow facies that exhibit only limited spinifex textures along their cooling margins. However, well-differentiated flows are interlayered within sequences dominated by poorly differentiated flows, indicating that the timing of ponding varied on a flow-by-flow basis. Poorly differentiated, non-cumulate flows, especially those with lobate sheet and flattened-pillow forms (rather than sheet flows) are spinifex textured along their margins and along fractures, indicating rapid crystallization due to extensive hydrothermal cooling and thermally constrained crystallization (Shore and Fowler 1999). Flattened pillows contain shelves that were interpreted by Shore (1996) as molten lava breakouts. However, the thicker parts of some lobate flows exhibit incomplete secondary selvages inside the major external selvages, suggesting that growth may have occurred by progressive inflation. Furthermore, these variations in flow morphologies indicate that the eruption rates waned and waxed through the komatiitic sequence.

Basaltic volcaniclastic deposit:
The basaltic volcaniclastic deposits were subdivided by Gibson and Gamble (2000) into 2 main volcanic facies: 1) distal facies that consists of well-bedded, framework-supported lapillistone units that are massive, normal and reversely graded, and moderately to well sorted; and 2) proximal facies of massive to poorly bedded, unsorted tuff breccia (*see* Fig. 3.2 for locations of stops 3.4 to 3.8).

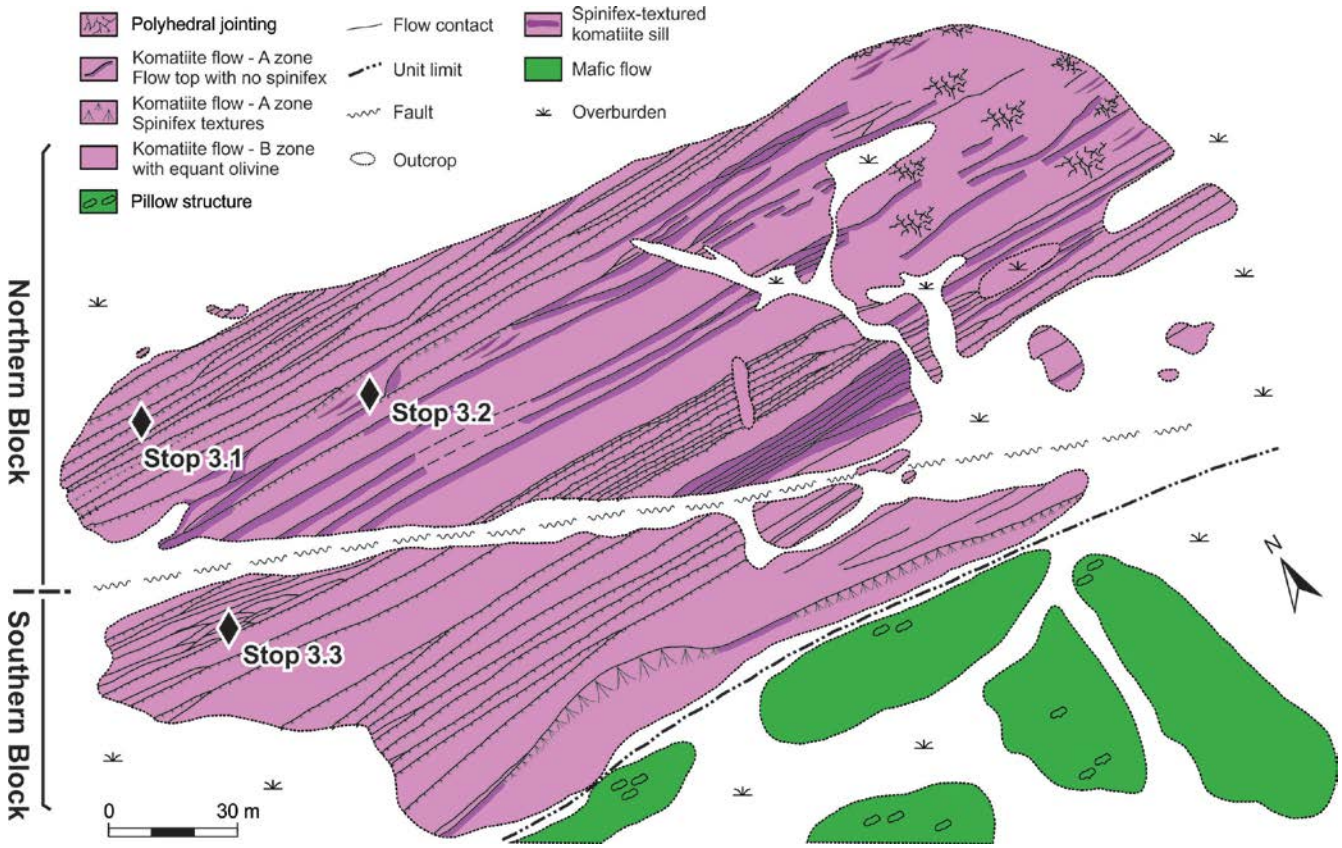

Figure 3.7. Geology of the Pyke Hill area showing locations of field trip stops 3.1 to 3.3 (modified from Pyke et al. 1973 and Arndt (1977).

4) Basaltic volcaniclastic unit:
(UTM Z18 NAD83 – 558777mE, 5383109mN)

Massive komatiite flows and the basaltic volcaniclastic unit are crosscut by a quartz diabase dike (Matachewan, ~2.45 Ma).

5) Thin differentiated komatiite flow:
(UTM Z17 NAD83 – 558538mE, 5383177mN)

Several spinifex-textured flows overlie the Potter volcaniclastic units. These komatiite flows are similar to flows that will be observed later, but are not as well exposed.

6) Proximal basaltic volcaniclastic unit:
(UTM Z17 NAD83 – 558535mE, 5383136mN)

Approximately 500 m east of the Potter mine area, the basaltic volcaniclastic rocks are massive to poorly bedded, unsorted and consist of globular, irregular "moulded" lapilli that resemble agglutinate, fluidal bombs, cored bombs, blocks, and armoured lapilli with less than 10% matrix containing fine, plate-like hyaloclastite shards and lapilli (Gibson and Gamble 2000). Accessory fragments of chert, carbonaceous mudstone, argillaceous mudstone, and massive sulfide account for less than 1% of the breccia.

The basaltic volcaniclastic rocks were previously interpreted to have been derived through quench fragmentation and autobrecciation of basaltic flows. However, the lack of basalt flows and in situ hyaloclastite, the abundance of fluidal and cored bombs, armoured lapilli, globular lapilli and the shear volume of breccia led Gibson and Gamble (2000) to propose an origin through "explosive fragmentation" rather than autobrecciation. The production of large volumes of lapilli-size granules is interpreted to be a product of the rapid eruption of low-viscosity mafic magma into a water column, where the magma was jetted into the water column, torn apart and quench fragmented. In this model, massive, poorly sorted tuff breccia containing globular, lapilli-size agglutinate and fluidal bombs are interpreted to represent vent-proximal deposits, similar to subaerial fire fountain and spatter rampart deposits. In contrast, well-bedded and well-sorted lapillistone deposits, typical of the mine area, are interpreted as high-particle-concentration mass flow and fall deposits that accumulated within a paleotopographic depression in the underlying komatiitic flow topography (Gibson and Gamble 2000).

7) Basaltic and komatiitic dikes/sills:
(UTM Z17 NAD83 – 558339mE, 5383144mN and UTM Z17 NAD83 – 558028mE, 5383048mN)

Basaltic and komatiitic sills are emplaced into the volcaniclastic succession interpreted by Gibson and Gamble (2000) as high-level synvolcanic intrusions. Evidence for this interpretation includes: 1) their fractured and autobrecciated upper and lower contacts with massive volcaniclastic material, massive sulfide and/or argillite injected along fractures that penetrate the massive sill interior; 2) locally chilled and sharp upper and lower contacts; 3) the development of hyaloclastite along chilled and perlitic-textured sill contacts and the mixing of this hyaloclastite with enclosing argillaceous mudstones and sulfide to form peperite; and 4) a basaltic composition that is identical to the volcaniclastic rocks (Gibson and Gamble 2000).

8) Distal volcaniclastic unit:
(UTM Z17 NAD83 – 558022mE, 5383006mN)

In the immediate mine area, the basaltic volcaniclastic rocks consist of well-bedded (decimetres to metres), framework-supported lapillistone units that are massive, normal graded, and moderately to well sorted. Fragment types include amygdaloidal, globular to angular, plate-like lapilli (<1 to 5 mm) of chloritized sideromelane and occasional armoured lapilli with lesser accessory fragments of olivine-porphyritic basalt, amygdaloidal aphyric basalt and plagioclase microlitic basalt. The matrix, which rarely exceeds 20% by volume of the hyaloclastite units, consists of: 1) albite and carbonate; 2) fine, massive chlorite; 3) amphibole and pyroxene; 4) graphitic argillaceous and carbonaceous sediments; and 5) massive sulfides. Well-bedded, basaltic volcaniclastic units host the massive sulfide mineralization (Gibson and Gamble 2000; Tardif et al. 2000).

Core display of the Potter copper-zinc volcanogenic massive sulfide deposit

9) Core display:

Mineralized diamond-drill core from the Potter Cu-Zn VMS deposit will be on display at the core shack during an extended lunch break, and will be discussed by Dave Gamble (Millstream Mines Ltd.). A selection of mineralized intervals and main features associated with the deposit will be shown.Five intervals have been selected from 5 diamond drilled holes to represent typical mineralized zones of 5 (A, B, C, D, and E zones) of the eleven, tabular, stacked massive to semi-massive sulfide mineable lenses at the Potter mine (see Fig. 3.8). All these lenses are vertical to steeply north dipping and are enveloped within zones of semi-massive to disseminated sulfides within the host volcaniclastic lithofacies.

10) Thick komatiite lava flow at 'Lava Lake':
The "Lava Lake" area (see Figs. 3.2 and 3.8 for location of Stop 3.10 to 3.13) is located immediately west of the Centre Hill Complex and approximately 1 km west of Pyke Hill. The "Lava Lake" area is very well exposed at surface, dominated by massive to weakly layered, medium-grained olivine adcumulate rocks (Fig. 3.9) and has been previously interpreted to represent an approximately 120 m thick "Lava Lake" that youngs toward the north (Arndt 1986). However, Houlé et al. (2002) suggest, based on geological mapping and drill core logging, that the "Lava Lake" is stratigraphically equivalent to the rocks exposed at Pyke Hill and youngs toward the south. This interpretation is supported by: 1) graded bedding in associated volcaniclastites and thin-bedded sediments within the upper part of the Middle Tholeiitic Unit; 2) chilled margin polarities; 3) asymmetric differentiation within flow units; 4) vesicle orientations; 5) fanned platy olivine spinifex; and 6) local asymmetric contacts in spinifex horizons within the komatiitic sequence. The remapping also suggests that the "Lava Lake" includes at least 6 mappable cooling units, and that it represents a series of thick sheet flows emplaced into a shallow depression, or a series of thick sheet flows overlain by a thin lava lake, rather than a thick lava lake. Thus, the Upper Komatiitic Unit in the Potter mine area is interpreted as sheet-flow facies komatiites that were channelized into a pre-existing depression, flanked by a levee facies represented by the multiple thin undifferentiated to differentiated flows at Pyke Hill.

11) Thin komatiite flows:
(UTM Z17 NAD83 – 557951mE, 5383074mN)

The base of the "Lava Lake" exposure is composed of several thin komatiite flows that exhibit some olivine and pyroxene spinifex-textured zones. Several relatively continuous vesicle-rich horizons are also present within or at the top of individual units. Multiple vesicle-rich horizons are interpreted to result from endogenous growth of these komatiite flows.

Figure 3.8. Oblique section (view looking easterly) of the interpreted mineralized zones at the Potter mine (from Gamble and Bettiol 2008).

12) Swirling olivine spinifex-textured:
(UTM Z17 NAD83 – 557927mE, 5383039mN)

The middle section of the "Lava Lake" exposure is characterized by the presence of unusual spinifex-textured zones previously interpreted as swirling olivine spinifex veins by Arndt (1986). However, field relationships (i.e., sharp lower contact and gradual upper contact) suggest those unusual zones are probably the result of partial melting and recrystallization of the spinifex-textured zones, due to residual heat from rapidly accumulated flows, as proposed for Honeymoon Well in Western Australia by Gole et al. (1990).

13) Serpentinization patterns:
(UTM Z17 NAD83 – 55887mE, 5382960mN)

Toward the upper part, the "Lava Lake" exposure is characterized by intense serpentinization. An irregular network of hierarchized bands of serpentine divides parts of the dunite/ peridotite into many irregular and

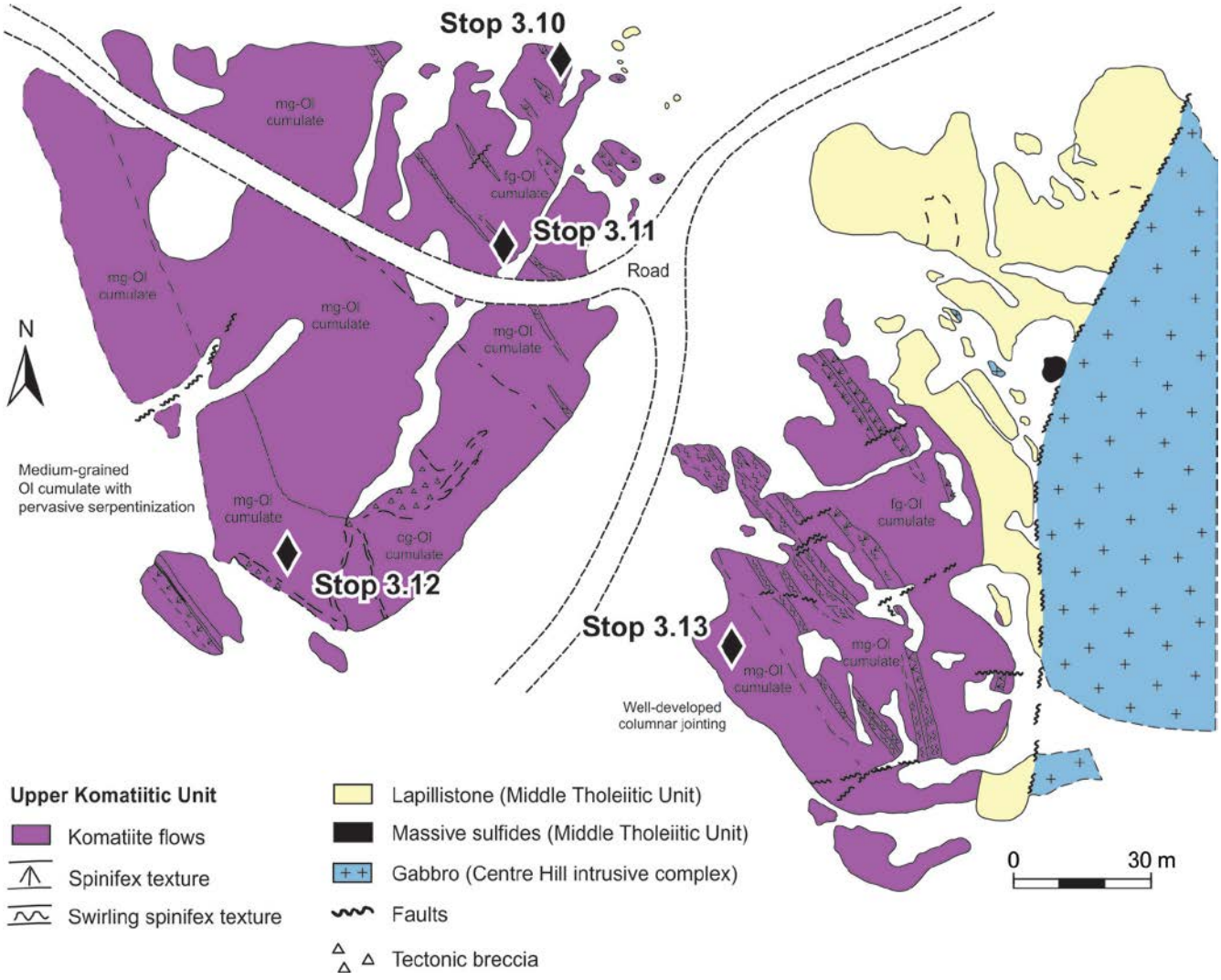

Figure 3.9. Geology of the "Lava Lake" area, showing locations of field trip stops 3.10 to 3.13 (modified from Arndt 1986).

randomly distributed remnants similar to those observed within a serpentinized olivine crystal in thin section.

14) Columnar jointing komatiite:
(UTM Z17 NAD83 – 557980mE, 5382948mN)

The upper part of the "Lava Lake" exposure is characterized by well-developed columnar jointing.

Layered mafic to ultramafic Centre Hill Complex:
The Centre Hill Complex is part of the tholeiitic differentiated ultramafic to mafic Munro Lake sill (Centre Hill Complex: south of the McCool syncline axis; and Munro Lake sill: north of the McCool syncline axis) and has been recently studied (e.g., Thériault and Fowler 1996). The Centre Hill exposure is the only area showing a complete section of the sill. The sill is characterized by the following lithostratigraphic units: a lower ultramafic cyclic unit (peridotite-clinopyroxenite), a middle unit of leucogabbro, and an upper mafic cyclic unit (BTG: branching-textured gabbro; CTG: clotted-textured gabbro) overlain by a marginal zone of fine-grained gabbro (Fig. 3.10, Thériault and Fowler 1996).

15) Harrisitic gabbro:
(UTM Z17 NAD83 – 558162mE, 5383050mN)

This stop marks the upper mafic cyclic unit characterized by alternating layers of the branching-textured gabbro (BTG) and clotted-textured gabbro (CTB). The layer of branching-textured gabbro (BTG) consist of spectacular harrisitic crystals of altered fayalite set in a gabbroic matrix, whereas the layers of clotted-textured gabbro (CTG) consists of centimetres-sized subspherical clots of clinopyroxene within a plagioclase-rich matrix (Thériault and Fowler 1996).

16) Igneous layering in the lower ultramafic unit:
(UTM Z17 NAD83 – 558423mE, 5382755mN)

This stop marks the lower ultramafic unit of the Centre Hill Complex. This unit is characterized by at least 6 cyclic subunits that consist of alternating layers of peridotite and clinopyroxenite. The cyclic repetition of the ultramafic layers within this unit has been interpreted by MacRae (1969) as periodic injection of new magma into the Centre Hill Complex magmatic chamber.

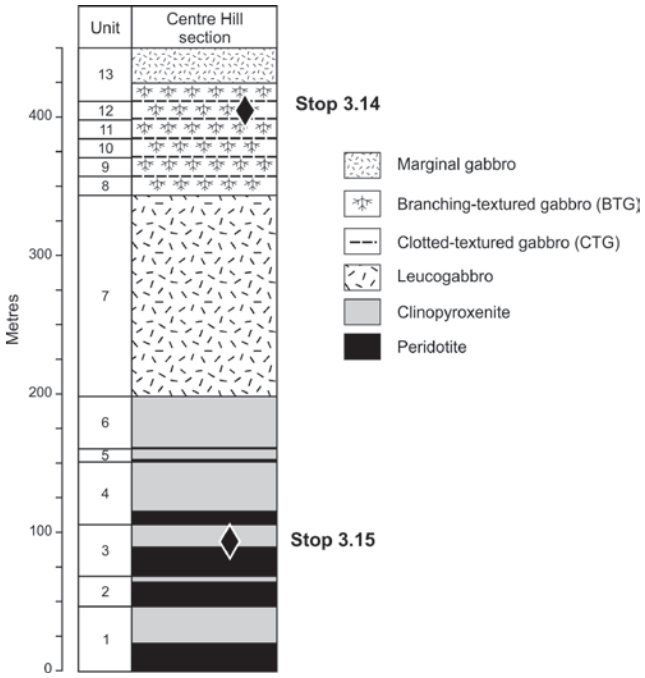

Figure 3.10. Stratigraphic section of the Centre Hill Complex showing main lithostratigraphic units and the approximate location of Stops 3.14 and 3.15 (after Thériault and Fowler 1996).

3.5 Acknowledgements

We are very grateful to Millstream Mines Ltd. for access to (E. Harrison) the Potter mine and to D. Gamble for information on the geology and mineralization on the property but also for participating to this field trip. We would also like to acknowledge previous contributions from many collaborators over the years such as H. Gibson, M. Lesher (Laurentian University) and A. Fowler (retired from University of Ottawa).

The guidebook has been patterned after previous field trips organized under the auspices of International Platinum Symposium held in Sudbury (Houlé et al. 2010) and for annual meetings of the Geological Association of Canada and the Mineralogical Association of Canada held in 2006 (Houlé et al. 2006), in 2008 (Houlé et al. 2008), and in 2015 (Pilote et al. 2015). The contributions from previous collaborators on those excursions and to those guidebooks were essential in the compilation of this field excursion and guidebook.

Our work in this area has been supported at various stages by financial support from the OGS (Project Unit 99-021) to C.M. Lesher, les Fonds de la nature et de la technologie Québec to MGH, the Natural Sciences and Engineering Research Council of Canada (NSERC) (DG 203171-98, -02, and -07) to C.M. Lesher, and the OGS and the GSC as part of the previous Targeted Geoscience Initiative program but also the Ni-Cu-Cr-PGE project under current Targeted Geoscience Initiative program of the GSC. Thanks to A.-A. Sappin for her help editing this contribution.

3.6 References

Arndt NT (1977) Thick, layered peridotite-gabbro lava flows in Munro Township, Ontario. Canadian Journal of Earth Sciences 14: 2620-2637.

Arndt NT (1986) Spinifex and swirling olivines in komatiite lava lake, Munro township, Canada. Precambrian Research 34: 139-155.

Ayer JA, Berger BR, Hall LAF, Houlé MG, Johns GW, Josey S, Madon Z, Rainsford D, Trowell NF, and Vaillancourt C (2005a) Geological compilation of the central Abitibi greenstone belt: Kapuskasing Structural Zone to the Québec border. Ontario Geological Survey, Preliminary Map P.3365, scale 1:250 000.

Ayer JA, Thurston PC, Bateman R, Dubé B, Gibson HL, Hamilton MA, Hathway B, Hocker SM, Houlé MG, Hudak G, Ispolatov VO, Lafrance B, Lesher CM, MacDonald PJ, Péloquin AS, Piercey SJ, Reed LE, and Thompson PH (2005b) Overview of results from the Greenstone Architecture Project: Discover Abitibi Initiative. Ontario Geological Survey, Open File Report 6154: 175 p.

Berger BR (2011) The Kidd–Munro Episode – Volcanism and Mineralization Between 2720 and 2710 Ma; in Results from the Targeted Geoscience Initiative III Kidd–Munro Project. Ontario Geological Survey, Open File Report 6258: 1-66.

Berger BR, Houlé MG, Dinel E, and Ayer JA (2009) The Kidd–Munro assemblage, Ontario: an update on the TGI project. Congrès Abitibi 2009, Abitibi Cuivre – Programme de Conférence, Rouyn-Noranda: 47-49.

Berger BR., Pilote P, Houlé MG, Ayer JA, Dinel E, and Bleeker W, (2011) Stratigraphy of the 2720-2710 Ma Kidd-Munro volcanic episode in the Abitibi greenstone belt: implication for base metals mineralization. In Yilgarn-Superior Workshop-Abstracts, Fifth International Archean Symposium, 10 September 2010: Geological Survey of Western Australia, Record 2010/20: 42-46.

Coad PR (1976) The Potter Mine. Unpublished MSc. Thesis, University of Toronto, Toronto, Canada: 239 p.

Gamble APD (2000) Geology of the Potter Cu-Zn-Co-Ag VMS mi ralization and exploration progress report to March 31, 2000 at Millstream Mines Ltd. Potter Mine exploration project. Dave Gamble Geoservices Inc., unpublished company report: 80 p.

Gamble APD and Bettiol EI (2008) Technical report on the resources at the Potter Mine property, Munro Township–Larder Lake Mining division on behalf of Millstream Mines Ltd. Technical Report under NI 43-101, filed May 29, 2008, with SEDAR® (see Sedar web site): 63 p.

Gibson HL (1998) A petrographic and geochemical study of the Potter Mine and interpretation on its volcanic environment, Munro Township, Ontario. Unpublished report, Millstreams Mines Ltd.

Gibson HL and Gamble APD (2000) A reconstruction of the volcanic environment hosting Archean seafloor and subseafloor VMS mineralization at the Potter Mine, Munro Township, Ontario, Canada. In Volcanic environments and massive sulfide deposits, Centre for Ore Deposit Research, University of Tasmania, Hobart, Tasmania, CODES Special Publication 3: 65-66.

Gole MJ, Barnes SJ, and Hill RE (1990) Partial melting and recrystallization of Archean komatiites by residual heat from rapidly accumulated flows. Contributions to Mineralogy and Petrology 105: 704-714.

Houlé MG, Lesher CM, Gibson HL, and Sproule RA (2002) Recent advances in komatiite volcanology in the Abitibi greenstone belt, Ontario; in Summary of Field Work and Other Activities 2002. Ontario Geological Survey, Open File Report 6100: 7-1 to 7-19.

Houlé MG, Péloquin SA, and Gibson HL (2006) Physical volcanology of komatiite-basalt association in Munro Township, Kidd–Munro assemblage, Ontario portion, Abitibi greenstone belt. In Mueller WU, Daigneault R, Pearson V, Houlé M, Dostal J, and Pilote P (eds), The komatiite-komatiitic basalt-basalt association in oceanic plateaus and calderas: Physical volcanology and textures of subaqueous Archean flow fields in the Abitibi greenstone belt, Geological Association of Canada–Mineralogical Association of Canada Joint Annual Meeting, Montréal 2006, Guidebook to Field Trip A3: 45-61.

Houlé MG, Ayer JA, Baldwin G, Berger BR, Dinel E, Fowler AD, Moulton B, Saumur B-M, and Thurston PC (2008) Field trip guidebook to the stratigraphy and volcanology of supracrustal assemblages hosting base metal and gold mineralization in the Abitibi greenstone belt, Timmins, Ontario. Ontario Geological Survey: Open File Report 6225: 84 p.

Houlé MG, Préfontaine S, Fowler AD, and Gibson HL (2009) Endogenous growth in channelized komatiite lava flows: evidence from spinifex-textured sills at Pyke Hill and Serpentine Mountain, western Abitibi greenstone belt, northeastern Ontario. Canada; Bulletin of Volcanology 71: 881-901.

Houlé MG, Lesher CM, Préfontaine S, Ayer JA, Berger BR, Taranovic V, Davis PC, and Atkinson BT (2010) Stratigraphy and physical volcanology of komatiites and associated Ni-Cu-(PGE) mineralization in the western Abitibi greenstone belt, Timmins area, Ontario: A field trip for the 11th International Platinum Symposium. Ontario Geological Survey, Open File Report 6255: 99 p.

Johnstone RM (1987) Geology of the Stoughton-Roquemaure Group, Beaty and Munro Townships, Northeastern Ontario. Unpublished M.Sc. Thesis, Carleton University, Ottawa, Ontario: 244 p.

Lesher CM (1989) Komatiite-associated nickel sulfide deposits; Reviews in Economic Geology 4: 44-101.

Lesher CM, Goodwin AM, Campbell IH, and Gorton MP (1986) Trace-element geochemistry of ore-associated and barren, felsic metavolcanic rocks in the Superior Province, Canada. Canadian Journal of Earth Sciences 23: 222-237.

MacRae ND (1963) Petrology of the Centre Hill Complex, Northern Ontario. Unpublished M.Sc. Thesis, Hamilton, Canada, McMaster University: 102 p.

MacRae ND (1969) Ultramafic intrusion of the Abitibi area, Ontario. Canadian Journal of Earth Science 6: 281-303.

Oliver JL, Rebagliati CM, and Haslinger RJ (1999) Summary exploration report - Potter Mine property, Munro Township, Ontario for the HDG Potter Exploration Limited Partnership of Hunter Dickinson Group Inc. and Millstream Mines Limited. Unpublished company report, Hunter Dickinson Group Inc.: 1-1 to 11-3.

Péloquin AS, Houlé MG, and Gibson HL (2005) Geology of the Kidd–Munro assemblage in Munro Township, and the Tisdale and Lower Blake River assemblages in Currie Township: Discover Abitibi Initiative. Ontario Geological Survey, Open File Report 6157: 94 p.

Pilote P, Lacoste P, David J, Daigneault R, McNicoll V, and Moorhead J (2015) La region de Val d'Or–Malartic: volcanology et évolution métallogénique. In Pilote P and Préfontaine S (eds), Stratigraphie, volcanologie et évolution métallogénique des régions de Val-d'Or-Malartic (Québec), Kirkland Lake et Timmins (Ontario), sous-province de l'Abitibi, American Geophysical Union-Geological Association of Canada–Mineralogical Association of Canada-Canadian Geophysical Union Joint Meeting, Montréal 2015, Guidebook to Field Trip: 5-28.

Préfontaine S (2003) Origin of spinifex texture in ultramafic sills at Serpentine Mountain and Pyke Hill, Abitibi Ontario; unpublished BSc thesis, University of Ottawa, Ottawa, Canada: 30 p.

Préfontaine S (2013) The definition, distribution and origin of hydrothermal alteration assemblages associated with the Potter volcanogenic massive sulfide deposit, Abitibi Greenstone Belt, Canada. Unpublished MSc thesis, Laurentian University, Sudbury, Canada: 78 p.

Préfontaine S, Gibson HL, Houlé MG, and Mercier-Langevin P (2012) Geochemical data and geological strips logs from the Potter deposit, Munro Township, Abitibi Greenstone Belt, Ontario. Ontario Geological Survey: Miscellaneous Release-Data 289.

Pyke DR, Naldrett AJ, and Eckstrand AP (1973) Archean ultramafic flows in Munro Township, Ontario. Geological Society of America Bulletin 84: 955-978.

Shore M (1996) Cooling and crystallization of komatiite flows; unpublished PhD thesis, University of Ottawa, Ottawa, Ontario: 211 p.

Shore M and Fowler AD (1999) The origin of spinifex texture in komatiites. Nature 397: 691-693.

Tardif NP, Gibson HL, Whitehead RES MacDonald CA, and Gamble APD (2000) Subaqueous firefountaining, hyaloclastite and massive sulfide mineralization. Presentation, Ontario Prospectors Association, Northeastern Ontario Mines and Minerals Symposium, April 18–19, Kirkland Lake, Ontario.

Thériault RD and Fowler AD (1996) Gravity driven and in situ fractional crystallization processes in the Centre Hill Complex, Abitibi Subprovince, Canada: evidence from bilaterally-paired cyclic units. Lithos 39: 41-55.

Chapter 4: (Day 2 – Part II) Duparquet gold camp

Jean Goutier
Ministère de l'Énergie et des Ressources naturelles du Québec

4.1 Introduction and stops

The Duparquet district is located north of Rouyn-Noranda, along the Porcupine-Destor Fault Zone (PDfz). It is the easternmost camp along the PDfz. The largest deposit of this area, Beattie deposit, is associated with large alkaline intrusions that are of Timiskaming age. These intrusions are emplaced in a Timiskaming sedimentary basin that contains large conglomerates (Fig. 4.1). Large blocks of syenite are comprised in the conglomerate. If time allows, a quick stop will be made along the highway to look at the syenites.

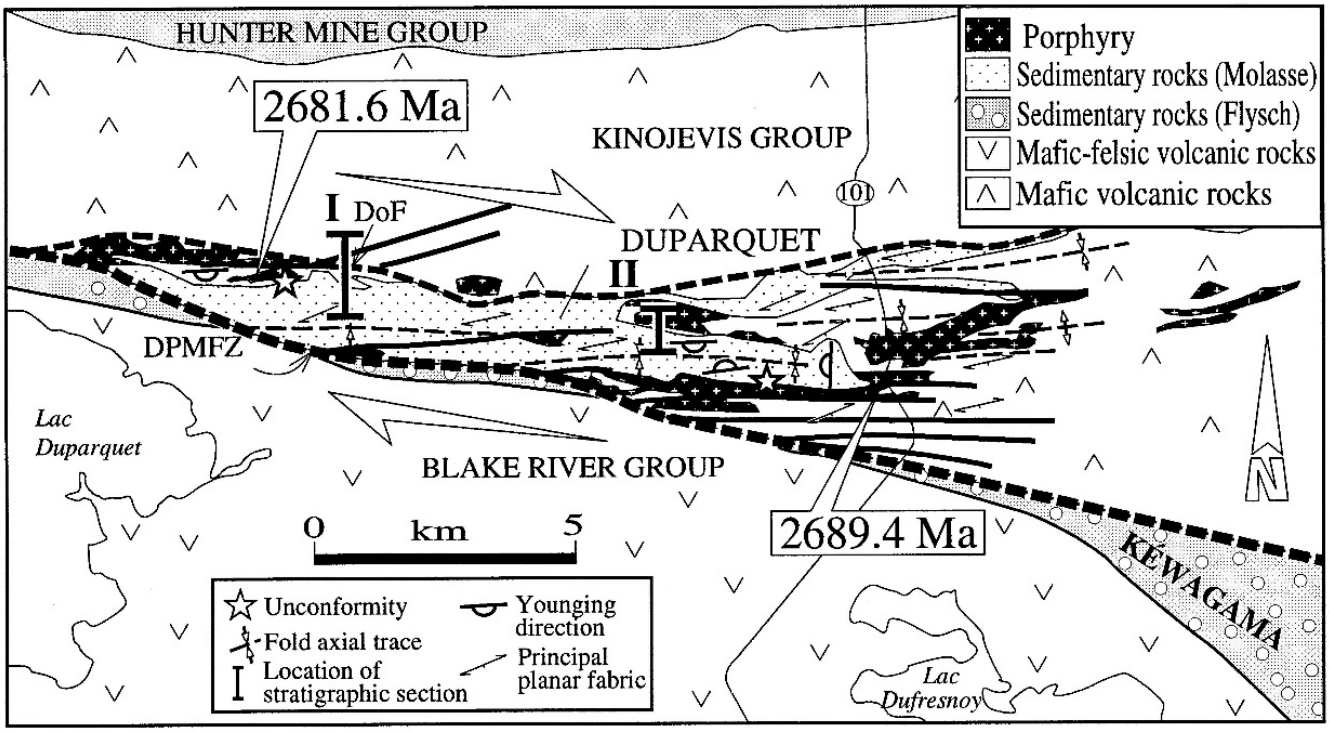

Figure. 4.1. Geological map of the Duparquet area including fault-bounded Duparquet basin and dated porphyry stocks. I and II indicate representative stratigraphic sections in basin. DPMFZ, Destor–Porcupine–Mannerille fault zone; DoF, Douchester fault. From Mueller et al. (1991), and Mueller and Corcoran (1998).

4.2 References

Mueller, WU, Donaldson JA, Dufresne D, Rocheleau M (1991) The Duparquet Formation: sedimentation in a late Archean successor basin, Abitibi greenstone belt, Quebec, Canada. Canadian Journal Earth Sci. 28: 1394-1406

Mueller WU, Corcoran PL (1998) Late-orogenic basins in the Archean Superior Province, Canada: characteristics and inferences. Sedimentary Geology 120: 177-203

Chapitre 5: (Day 3 – Part I) Geology of the Blake River Group

Jean Goutier
Ministère de l'Énergie et des Ressources naturelles du Québec

5.1 Introduction and objectives

The Blake River Group is a unique Archean sequence for numerous reasons including its precious and base metal endowment, its state of preservation, the large number of outcrops, its access, and a wealth of geoscientific studies.

A detailed description of the Blake River Group geology is not be provided here for conciseness. Readers are referred to the Geological Association of Canada-Mineralogical Association of Canada 2011 field trip guidebook by Mercier-Langevin et al. (2011) that is entirely devoted to the Blake River Group and its mineralization. Readers are also referred to McNicoll et al. (2014) paper on the most recent U-Pb ages of the group and the chronological position of the VMS lenses. A digital copy of the 2011 guidebook (which can also be downloaded for free from the Geological Survey of Canada website and the Ministère de l'énergie et des Ressources naturelles du Québec) will be given to the participants.

The Blake River part of the FT-06 field trip will give participants the opportunity to observe some of the principal volcanic facies of the Blake River Group. It will also allow for the examination of typical alteration zones associated with VMS deposits and occurrences plus some exhalative units that are characteristic of the Noranda camp. Most of the description stops come from the various field trip guidebooks to which the author contributed (Péloquin et al. 1995, 1996; Goutier et al. 2009; Goutier et al. 2011; Monecke et al. 2017). Some information was updated such as a table of geochemical analyses of the rocks present at the various stops. Up-to-date maps will also be provided to participants. These last two items will be provided digitally and/or on site.

5.2 Program and stops

Stop 1: Facies variations in basalts from a lava plain

Coordinates
UTM, NAD83, zone 17, 648180 m E, 5343080 m N

Stop description: Outcrops near parc Lapointe, within the city limits of Rouyn-Noranda, expose a succession of submarine mafic lava flows (Fig. 5.1). The strain intensity in this area is very low and the metamorphic grade is relatively low at greenschist facies, allowing for the very good preservation of typical subaqueous mafic-intermediate flows. A lava plain setting has been proposed by Dimroth et al. (1982) to explain the nature and architecture of such widespread tholeiitic lava flows near the stratigraphic base of the Blake River Group (Rouyn-Pelletier and Hébécourt formations). These outcrops, and other outcrops scattered elsewhere in the region, allowed Dimroth et al. (1976, 1978) to develop facies models for mafic subaqueous lavas, in which massive lavas grade laterally or vertically into pillowed flows and then fragmental facies such as pillow breccias and hyaloclastite (Fig. 5.1). The flows near parc Lapointe are oriented WNW and dip steeply to the NNE. Gabbroic sills invade the volcanic sequence and can be difficult to differentiate from massive lavas.

Geochemical analyses from this outcrop indicate same composition for pillowed flow, massive flow, and gabbroic sill (Appendix 1 – digital supplement). The trace element ratios indicate a tholeiitic affinity on both the Barrett and MacLean (1999) and Ross and Bédard (2009) discrimination diagrams.

Stop 2: Outcrops at the West Zone

Coordinates
UTM, NAD83, zone 17, 646475 m E, 5346275 m N

Stop description: The West Zone outcrop (formely Remnor "West Zone") represents a well preserved felsic sequence, located in the footwall of the Horne deposit, according to Kerr and Gibson (1993). The outcrop is located approximately 1 km to the west of the central Horne deposits and represents the best exposed lower section of the Horne stratigraphy (Monecke et al. 2008).

These outcrops were stripped in 1987 by Remnor to better understand the stratigraphy of the Horne sequence and the West Zone 165,000 t at 4.53 g/t Au and New Zone 98,500 t at 5.1 g/t Au (unpublished). A very detailed surface mapping (see Fig. 24 in Mercier-Langevin et al. 2011) was carried out by Monecke et al. (2008) and Monecke and Gibson (2013), while the drilling study was carried out by Laurin (2010). Many of the outcrops were sandblasted in 2008 as part of the GSC TGI-3 project and MERN Plan Cuivre. The objective was to remove the alteration crust associated with the oxidation of sulfides and better see the volcanic structures (Fig. 5.2). The oxidation process is quite rapid as these sandblasted areas are already heavily stained and some textures are getting more difficult to see. During the summer of 2017, part of the SE sector was also modified (e.g. fence was removed, land was backfilled).

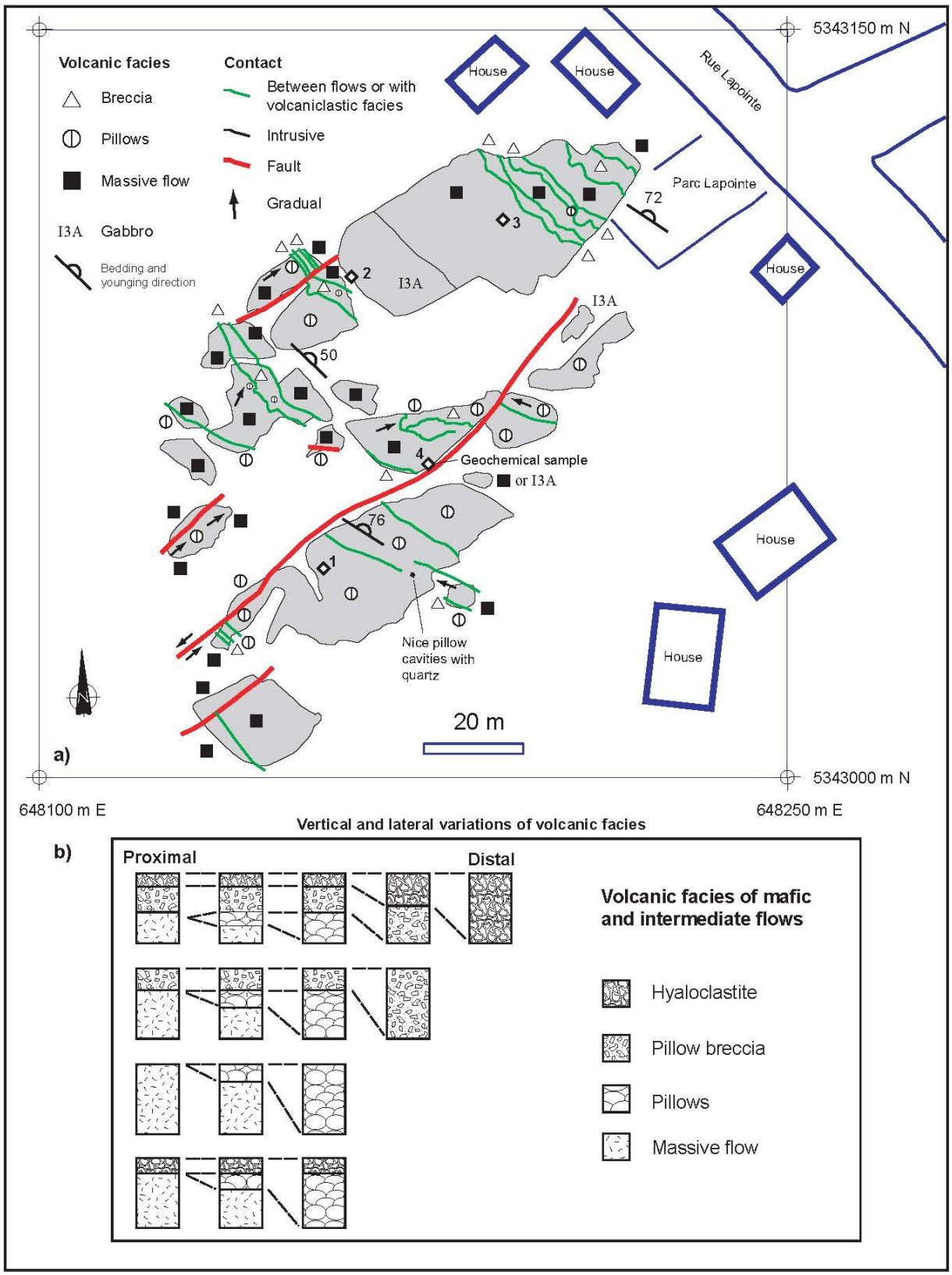

Figure 5.1. a Map of volcanic facies variations in tholeiitic basalts SW of parc lapointe in Rouyn-Noranda (stop 1). Map grid is UTM nad 83 zone 17. **b** Schematic facies variations likely to be encountered in mafic to intermediate lava flows. After Dimroth et al. (1976, 1978).

The lower portion of the West Zone succession is composed of a proximal facies association comprising aphyric rhyolite flow and associated juvenile volcaniclastic rocks that formed by autobrecciation and quench fragmentation (Monecke et al. 2008). The alteration of this rhyolite is materialized by the presence of sericite, epidote, chlorite, pyrite, carbonate, and numerous fine manganese garnets (porphyroblasts). To the east, siliceous, chloritic, and pyritic alterations increase. This rhyolite has a transitional affinity (Appendix 1 – digital supplement). According to the diagram of Hart et al. (2004), it is located at the transition between the rhyolites of FII and FIIIa types. This unit provided zircons that gave an age of 2702.2 ±0.9 Ma (McNicoll et al. 2014) for the base of the Horne sequence. This dating, and dating of the rocks hosting the nearby Quemont deposit are important because they indicate that these Au-rich VMS systems formed in the lower part of the Blake River. The rhyolitic flow is overlain by voluminous, coarse volcaniclastic deposits. In this part of the sequence, the beds are thick and weakly graded bedded.

Figure 5.2. a Stop 2. West Zone. Industrial technique of sandblasting with magnetite.

Figure 5.2. b. Example of a part of outcrop cleaned on the left and of a part not cleaned on the right.

The upper portion of the exposed West Zone succession is dominated by a large rhyolite unit that shows a distinct flow banding. Columnar jointing is locally well developed. The rhyolite unit is typified by a core zone that contains abundant mafic xenoliths. The xenoliths range from 1-2 cm to 1.5 m in size (Oseguera 2014). Contacts between the xenoliths and the enclosing rhyolite are sharp but range from straight to irregular and scalloped. Flow banding within the host unit typically envelop the xenoliths. The contact relationships between the mafic xenoliths and the rhyolite suggest a reaction zone between consolidated mafic clasts and felsic magma. A coarser grain size and the presence of zinc-bearing mineralization (1.5 % Zn, Appendix 1 – digital supplement) in the mafic clasts support this interpretation.

The upper contact between the rhyolite and the enclosing volcaniclastic facies is sharp. However, logging of historic drill core shows that the stratigraphic position of the upper rhyolite contact varies along strike and down dip, implying that the margin of the rhyolite unit was at least locally intrusive. Additional constraints are provided by the occurrence of two large (150 x 100 cm and 65 x 33 cm, respectively) xenolith-bearing rhyolite clasts in the volcaniclastic facies that overlies the rhyolite, as observed in outcrop. Incorporation of rhyolite clasts into the volcaniclastic deposits provides evidence that the rhyolite locally emerged at the paleoseafloor. The rhyolite may have breached the seafloor during emplacement or, alternatively, it became exposed during synvolcanic faulting or broken during the volcanic explosion.

The final unit of volcaniclastic rocks occurs stratigraphically above the rhyolite in the northern portion of the West Zone outcrop. The summit of these outcrops exposes a superb felsic volcaniclastic sequence. Unlike the volcanoclastites of the central part, the beds are thin, well graded and have erosional channels. The center of the outcrop is characterized by a fine sequence with parallel lamination, grading to cross-lamination. The light burgundy color of these rocks is associated with the abundance of very fine manganese garnets (same composition of garnet in rhyolite, Appendix 1 – digital supplement). The block present in this sequence is interpreted as a product of ballistic fallout.

The last part of the outcrop is marked by a drastic change in particle size and composition with irregular clasts of VMS (Fig. 5.3). There is a 2.6 m thick, graded bed with planar laminated on the top. The base contains numerous fragments of massive pyritic sulfides, some of which are nearly 30 cm in diameter. A geochemical analysis of one of these fragments indicates very low levels of Cu, Zn, and Ag but an anomalous content of 699 ppm Au (P. Mercier-Langevin, unpublished data: Appendix 1 – digital supplement).

This volcanic sequence is cut by three mafic dikes. This type of dikes is very common in the area and becomes very dense across the main mineralized zones of Horne.

Stop 3: Dufresnoy gabbro

Coordinates

UTM, NAD83, zone 17, 644544 m E, 5351905 m N

Stop description: One of the characteristics of the Blake River Group is the abundance of mafic and intermediate intrusions (dikes and sills) of decametric to kilometric thickness. Originally, these rocks were described as quartz diorites because the majority of pyroxenes were replaced by amphibolites, and quartz was frequently noted. The geochemical composition of these rocks, however, indicates that they are mainly metagabbros (Kuiper 2010, Appendix 1 – digital supplement). In addition, several of these intrusions have a similar age of 2698 Ma (McNicoll et al. 2014).

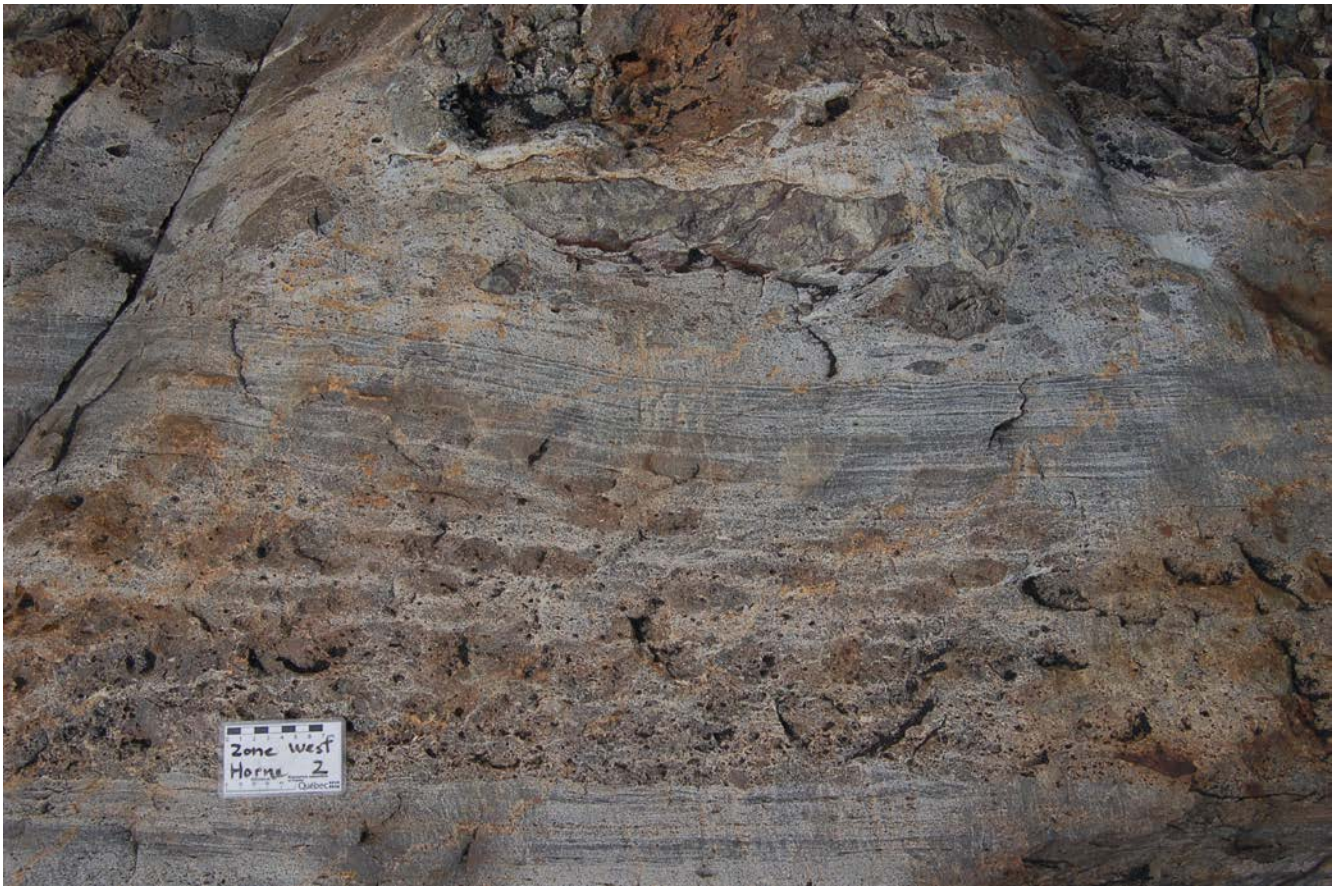

Figure 5.3. Stop 2. West Zone. Example of the volcanoclastite bed containing irregularly shaped of VMS fragments in the northern outcrop of the West Zone. The photo was taken in 2008, just after the industrial sandblasting.

The Dufresnoy gabbro is one of these intrusions. It has a thickness of several hundred metres. It is oriented NNW-SSE and dips moderately (50º) to the NNE (Fig. 5.4). The gabbro cuts the host sequence of the northern and southern central camp VMS deposits. This stop is a U-Pb sampling site. The dated sample gave an age of 2697.9 ±0.8 Ma (McNicoll et al. 2014), which is similar to the age obtained for the Lac Turcotte dacite (2698.3 +1.2/–1.0 Ma, David et al. 2010) of the central camp. This age is similar to the upper member of the Bousquet Formation and indicates simultaneous graben-filling (Noranda formation) and calc-alkaline volcanism (Bousquet Formation). The age and setting of the Dufresnoy gabbro is therefore important in constraining the age of the central camp VMS deposits. The exposed gabbro at stop 3 is medium to coarse-grained with decimetre-scale pegmatitic sections (Fig. 5.5). These sections contain more Zr content (211 ppm, Appendix 1 – digital supplement) compare to medium and coarse-grained sections (44.9 to 84 ppm Zr, Appendix 1 – digital supplement). This outcrop presents textures that are similar to those observed in gabbros of same age of the Rouyn-Noranda area (Kuiper 2010; McNicoll et al. 2014).

In front of this outcrop, the view exposes a perpendicular section through the sequence containing the VMS deposits of the northern part of the Mines sequence. The sequence is composed at the base of the Waite Rhyolite, followed by the mineralized level containing the VMS deposits of Old Waite, Vauze, East Waite, and Norbec (Lake Dufault) and covered by the Amulet mafic flows. This level is an exhalative horizon correlates with the “Main Contact”. It consists of finely laminated tuff and chert, with varying amounts of sulfides. Its thickness varies between a few centimetres and 5 metres near the Norbec VMS deposit (Cattalani et al. 1993).

Gabbroic injections, like that of Dufresnoy, cut and

raised the sequence, giving an appearance of inverse fault motion. It would be a relative movement associated with injections and a volcanic piston phenomenon (Fig. 5.6).

Stop 4: Metamorphosed synvolcanic alteration zones, Amulet A

Coordinates
UTM, NAD83, zone 17, 643271 m E, 5352143 m N

Stop description: The southern central camp contains several VMS deposits at the same stratigraphic position (Fig. 5.4), correlated in part with northern central camp VMS deposits. The Amulet A deposit is one of the typical examples of Noranda-type VMS mineralization. This deposit shows a stacking of several lenses between andesite and basaltic andesite flows (see figure 10 in Price 1953). This slightly differs from the northern central camp where deposits are rather hosted in a felsic-andesitic sequence. Mineralized levels are marked by more or less extensive exhalites that extend over several kilometers. The Amulet Upper A orebody was discovered in 1927 and Lower A orebody subsequently found in 1938 while testing for further massive sulfide mineralization in the alteration pipe below the Upper A orebody. The size of the deposits in this sector contrasts with those of Horne and the DBL camp that are much larger (Table 1.1).

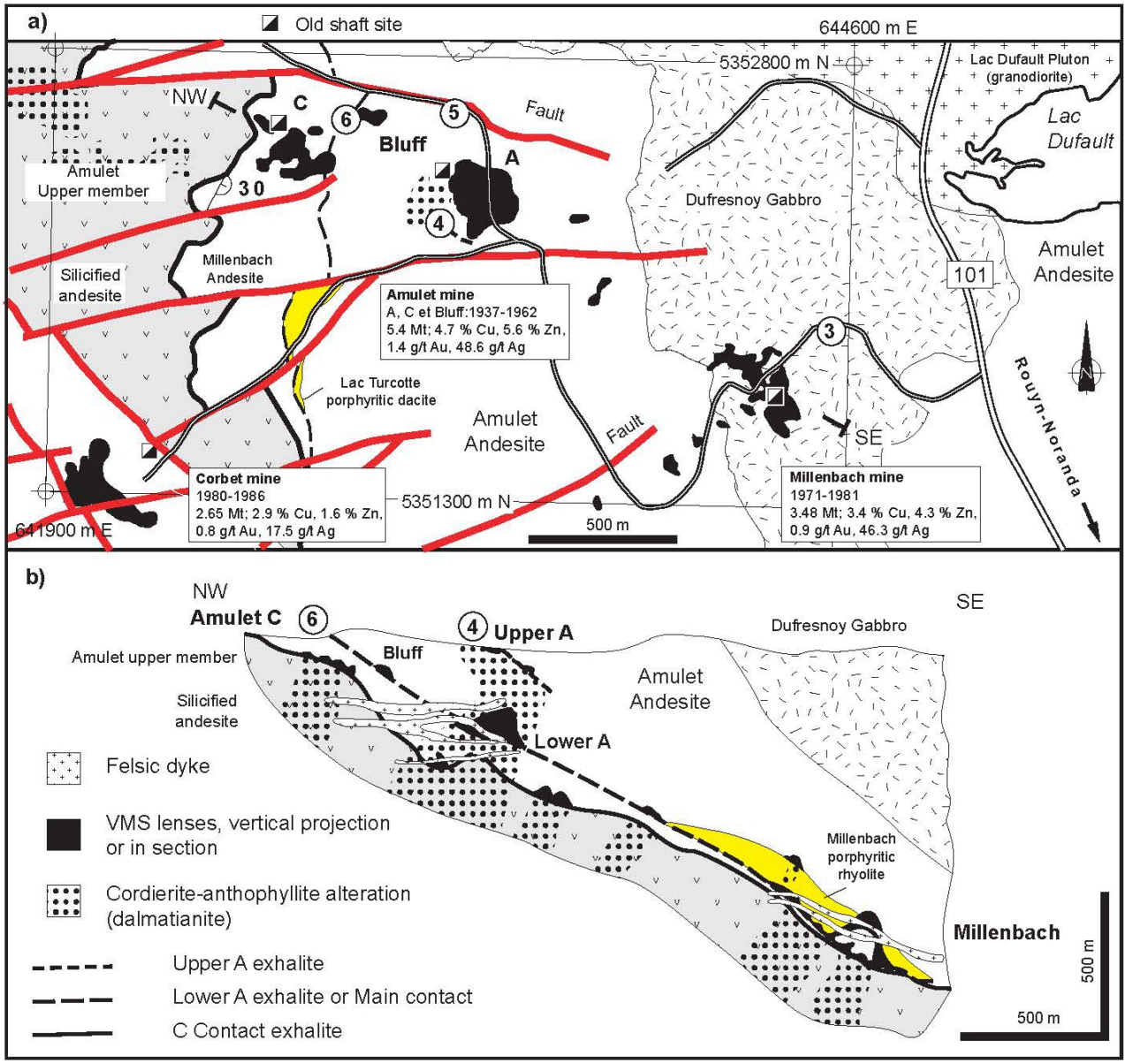

Figure 5.4. Stops 3 to 6. **a** Geological map of the southern central camp showing the location of the former Amulet, Millenbach, and Corbet mines, and the position of stops 3 to 6. **b** Geological section showing the location of the VMS lenses of the Amulet-Millenbach cluster along two distinct exhalative units that join near the Millenbach deposit. Most of the hydrothermal alteration is found in the footwall sequence. These alteration zones consist of porphyroblastic chlorite, anthophyllite, and cordierite ("dalmatianite") due to contact

metamorphism around the Lac Dufault Pluton. Modified from Knuckey et al. (1982), Gibson (1989), Bertrand (1990), and Péloquin et al. (1995, 1996).

The strata of this region are N-S oriented with an average dip of 30º. The alteration surrounding the Amulet orebodies is distinctive because of the effect of an amphibolite facies contact metamorphism aureole around the Lac Dufault pluton (granodiorite, 2690 +2.2/2.0 Ma, Mortensen 1993). Typical alteration zones (sericite-chlorite) of VMS deposits were transformed into high-temperature metamorphic assemblages (now partly retrograded to greenschist conditions).

Figure 5.5. Stop 3. Pegmatitic pods in the Dufresnoy Gabbro. These pods are richer in Zr and have been sampled for the U-Pb dating of the gabbro.

Three types of assemblages were recognized during mine operation, from proximal to distal (Price 1953): cordierite-anthophyllite rosette-type, high chlorite-cordierite type, and biotite-cordierite-sericite type. The spotted texture of the volcanic alteration is referred to as "dalmatianite" or "spotted dog" due to the mottled texture of ovoid porphyroblasts of cordierite, highlighted by weathering (de Rosen-Spence 1969). The degree of preservation of the cordierite varies greatly from fresh to completely retrograded. Below VMS lenses, cordierite-anthophyllite rosette-type assemblage also contains, locally, andradite, hedenbergite, and ilvaïte (de Rosen-Spence 1969).

Points to note at this stop are:

1) Near the glory hole there is an excellent view of the Horne smelter to the south. The low depression occupied by lac Dufault to the east marks the position of the Lac Dufault Pluton.
2) Well developped dalmatianite is present around the glory hole and pillowed margins can be recognized through the heavy cordierite spotting. Quartz and pyrite are present in pillow selvage.
3) The presence of felsic dikes crosscutting the andesitic sequence. The abundance of felsic and intermediate dykes is an exploration criterion that reflects proximity to volcanic vents.
4) An exhalite tuff found on strike from the Upper A Amulet orebody is exposed in the trench along the Corbet mine road.
5) On the other side of the road, there is the disappearance of the dalmatianite texture and a change of alteration characterized by spots of quartz, epidote with very few sulfides.

Stop 5: Columnar jointing in lava of the Amulet Andesite

Coordinates
UTM, NAD83, zone 17, 643229 m E, 5352635 m N

Stop description: The southern outcrop represents an excellent exposure of columnar jointing in a thick, basaltic andesite flow belonging to the Amulet Andesite.

Stop 6: Exhalite of the Bluff area

Coordinates
UTM, NAD83, zone 17, 642886 m E, 5352578 m N

Stop description: Several exhalites (Ridler, 1971) are known from the southern central camp, located in between andesitic-andesitic sequence or felsic-andesitic sequence (Fig. 5.4B). These marker horizons contain chert, sulfides, and volcanoclastic components (Kalogeropoulos and Scott 1989; Appendix 1 – digital supplement), and have been used extensively and successfully for VMS exploration in the central camp. Stop 6 exposes the Lower A (Amulet) exhalite also known as the "Main Contact" or the "Mine Contact". The exhalite is 15 to 35 centimetres thick and drapes over megapillows from the Millenbach andesite.

Stop 7: Moosehead massive sulfide showing

Coordinates
UTM, NAD83, zone 17, 642048 m E, 5352801 m N

Stop description: The Moosehead showing represents a small massive sulfide lens. Although uneconomic, all key relationships of the VMS deposits of the Noranda Main camp are present at this location: footwall alteration, exhalite, VMS lens, weakly-altered hanging-wall rock, or cap rock, and different dikes. The massive sulfide lens occurs at the contact between the Amulet Upper member and the Millenbach Andesite, which is marked by the C Contact Tuff (see figure 10 in Watkinson 1990). At Moosehead, the volcanic footwall shows clear dalmatianite spotting in which the cordierite porphyroblasts are retrograded to biotite, pinnite, and chlorite. Close to the main outcrop, footwall pillowed lava is strongly altered with pyrite stringers and clusters. The visible decimetric VMS lenses (sphalerite, pyrite, chalcopyrite, and magnetite) are present at the base of the northern part of the main outcrop. Many rock samples of VMS are present in the plane portion of the sector. Very small portions of the exhalite level (chert and pyrite) are visible in the eastward extension of the VMS lens. The exhalite has an

average dip of 30° towards the south. This level is capped and probably cut by a massive flow of Millenbach Andesite. A pillowed portion of this flow is present just over the VMS lens and on the top of the outcrop, in the NE portion. The alteration of this flow is characterized by millimetric to centimetric clusters of epidote and quartz, but also by the presence of fine biotite grains in the groundmass, visible in thin sections (ex. 1.13% K_2O, Appendix 1 – digital supplement). This Millenbach Andesite is cut by three types of dikes: mafic, intermediate, and felsic. The mafic and felsic dikes cut Millenbach Andesite, while the intermediate dike cuts all. The felsic dike is feldspar- phyric and clearly more magnetic than the surrounding andesite. We used a susceptibility meter to trace the new contacts between the felsic dike and the andesite (Goutier, unpublished map, 2017). The abrupt variations of magnetic susceptibility and the sharp contacts do not indicate a magma mingling (T. Smith hypothesis on his map - see figure 10 in Watkinson 1990 - and reported by Monecke et al. 2017), but rather a clear intrusive contact.

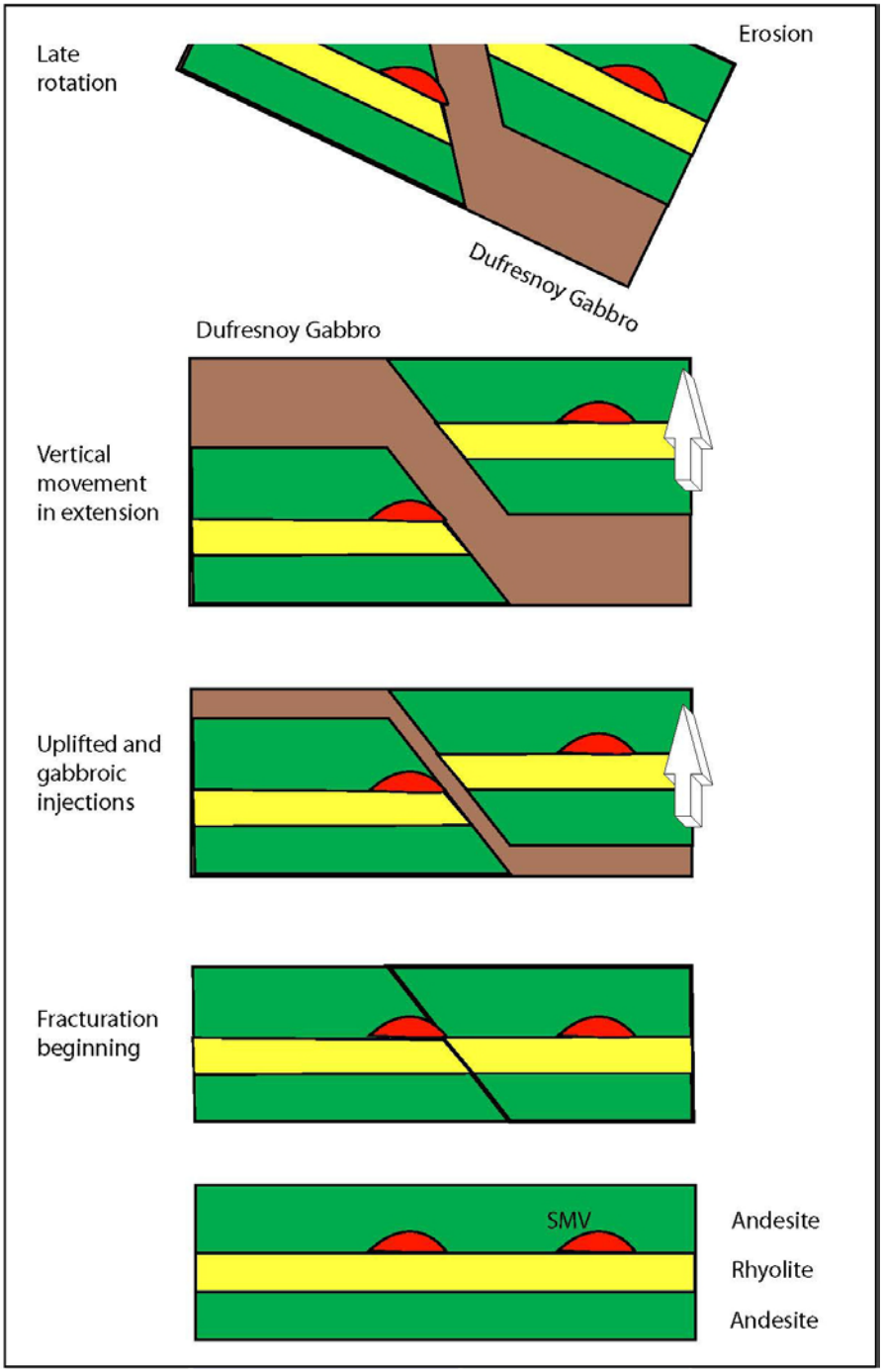

Figure 5.6. Diagram illustrating an injection of major gabbroic intrusions and the uplift of volcanic sequences in a caldera, giving an

appearance of inverse apparent motion. The subsequent rotation of the strata shows the current dip that can be seen from stop 3

5.3 References

Barrett TJ, MacLean WH (1999) Volcanic sequences, lithogeochemistry, and hydrothermal alteration in some bimodal volcanic-associated massive sulphide systems, *In* Barrie CT, Hannington MD (eds), Volcanic-associated massive sulphide deposits: processes and examples in modern and ancient settings: Reviews in Economic Geology 8: 101-131.

Bertrand, P (1990) Central Mine Sequence Stratigraphy Field Trip: *In* Sullivan JR, Côté R, Bertrand P, Chartrand F, Gaulin R, Lacroix S, Racicot D (eds), The Northwestern Quebec Polymetallic Belt: Excursion Guidebook, Rouyn-Noranda: The Canadian Institute of Mining and Metallurgy: 27-35.

Cattalani S, Barrett TJ, MacLean WH, Hoy L, Hubert C, Fox JS (1993) Métallogénèse des gisements Horne et Quemont (région de Rouyn-Noranda): Ministère des Ressources naturelles: Report ET 90-07, 121 p.

David J, Vaillancourt D, Bandyayera D, Simard M, Dion C, Goutier J, Dion C, Barbe P (2010) Datations U-Pb effectuées dans les sous-provinces d'Ashuanipi, de La Grande, d'Opinaca et d'Abitibi en 2008−2009: Ministère des Ressources naturelles et de la Faune, Québec: Report RP 2010-11: 37 p.

de Rosen-Spence A (1969) Genèse des roches à cordierite-anthophyllite des gisements cupro-zincifères de la région de Rouyn-Noranda, Québec, Canada: CJES 6: 1339-1345.

Dimroth E, Larouche C, Trudel P (1976) Fifth progress report on volcanological and sedimentological work in Rouyn-Noranda area: Ministère des Richesses naturelles: report DP-500: 38 p., 1 map.

Dimroth E, Cousineau P, Leduc M, Sanschagrin Y (1978) Structure and organisation of Archean subaqueous basalt flows, Rouyn-Noranda area, Quebec, Canada: CJES 15: 902-918.

Dimroth E, Imreh L, Rocheleau M, Goulet N (1982) Evolution of the south-central part of the Archean Abitibi belt, Quebec. Part I: stratigraphy and paleogeographic model: CJES 19: 1729-1758.

Gibson HL (1989) The Mine sequence of the Central Noranda Volcanic Complex: geology, alteration, massive sulphide deposits and volcanological reconstruction: Ph.D thesis: Carleton University, Ottawa, Canada: 800.

Goutier J, McNicoll V, Dion C, Ross PS, Mercier-Langevin P (2009) Portrait des grandes unités du Groupe de Blake River et leur relation avec les sulfures massifs volcanogènes: Congrès Abitibi 2009 – Abitibi Cuivre, Rouyn-Noranda, September 28th, 2009, Excursion Guidebook: Ministère des Ressources naturelles et de la Faune, Québec, report MB 2009-10 (GM 64196): 9-28.

Goutier J, Ross PS, McNicoll V, Dion C, Mercier-Langevin P, Thurston P, Dubé B, Gibson H (2011) Day 1: Geology, stratigraphy and geochronology of the Blake River Group and relationships with VMS deposits: *In* Mercier-Langevin P, Goutier J, Ross PS, McNicoll V, Monecke T, Dion C, Dubé B, Thurston P, Bécu V, Gibson H, Hannington M, Galley A (eds), The Blake River Group of the Abitibi greentsone belt and its unique VMS and gold-rich VMS endowment: GAC–MAC–SEG–SGA Joint Annual Meeting, Ottawa 2011: Guidebook to Field Trip 2B: Geological Survey of Canada, Open File 6869: 10-21.

Hart TR, Gibson HL, Lesher CM (2004) Trace element geochemistry and petrogenesis of felsic volcanic rocks associated with volcanogenic massive Cu-Zn-Pb sulfide deposits: Econ Geol 99: 1003–1013.

Kalogeropoulos SI, Scott SD (1989) Mineralogy and geochemistry of an Archean tuffaceous exhalite: the Main Contact Tuff, Millenbach mine area, Noranda, Quebec: CJES 26: 88-105.

Kerr DJ, Gibson HL (1993) A comparison of the Horne volcanogenic massive sulfide deposit and intracauldron deposits of the Mine Sequence, Noranda, Quebec: Econ Geol 88: 1419-1442.

Knuckey MJ, Comba CDA, Riverin G (1982) Structure, metal zoning and alteration at the Millenbach deposit, Noranda, Quebec: *in* Hutchinson RW, Spence CD, Franklin JM (eds), Precambrian sulphide deposits: Geological Association of Canada Special Paper 25: 255-295.

Kuiper D (2010) Geology, geochemistry and geochronology of the Dufault, Séguin, and Horseshoe gabbroic-dioritic intrusions, Blake River Group (2704-2695 Ma), Abitibi Subprovince, Québec: Master thesis, Laurentian University, Sudbury, Canada: 130 p.

Laurin J (2010) Geology, gold mineralization and alteration of the Horne West property Rouyn-Noranda: Master thesis, University of Ottawa, Ottawa, Canada: 161 p.

McNicoll V, Goutier J, Dubé B, Mercier-Langevin P, Ross PS, Dion C, Monecke T, Legault M, Percival J, Gibson H (2014) U–Pb geochronology of the BlakeRiver Group, Abitibi Greenstone Belt, Québec, and implications for base metal exploration: Econ Geol 109: 27-59.

Mercier-Langevin P, Goutier J, Ross PS, McNicoll V, Monecke T, Dion C, Dubé B, Thurston P, Bécu V, Gibson H, Hannington M, Galley A (2011) The Blake River Group of the Abitibi greentsone belt and its unique VMS and gold-rich VMS endowment: GAC–MAC–SEG–SGA Joint Annual Meeting, Ottawa 2011: Guidebook to Field Trip 2B: Geological Survey of Canada, Open File 6869: 61 p. doi:10.495/288757.

Monecke T, Gibson HL (2013) Surface geology of the giant Horne volcanic-hosted massive sulphide deposit, Rouyn-Noranda, Quebec: Geological Survey of Canada, Open File 4712: 5 p., 6 sheets, doi:10.4095/292870.

Monecke T, Gibson H, and Goutier J (2017) Massive sulfide deposits of the Noranda camp: Reviews in Economic Geology, v. 19, in press.

Monecke T, Gibson H, Dubé B, Laurin J, Hannington MD, Martin (2008) Geology and volcanic setting of the Horne deposit, Rouyn-Noranda, Quebec: initial results of a new research project: Geological Survey of Canada, Current Research 2008-9: 16 p.

Mortensen JK (1993) U-Pb geochronology of the eastern Abitibi Subprovince. Part 2: Noranda – Kirkland Lake area: CJES 30: 29-41.

Oseguera O (2014) The significance of magma mingling and mixing during the formation of the host-rock sucessions of Archean massive sulfide deposits in the Noranda camp: Master thesis, Colorado School of Mines, Golden, USA: 117 p.

Péloquin AS, Verpaelst P, Goutier J (1995) Blake River volcanism: *In* Couture JF, Goutier J (eds), Metallogeny and Tectonic Evolution of the Rouyn-Noranda Region: ICM Section Rouyn-Noranda, Field Trip Guidebook: 23-32.

Péloquin AS, Verpaelst P, Goutier J (1996) Le volcanisme du Groupe de Blake River: *In* Couture JF, Goutier J (eds), Métallogénie et évolution tectonique de la région de Rouyn-Noranda: Ministère des Ressources naturelles, Québec: report MB 96-06: 23-32.

Price P (1953) Waite Amulet mines Ltd: *In* Price, P (chairman), Geology and Mineral Deposits of Northwestern Quebec: GSA-GAC: guide book for field trip No. 10: 18-20, maps 8-10.

Ridler RH (1971) Analysis of archean volcanic basins in the Canadian Shield using the exhalite concept: Can Inst Min Met Bull 64 (abstract): 20.

Ross PS, Bédard JH (2009) Magmatic affinity of modern and ancient subalkaline volcanic rocks determined from trace-element discriminant diagrams: CJES 46: 823-839.

Watkinson DH (1990) Mineral deposits of Noranda, Quebec and Ontario [field trip 4]: IAGOD – Geological Survey of Canada: Open file 2189: 52 p.

Chapitre 6: (Day 3 – Part II) The Horne 5 deposit

Alexandre Krushnisky
Institut national de la Recherche scientifique – Centre Eau Terre Environnement

Patrick Mercier-Langevin
Natural Resources Canada – Geological Survey of Canada

Pierre-Simon Ross
Institut national de la Recherche scientifique – Centre Eau Terre Environnement

Jean Goutier
Ministère de l'Énergie et des Ressources naturelles du Québec

Claude Pilote
Falco Resources inc.

Claude Bernier
Falco Resources inc.

Lyndsay Moore
McGill University

6.1 History and geological context of the Horne deposit

The discovery of the Horne deposit in 1923 was a critical step in the development of the Abitibi, which would quickly establish itself as one of the world's most productive mining regions (Gibson et al. 2000). During its production history, from 1927 to 1976, the Horne mine yielded a total of 53.7 Mt of ore at 6.06 g/t Au (327.6 t, or 11.6 Moz Au), 2.22% Cu, and 13.0 g/t Ag, extracted largely from the giant Upper H and Lower H orebodies by Noranda Mines Ltd. (Kerr and Mason 1990; Mercier-Langevin et al. 2011a). The Horne deposit thus represents the largest gold-rich volcanogenic massive sulfide (VMS) deposit in the world (Poulsen and Hannington 1996; Dubé et al. 2007; Mercier-Langevin et al. 2011b; Fig. 1.5).

The Horne 5 deposit (often termed "No. 5 zone") is a sheet-like sulfide body that is located downdip, but stratigraphically above, the H orebodies (Kerr and Mason 1990). It was extensively drilled by Noranda Mines Ltd. and was only superficially exploited during the life of the Horne mine. Ongoing drilling by Falco Resources Ltd. has allowed the company to define a new resource for the Horne 5 deposit (including measured, indicated, and inferred resources) that amounts to 113.4 Mt at 1.54 g/t Au (174.9 t, or 5.63 Moz Au; Falco Resources, press release, October 2016), with significant Ag, Cu, and Zn as by-products.

The Horne deposit is located in the Blake River Group (BRG) along the southern portion of the Noranda camp (Fig. 6.1). The deposit extends from the surface to a depth of more than 2500 meters within the Horne Block, an east-west trending structural block wedged between the Horne Creek and Andesite faults (Cattalani et al. 1993). A steeply dipping, north-facing sequence of dominantly coherent felsic volcanic rocks, interpreted as submarine lava flows and/or domes, and related autoclastic breccias and redeposited volcaniclastic units comprises the host rocks to the Horne deposit (Price 1934; Kerr and Mason 1990; Monecke et al. 2008). A swarm of mafic to intermediate dikes is also present and becomes more prevalent at shallower depths with many of these dikes cross-cutting the host succession. Recent U-Pb dating of a coherent rhyolite at the base of the felsic sequence (2702.2 ± 0.9 Ma; McNicoll et al. 2014) indicates that the rocks in the block are amongst the oldest in the BRG and pre-date the Noranda "central mine sequence" and its archetypal Cu-Zn VMS deposits by approximately four million years (McNicoll et al. 2014). Most of the felsic rocks contained in the Horne Block are affected by pervasive sericitization, and possible silicification, consistent with relatively low-temperature, diffuse hydrothermal discharge (MacLean and Hoy 1991). Evidence for higher temperature, more focused hydrothermal fluid flow typically associated with Cu-Au mineralization is seen in the discordant zones of Fe-chlorite alteration that cross-cut pervasive sericite ± quartz alteration in the Upper and Lower H zones. Deformation of the Horne Block is of variable intensity, but moderate to strong in general, the entire succession being tilted and somewhat rotated relative to the bounding successions (Price 1948; Poulsen et al. 2000).

Important differences distinguish the Horne 5 deposit from the Upper and Lower H zones, such as: 1) mineralization within the Horne 5 deposit and the average low gold grades differ significantly from the larger, more gold-rich (6.06 g/t) massive sulfide bodies of the H zones; 2) the pyrite-rich Horne 5 deposit contains only minor chalcopyrite and very rare pyrrhotite, which is in contrast with the pyrite-pyrrhotite-chalcopyrite assemblage of the H

zones (Price 1934); and 3) the mostly sub-microscopic ("invisible'') gold occurrence in the Horne 5 deposit is unlike the visible to microscopic native gold and Au-tellurides in the Upper and Lower H massive sulfides and their associated chlorite-rich veinlets (Price 1934).

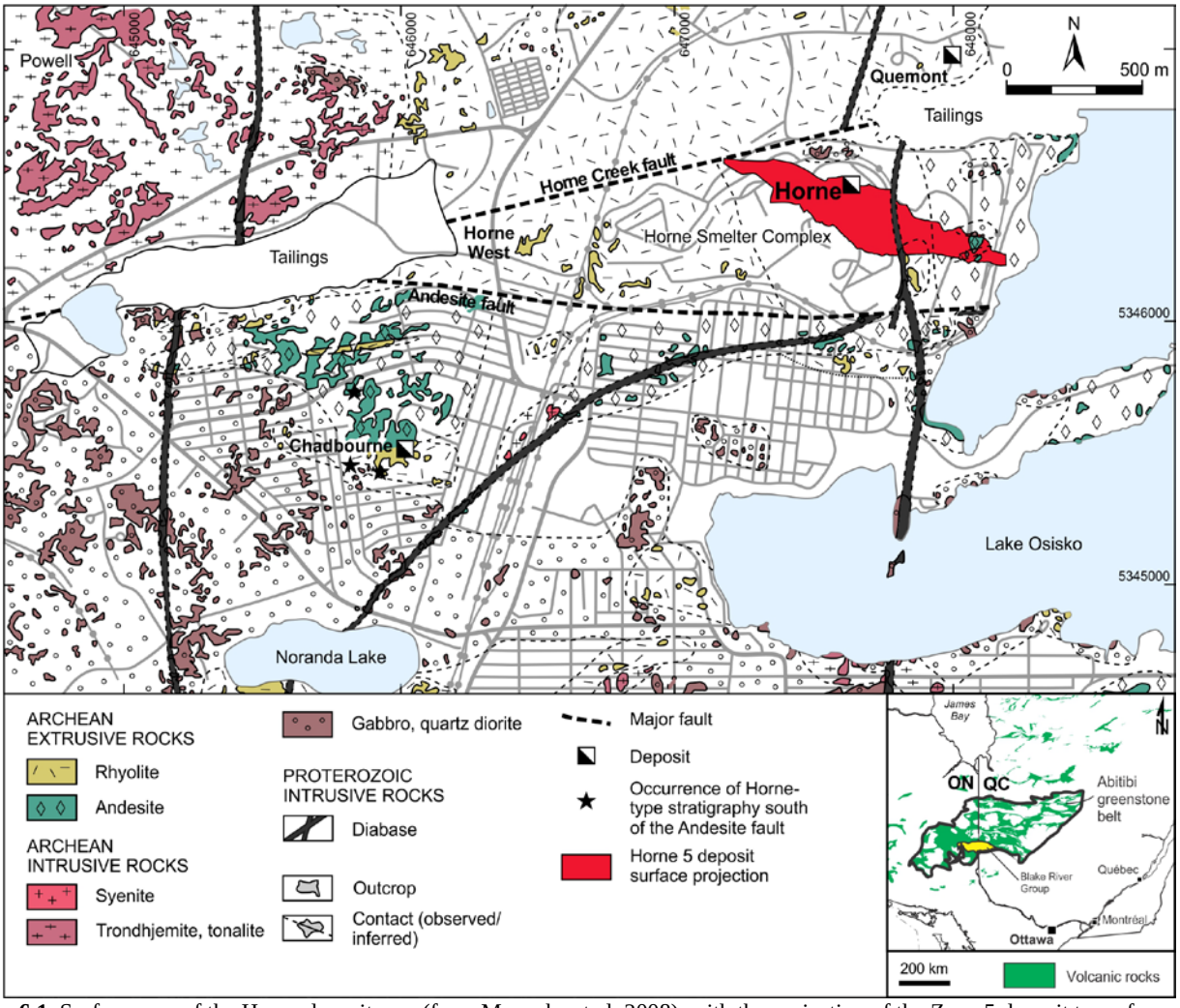

Figure 6.1. Surface map of the Horne deposit area (from Monecke et al. 2008), with the projection of the Zone 5 deposit to surface.

Initial studies at the Horne deposit identified and documented the host lithologies and provided detailed descriptions of the mineralized zones (Cooke et al. 1931; Price 1934; Suffel 1935). An epigenetic model for the mineralization was favored by these authors, with sulfides and gold being emplaced after the late diabase dikes. More recent studies (e.g., Kerr and Mason 1990; Barrett et al. 1991; Cattalani et al. 1993; Kerr and Gibson 1993), in addition to the work by Sinclair (1970) on the Horne 5 deposit, helped demonstrate the synvolcanic origin for the mineralization. According to these authors, the host volcaniclastic units were deposited within what has been interpreted as a synvolcanic fault-bounded "graben" structure on the flanks of a submarine felsic edifice. Mineralization formed by infiltration of primary pore space and by sub-seafloor replacement of permeable host fragmental rocks. Entrapment of fluids and metals under the seafloor likely contributed to the important size of the deposit, isolating fluids from dilution in seawater and favoring zone refining processes. However, the presence of massive sulfide clasts within the Horne 5 deposit (Sinclair 1970), as well as in the Horne West zone (Monecke et al. 2008; Laurin 2010), suggests that at least some massive sulfide lenses were formed at the seafloor or near-seafloor interface. Differences in the style of mineralization and the metal content between the Upper and Lower H zones and the Horne 5 deposit can be attributed to their position on the volcanic edifice. The large, Au- and Cu-rich H orebodies formed proximal to the vent area, where high-temperature hydrothermal discharge would have been favored, whereas the Horne 5 deposit formed more distally from a lower-temperature hydrothermal system (Taylor et al. 2014). Much more information about the VMS deposits of the Noranda camp can be found in Monecke et al (2017,

in press) given in Supplement D.

6.2 Program for the visit

We will stop at Falco Resource's Noranda core facility. We will first have a short introductory presentation on the Horne 5 project, followed by the observation of drill hole (ddh) H5-15-07C, which is part of a group of recently drilled deep exploration drill holes in Zone 5. A description of some of the key intersections from ddh H5-15-07C is given below.

6.3 Horne 5 mineralized drill core observation: ddh H5-15-07C

6.3.1 Introduction

Drill hole H5-15-07C presents a variety of features characterizing the mineralized zone of the Horne 5 deposit. Ddh H5-15-07C intersects a high-grade gold zone (cut-off of 2.5 g/t Au) in the center of the deposit (high-grade zone A, see Fig. 6.2).

The deposit is hosted in subvertically-dipping felsic volcaniclastic units. Gold and silver mineralization is associated with a sulfide assemblage of pyrite with lesser sphalerite and chalcopyrite. The mineralization forms a series of stacked semi-massive to massive lenses intercalated with extended zones of disseminated and stringer sulfides (Fig. 6.3). Sericite alteration predominates within and proximal to the mineralized zone, and its intensity and style vary in conjunction with the style of mineralization. Gold and silver grades correlate well with the abundance of sulfides in core and with S values, as well as with Te grades. Distribution of Au within the mineralized zone is controlled in large part by the primary permeability of the host rocks, but deformation events may be responsible for modifications to the Au distribution within the mineralized lens, which is still under study.

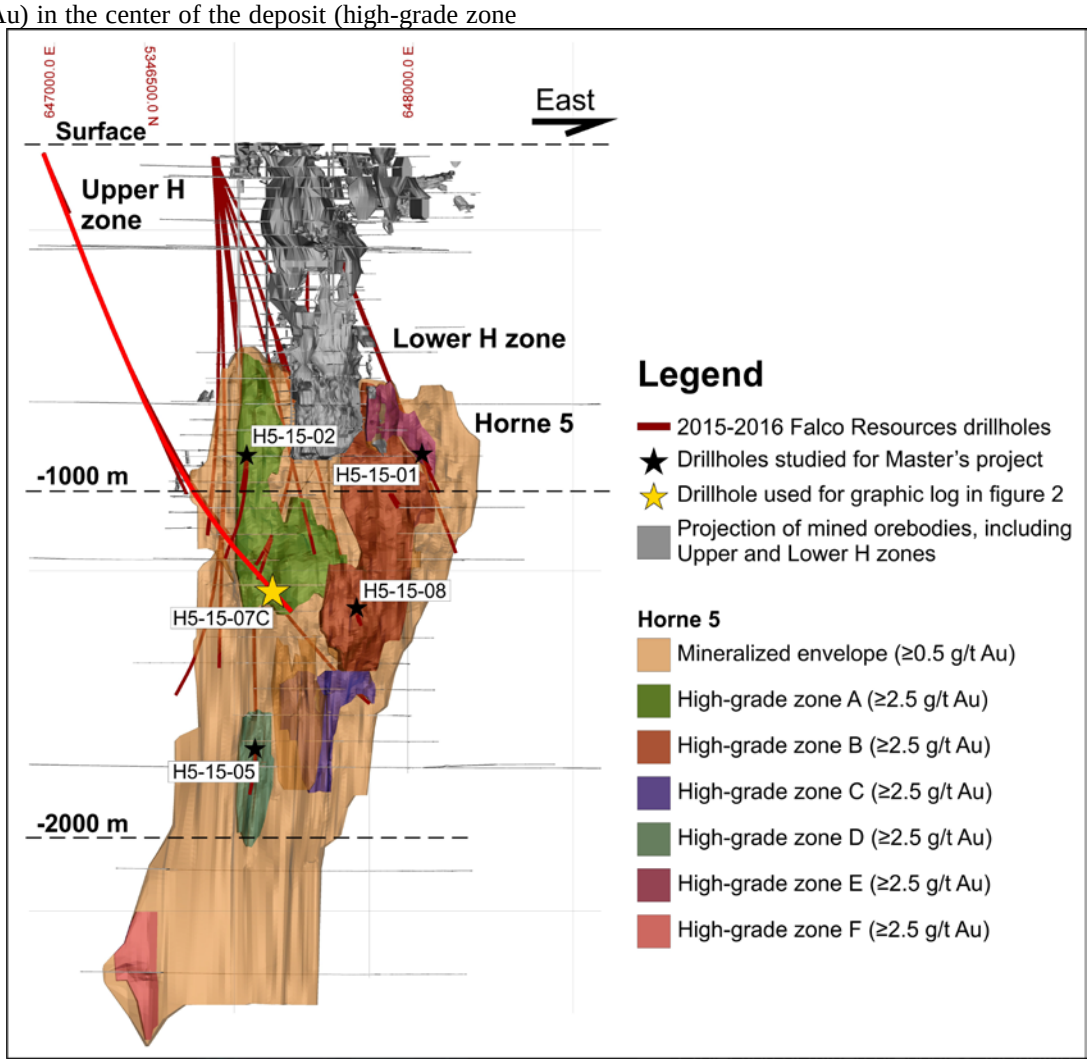

Figure 6.2. 3-D model of the Horne 5 deposit showing the mineralized gold envelope (cut-off at 0.5 g/t) and the higher grade gold zones (cut-off at 2.5 g/t), as well as the location of drill hole H5-15-07C (model generated by InnovExplo for Falco Resources Ltd.). Mine workings of the exploited Upper H and Lower H zones are also shown in grey.

6.3.2 Hangingwall lithofacies and alteration (1582.9-1620.8 m)

The rocks overlying the Horne 5 deposit consist of massive to graded volcaniclastic deposits. Lapilli-sized fragments are siliceous and of felsic composition, with variable amounts of lithic clasts, set in a fine-grained matrix comprising an assemblage of chlorite-epidote-sericite (Fig. 6.4A). Sericite and potassium feldspar are also present on the margins and along thin fractures in the felsic fragments. Traces to 5% finely disseminated pyrite are found in the matrix of the volcaniclastic units, and more rarely within the felsic fragments.

Directly above the uppermost massive sulfide lens are a series of fine-grained felsic volcanic rocks intercalated with felsic volcaniclastic deposits. The fine-grained volcanic units are interpreted as felsic intrusions that were emplaced within unconsolidated and wet volcaniclastic deposits (Fig. 6.4B). Evidence includes fragments of the intrusion in the volcaniclastic units, and vice-versa, and sharp erosional contacts with abrupt changes in grain size. Flow banding textures are also developed within this volcanic unit, with chlorite and disseminated pyrite preferentially developed in coarser-grained bands. These fine-grained volcanic units are significantly less altered than the host volcaniclastic units. Thus, they likely acted as cap rocks to ascending hydrothermal fluids which formed the underlying massive sulfide lens.

A small chlorite-rich interval within the volcaniclastic units contains 2-5% Mn-bearing garnet, 3-5% finely disseminated magnetite and pyrite and weak fracture-hosted carbonate (Fig. 6.4C).

6.3.3 Uppermost massive sulfide and underlying stringer zone (ddh H5-15-07C, 1620.8-1631.0 m)

A 2 m-long interval of massive sulfides represents the upper part of the mineralized zone in ddh H5-15-07C (Point A on Fig. 6.3). These massive sulfides have a sharp lower contact (Fig. 6.4D) and an upper contact cut by an unaltered and non-mineralized mafic intrusion. Pyrite is the dominant mineral, but 1-2% fracture-hosted chalcopyrite and traces of sphalerite are also present (Fig. 6.4E). Within the Horne 5 deposit, zones of massive sulfides are usually associated with the highest Au and Ag grades, as well as Cu, Zn, and Te. The sulfide zones are also enriched in As, Co, Bi, Sb, Sn, and In are also present (Fig. 6.3).

The underlying zone consists of auriferous stringer pyrite mineralization within strongly altered felsic volcaniclastic units. Alteration consists of strong pervasive sericitization of the host felsic rock. A well-developed foliation is present throughout this zone, suggesting that the sericite-rich rock has accommodated a significant portion of the deformation.

6.3.4 Massive sulfide clasts and mafic intrusions (ddh H5-15-07C, 1675.2-1692.2 m)

Within the host volcaniclastic deposits, numerous massive sulfide blocks are present at various levels in the stratigraphy (e.g., Point B on Fig. 6.3). Some contain significant gold and silver grades (e.g., 6.6 g/t in block shown in Fig. 6.4F), as well as base metals. Most are composed of pyrite with traces of sphalerite and chalcopyrite. These blocks are usually flattened and/or stretched to variable degrees. Disseminated to massive pyrite hosted in the matrix of the volcaniclastic units can also be observed throughout. Some of the felsic fragments are partly replaced by pyrite (Fig. 6.4G). Also present within this interval are two mafic intrusions that crosscut the volcaniclastic units. These gold-barren intrusions are pervasively chloritized ± epidotized and weakly foliated.

6.3.5 Lowermost massive sulfide interval and overlying felsic coherent unit (ddh H5-15-07C, 1708.5-1735.8 m)

Above the massive sulfide zone, felsic lapilli tuff and finely graded tuff deposits are intruded by a felsic coherent unit (Point C on Fig. 6.3). Tuff units are normally graded towards the top of the hole, and finely disseminated pyrite is found in the matrix of the coarser-grained layers. A few chlorite-rich intervals contain coarsely recrystallized pyrite and dark red sphalerite.

The felsic intrusion (dike or sill, lobe or dome) occurs below these volcaniclastic deposits. At its upper contact, the intrusion mixes with the enclosing volcaniclastic units, and fragments of the intrusion are found in fine tuff deposits, suggesting the intrusion was emplaced in unconsolidated rocks. Mineralization and alteration within the felsic intrusion consists of disseminated and stringer pyrite and weak pervasive sericitization, increasing progressively in abundance and intensity towards the massive sulfide zone.

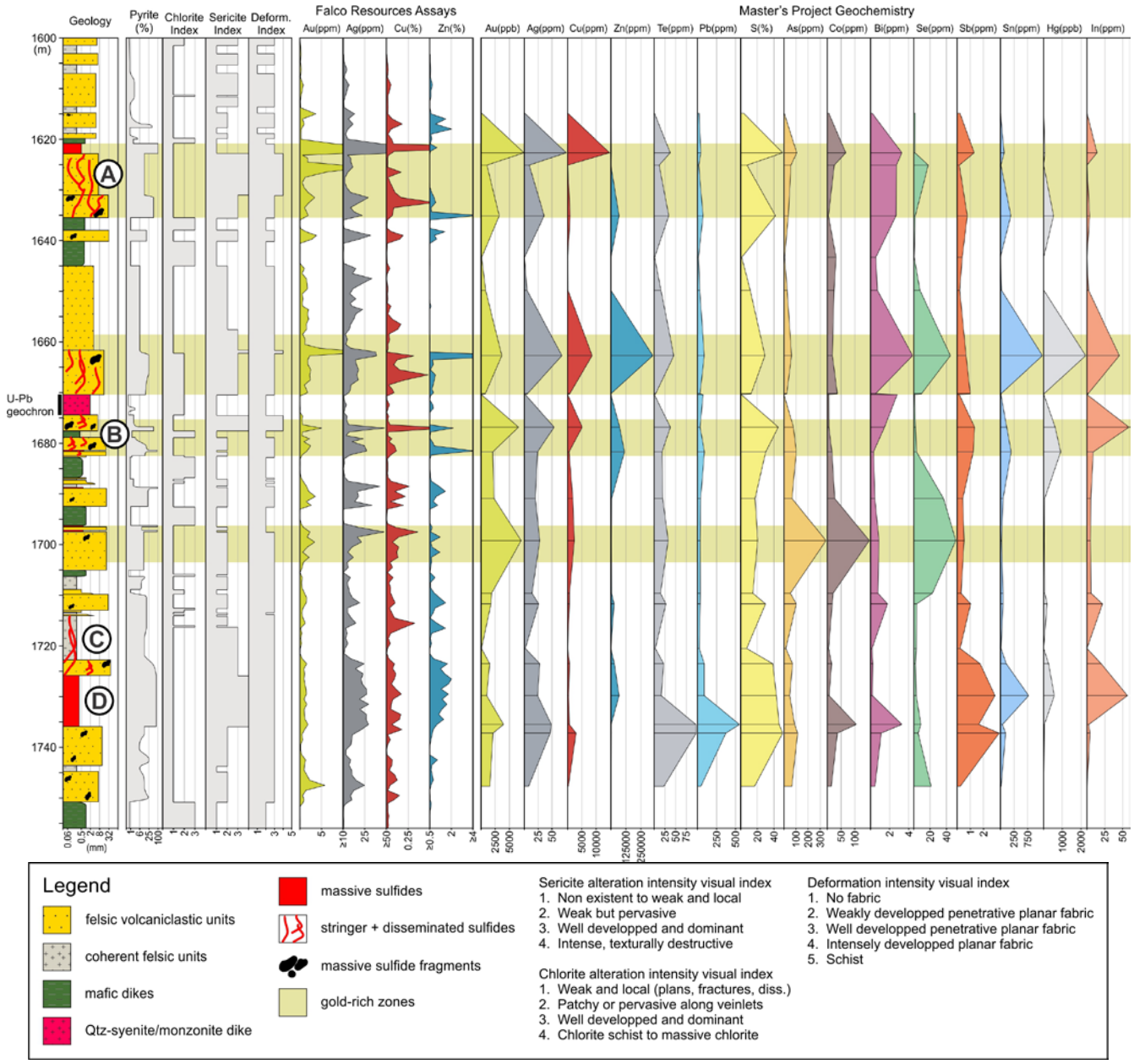

Figure 6.3. Schematic stratigraphic section and geochemical profile along mineralized zones of drill hole H5-15-07C (previous page) with accompanying legend (above). Downhole plots display abundance of sulfides, intensity of chlorite and sericite alteration, intensity of deformation, and metal profiles. The visual index represents a series of criteria used to quantify the intensity of alteration and deformation during fieldwork.

The underlying massive sulfide interval consists of fine to medium-grained granoblastic pyrite with up to 5% dark red disseminated and stringer sphalerite and traces of remobilized chalcopyrite. Sulfides were emplaced in a coarse-grained felsic volcaniclastic deposit, probably a tuff breccia or breccia, which offered a high permeability to circulating hydrothermal fluids. These massive sulfides show many features typical of sub-seafloor replacement (Fig. 6.4H). Evidence include permeable host volcaniclastic deposits, the presence of relict felsic fragments, texturally identical to the host volcaniclastic units, and gradual contacts from massive to semi-massive to disseminated outwards into the host rocks. The overlying felsic coherent unit probably acted as a cap rock to ascending hydrothermal fluids, focusing them along this specific horizon. Many massive sulfide fragments are also distinguishable within the massive sulfide interval, and were likely emplaced with the volcaniclastic deposits. Significant Ag, Cu, Zn, Te, Pb, Co, Bi, Sb, Sn, Hg, and In are present within this massive sulfide zone. Gold grades throughout this zone are relatively low compared with massive to semi-massive intervals higher in the stratigraphy.

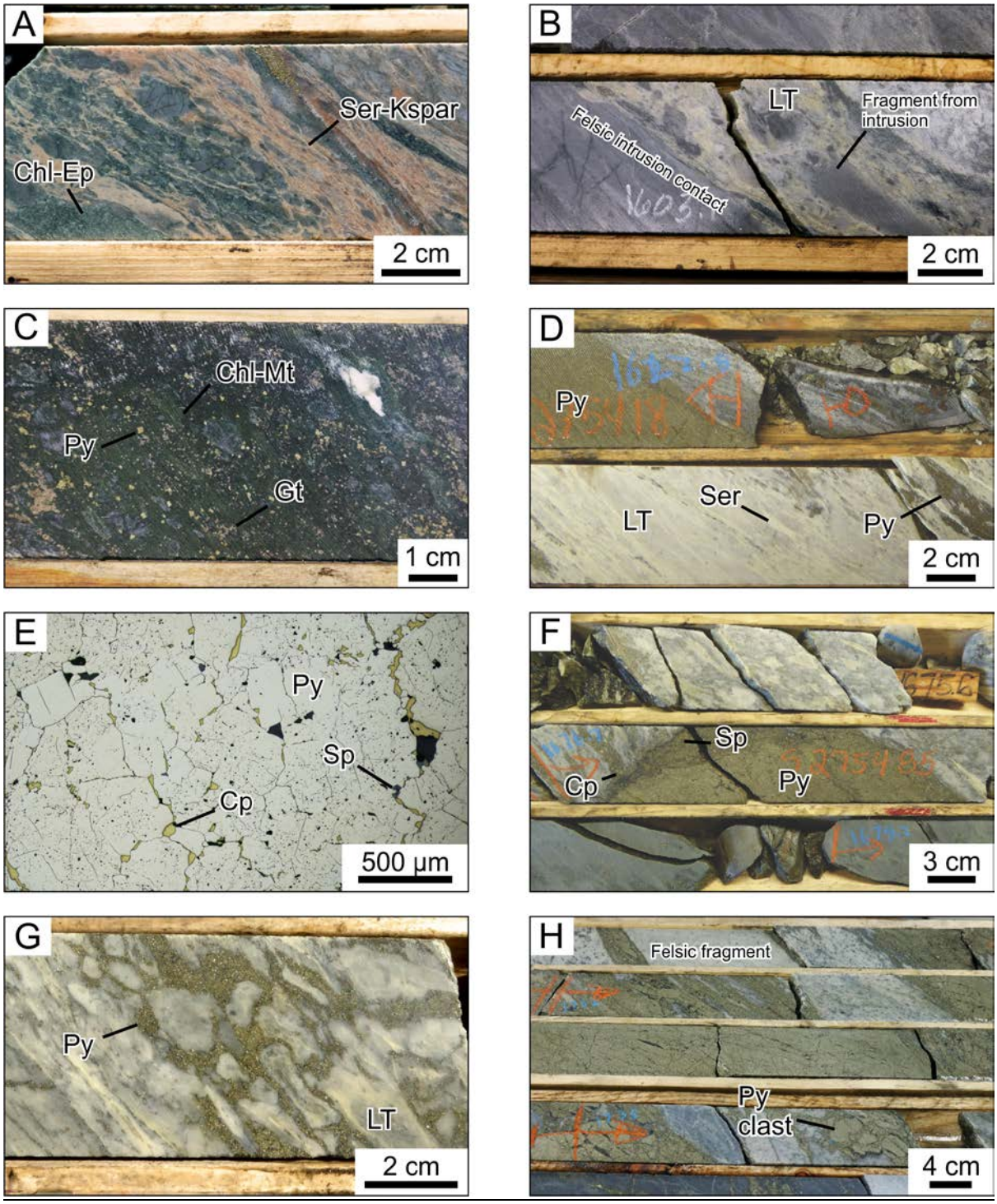

Figure 6.4. **a** Ser-Chl-Ep alteration assemblage typical of the hangingwall to the Horne 5 deposit. **b** Felsic intrusion within volcaniclastic deposits, with peperite-like textures at one contact. **c** Disseminated garnet porphyroblasts, pyrite and magnetite associated with a chlorite-rich zone within felsic volcaniclastic units. **d** Massive sulfide lens (mostly pyrite) and underlying stringer zone within bleached and strongly sericitized lapilli tuffs. **e** Photomicrograph of massive sulfide shown in d, showing abundance of recrystallized pyrite and interstitial chalcopyrite and sphalerite. **f** Massive sulfide block within a felsic lapilli tuff unit, containing pyrite and lesser sphalerite and chalcopyrite along the margins. **g** Felsic lapilli tuff fragments partly replaced by fine-grained pyrite. **h** Replacement-style massive sulfide, containing relict felsic fragments from host rocks and several massive sulfide clasts. Abbreviations: Chl = chlorite, Cp = chalcopyrite, Ep = epidote, K-spar = potassium feldspar, Gt = garnet, LT = lapilli tuff, Mt = magnetite, Py = pyrite, Ser = sericite, Sp = sphalerite.

6.3.6 Footwall lithofacies and alteration (ddh H5-15-07C, 1735.8-1751.8 m)

Massive felsic lapilli tuff deposits underlie the lowermost massive sulfide zone in ddh H5-15-07C (Point D on Fig. 6.3). These volcaniclastic units contain several dark grey lithic blocks hosting very finely disseminated pyrite, as well as massive sulfide fragments. Weak patchy sericite alteration is present in the matrix of the volcaniclastic rocks. Minor chalcopyrite stringers are present close to the overlying massive sulfides. The hole ends in a fine-grained mafic intrusion or flow.

6.4 References

Barrett TJ, Cattalani S, MacLean WH (1991) Massive sulfide deposits of the Noranda area, Quebec. I. The Horne mine: Can Jour Earth Sci 28: 465–488

Cattalani S, Barrett TJ, MacLean WH, Hoy L, Hubert C, Fox JS (1993) Métallogenèse des gisements Horne et Quemont (région de Rouyn-Noranda): MRN ET 90-07, 132 p

Cooke HC, James WF, Mawdsley JB (1931) Geology and ore deposits of Rouyn-Harricanaw region, Quebec: Geological Survey of Canada Memoir 166, 314 p

Dubé B, Gosselin P, Mercier-Langevin P, Hannington M, Galley A (2007) Gold-rich volcanogenic massive sulphide deposits. In Goodfellow WD (ed) Mineral Deposits of Canada: A Synthesis of Major Deposit-Types, Disctict Metallogeny, the Evolution of Geological Provinces, and Exploration Methods, Geological Association of Canada, Mineral Deposits Division, Special Publication 5, pp 75-94

Gibson HL, Kerr DJ, Cattalani S (2000) The Horne mine: geology, history, influence on genetic models, and a comparison to the Kidd Creek mine: Explo Mining Geol 9: 91–111

Kerr DJ, Gibson HL (1993) A comparison of the Horne volcanogenic massive sulfide deposit and intracauldron deposits of the Mine Sequence, Noranda, Quebec: Econ Geol 88: 1419–1442

Kerr DJ, Mason R (1990) A re-appraisal of the geology and ore deposits of the Horne mine complex at Rouyn-Noranda, Quebec: Canadian Institute of Mining and Metallurgy, Special Volume 43: pp. 153–165

Laurin J (2010) Geology, gold mineralization and alteration of the Horne West Property Rouyn-Noranda: Unpublished MSc thesis, University of Ottawa, 172 p.

MacLean WH, Hoy LD (1991) Geochemistry of hydrothermally altered rocks at the Horne Mine, Noranda, Quebec: Econ Geol 86: 506–528

McNicoll V, Goutier J, Dubé B, Mercier-Langevin P, Ross PS, Dion C, Monecke T, Legault M, Percival J, Gibson H (2014) U-Pb geochronology of the Blake River Group, Abitibi greenstone belt, Quebec, and implications for base metal exploration: Econ Geol 109: 27–59

Mercier-Langevin P, Goutier J, Ross PS, McNicoll V, Monecke T, Dion C, Dubé B, Thurston P, Bécu V, Gibson H, Hannington M, Galley A (2011a) The Blake River Group of the Abitibi greenstone belt and its unique VMS and gold-rich VMS endowment. GAC-MAC-SEG-SGA Joint Annual Meeting 2011, Ottawa, Field Trip 02B guidebook; Geological Survey of Canada, Open File report 6869, 61 p.

Mercier-Langevin P, Hannington MD, Dubé B, Bécu V (2011b) The gold content of volcanogenic massive sulfide deposits: Min Dep 46: 509–539

Monecke T, Gibson HL, Dubé B, Laurin J, Hannington MD, Martin L (2008) Geology and volcanic setting of the Horne deposit, Rouyn-Noranda, Quebec: initial results of a new research project: Geological Survey of Canada Current Research 2008-9, 16 p.

Poulsen KH, Hannington MD (1996) Volcanic-associated massive sulphide gold, *in* Eckstrand OR., Sinclair WD, Thorpe RI, eds, Geology of Canadian Mineral Deposit Types, Geological Survey of Canada, Geology of Canada Series no. 8, p. 183–196.

Poulsen KH, Robert F, Dubé B (2000) Geological classification of Canadian gold deposits: Geological Survey of Canada Bulletin 540, 113 p.

Price P (1934) The geology and ore deposits of the Horne Mine, Noranda, Quebec: The Transactions of the Canadian Institute of Mining and Metallurgy and of the Mining Society of Nova Scotia 37: 108–140

Price P (1948) Horne Mine: Structural geology of Canadian ore deposits, Canadian Institute of Mining and Metallurgy, p. 763–772

Sinclair WD (1970) Geology of the No. 5 Zone, Horne mine, Noranda, Quebec, Canada: Unpublished MS thesis, University of Wisconsin, 69 p.

Suffel GG (1935) Relations of later gabbro to sulphides at the Horne Mine, Noranda, Quebec: Econ Geol 30: 905–915

Taylor BE, de Kemp EA, Grunsky E, Martin L, Maxwell G, Rigg D, Goutier J, Lauzière K, Dubé B (2014) Three-dimensional visualization of the Archean Horne and Quemont Au-bearing volcanogenic massive sulfide hydrothermal systems, Blake River Group, Quebec: Econ Geol 109: 183–203

Chapter 7: (Day 4) Au-rich VMS deposits of the Doyon-Bousquet-LaRonde mining camp – The LaRonde Penna mine

Patrick Mercier-Langevin
Natural Resources Canada – Geological Survey of Canada

Benoît Dubé
Natural Resources Canada – Geological Survey of Canada

David Pitre, Jean-François Bégin, Annie Laberge, and Linda Burke
Agnico Eagle Mines ltd, LaRonde Division

7.1 Introduction

The LaRonde Penna mine is located approximately 45 km east of Rouyn-Noranda, in the southern part of the Abitibi greenstone belt. It is the easternmost mine in the Doyon-Bousquet-LaRonde mining camp (Figs. 7.1 and 7.2). Production at the LaRonde Penna deposit started in 2000, and 39 Mt of ore were extracted, for a total production of 115.4 t Au, or 3.71 Moz (table 7.1). It is one of the largest Au deposits in Canada with a total content (production, reserves, and resources) of 70 Mt of ore at 4.17 g/t Au for approximately 292 t Au, or 9.37 Moz (Table 7.1). It is also the largest Ag, Cu, and Zn producer in Québec. Its significant size also makes the LaRonde Penna deposit one of the largest Canadian VMS deposits. It is second to Horne amongst the gold-rich VMS deposits (Fig. 1.5).

Table 7.1. Total production, reserves and resources[1] at the end of 2016 (December 31, 2016) for the Doyon-Bousquet-LaRonde mining camp

			Cumulative production									Total gold budget (*in situ*)			
			Tonnage	Au	Au	Au	Au	Au	Ag	Cu	Zn	Tonnage	Au	Au	Au
Deposit				(g/t)	(tonnes)	(tonnes)	(Moz)	(Moz)	(tonnes)	(tonnes)	(tonnes)				
Type	Mine	Year	(Mt m)	*in situ*	prod.	*in situ*	prod.	*in situ*	prod.	prod.	prod.	(Mt m)	(g/t)	(t)	(Moz)
Au-rich volcanogenic massive (±semi-massive) sulfide lenses, and Au-rich sulfide veins, stockworks and disseminations															
	Dumagami	1988-1999	7.33	6.84	46.01	50.12	1.48	1.61	85.79	34,196	4994	7.33	6.84	50.11	1.61
	LaRonde Penna[2]	**2000-2016**	**38.99**	**3.24**	**115.4**	**126.40**	**3.71**	**4.07**	**1,682**	**80,542**	**733,732**	**69.97**	**4.17**	**291.45**	**9.37**
	Bousquet 2	1990-2002, 2007	8.22	8.56	66.64	70.31	2.14	2.26	0.42	45,804	20	10.31	7.95	81.99	2.64
	Bousquet 1	1978-1996	7.45	5.70	39.49	42.45	1.27	1.36				7.45	5.30	42.45	1.36
	Bousquet 1 (LZ5)[3]											18.04	2.79	50.50	1.62
	Ellison											2.35	3.41	8.00	0.26
Epizonal "intrusion-related" sulfide-rich Au-Cu vein systems															
	Doyon	1980-2009	31.62	5.53	167.95	174.94	5.40	5.62				34.10	5.45	185.78	5.97
	Westwood[2]	2013-2016	1.33	6.89	8.71	9.16	0.28	0.29				14.09	10.49	147.76	4.75
	Mooshla A	1939-1940	0.004	29.66	0.13	0.13	0.01	0.01				0.004	29.66	0.13	0.01
Shear-hosted sulfide-rich Au-Cu vein systems															
	Mouska	1989-2011	2.13	12.69	25.67	27.08	0.83	0.87		437		2.44	12.99	31.67	1.02
	Mic Mac	1942-1947	0.72	4.62	3.34	3.34	0.11	0.11		1150		0.72	4.62	3.34	0.11
	Orion-B2 shear											0.50	6.00	3.00	0.10
	TOTAL camp DBL		**97.79**	**5.15**	**473.34**	**503.93**	**15.23**	**16.20**	**1,768**	**162,129**	**738,746**	**167.30**	**5.36**	**896.18**	**28.82**

Mt m = million metric tonnes
Moz = million ounces
[1]Global gold endowment figures (Total metal budget in situ) include total historical production (in situ) plus current reserves and resources data taken from public sources and are for comparison purposes only - Please refer to Iamgold and Agnico Eagle Mines websites for details
[2]Current producers
[3]Development stage

For conciseness, only information specific to the August 2017 SGA field trip visit are given here; readers are referred to Mercier-Langevin et al. (2017) for the relevant information about to the LaRonde Penna mine visit and the deposit and camp geology.

7.2 Tour Program

There are two parts to the LaRonde Penna mine visit, with an underground tour in the morning, and drill core and outcrops observations in the afternoon.

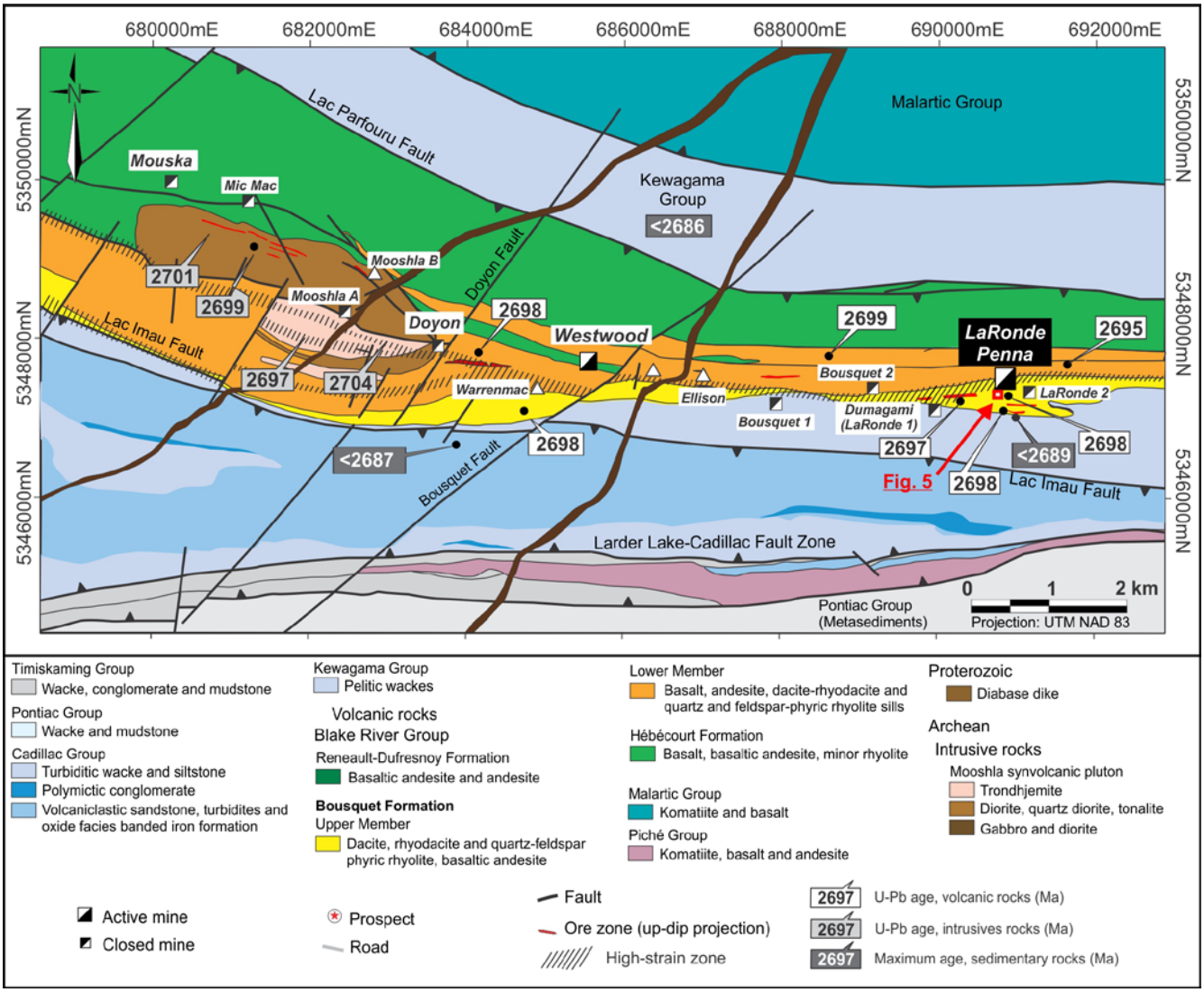

Figure 7.1. Geology of the Doyon-Bousquet-LaRonde mining camp. From Mercier-Langevin et al. (2017).

7.2.1 Morning

Arrival at the mine is scheduled at 07h00. There will be a breif introduction and participants will be geared up for the undergroud tour.

Stop 1: Lunch room on level 278 (2780 m below surface) for a discussion about the mine and the geology of the deposit.

Stop 2: GAL-EXPL 290W, underground diamond drilling for exploration program of LaRonde 3.

Stop 3: PS-290-20-129, typical transversal development within footwall of 20 North Zone and well-exposed Au ±Cu-Ag-Zn mineralization.

Stop 4: CH-296-20-116, draw point for 20 North Zone.

Stop 5: Conveyor drift, level 292, loading at the start of coarse conveyor.

Stop 6: Main garage and warehouse on level 278 Main garage.

Return to surface will be at around 11h30 and lunch will be served in the meeting room of the main office building. Discussion with mine staff during lunch time.

7.2.2 Afternoon

We will look at representative drill core in the afternoon of both mineralization and altered host rocks. We will first look at core from two drill holes (DDH 3146-05, DDH 3220-04, and DDH 3170-11b) that were studied in detail a few years ago (Dubé et al. 2007; Mercier-Langevin et al. 2007a, b, c, d) and that show contrasting styles of alteration in proximity to the 20 North lens. Spectacular intersections of high-grade mineralization from DDH LR-290-056, LR-290-056A, and LR-290-061 will also be laid out at the core shack. The tour will end with two brief stops on outcrops near the headframe where the footwall rhyodacite dome is exposed.

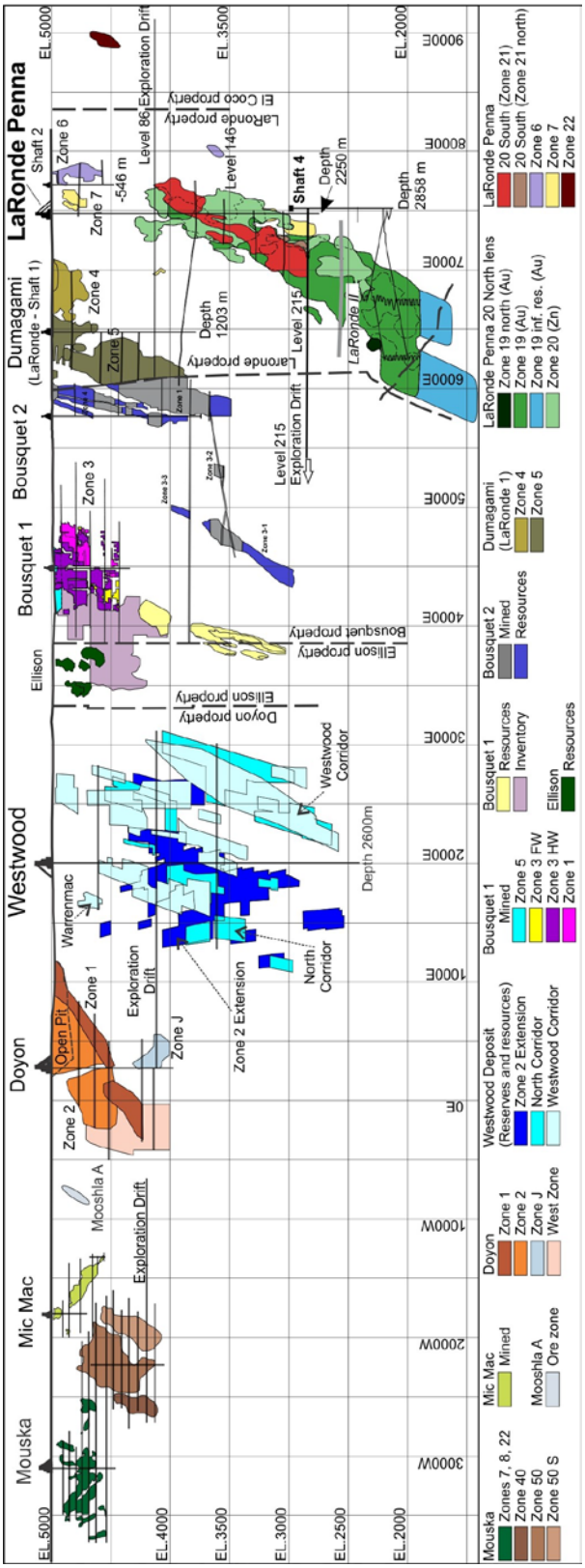

Figure 7.2. Composite longitudinal view (looking north) of the Doyon-Bousquet-LaRonde mining camp. The outline of zones include production, reserves, and resources, including some historical, non-NI-43-101 compliant reserves and resources. From Mercier-Langevin et al. (2017).

Stop 7: DDH 3146-05: Drill core from one hole intersecting most of the upper member of the Bousquet Formation will be laid out to display the main alteration styles and mineralization assemblages associated with the 20 North and 20 South lenses in the upper levels of the deposit (Fig. 7.3). Details are given in Dubé et al. (2007) and Mercier-Langevin et al. (2017).

Stop 8: DDH 3220-04: Parts of the drill hole DDH 3220-04 will be laid out to study the aluminous alteration assemblage associated with the 20 North lens at LaRonde Penna in the lower levels of the deposit (Fig. 7.3), and to allow comparison with DDH 3146-05 that intersects the ore and its alteration zones higher in the deposit. DDH 3220-04 represents an excellent example of the aluminous assemblages and the zonation towards the ore. Details are given in Dubé et al. (2007) and Mercier-Langevin et al. (2017).

Stop 9: DDH 3170-11b: Very intense aluminous and silicic alteration can be studied in drill core DDH 3170-11b (Fig. 7.3). The section shows the depth extension of the 20 North lens where the ore consists of semi-massive sulfides that are hosted in strongly silicified, altered felsic rocks (Unit 5.2b).

Stop 10: DDH LR-290-056: This exploration drill hole intersected the 20 north lens (19N, 19, and 20 zones) at a depth of approximately 3.4 km (3400 m from surface, in one of the deepest extensions of the lens, on its western side. The Zone 19 intersection has weighted average grade of 14.97 g/t Au over 21.5 m (9.5 m true thickness). This intersection also grades 0.2 wt.% Cu. The intersection is underlain by sulfidized rhyodacite (unit 5.2b). The ore zone consists of semi-massive pyrite-chalcopyrite ±sphalerite with traces of tellurides and electrum in a strongly silicified and aluminous host rock (quartz-biotite-sericite and quartz-sericite-kyanite-andalusite ±staurolite). The immediate hanging-wall rocks consist of sulfidized and sericitized intermediate to felsic volcanic rocks (rhyodacite, unit 5.5).

Stop 11: DDH LR-290-056A: This exploration drill hole intersected the 20 north lens (19N, 19, and 20 zones) at a depth of approximately 3.4 km (3400 m from surface, in one of the deepest extensions of the lens, on its western side (Figs. 7.3 and 7.4). The Zone 19 intersection has weighted average grade of 28.09 g/t Au over 16.5 m (9.3 m true thickness). This intersection has 0.46 wt.% Cu. The intersection is underlain by sulfidized, biotite-sericite-quartz-altered rhyodacite (unit 5.2b). The ore zone consists of semi-massive pyrite-chalcopyrite ±sphalerite with traces of tellurides and electrum in a strongly silicified and aluminous host rock (quartz-staurolite-kyanite-andalusite ±sericite). The immediate hanging-wall rocks consist of sulfidized and sericitized intermediate to felsic volcanic rocks that are biotite and garnet (porphyroblasts)-altered

away from the ore zone (rhyodacite, unit 5.5).

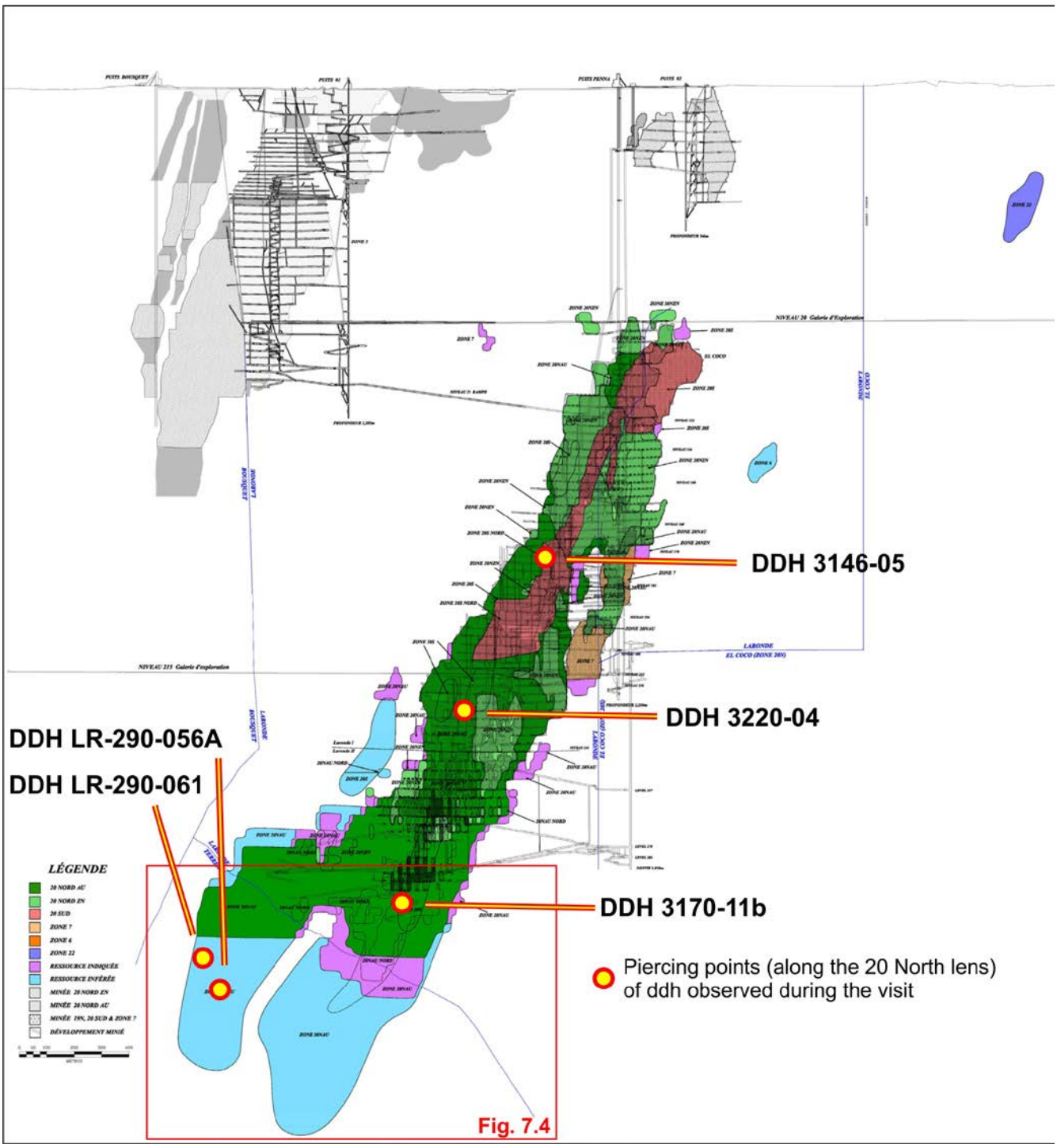

Figure 7.3. Longitudinal view of the LaRonde Penna mine (looking north). Figure courtesy of Agnico Eagle Mines ltd.

Stop 12: DDH LR-290-61: This exploration drill hole intersected the 20 north lens (19N, 19, and 20 zones) at a depth of approximately 3.3 km (3300 m from surface, in one of the deepest extensions of the lens, on its western side (Figs. 7.3 and 7.4). The Zone 19 intersection has weighted average grade of 13.77 g/t Au over 14.6 m (8.1 m true thickness). It also contains significant Zn (2.89 wt.% over 8.1 m), with 1.31 wt.% Cu on that same interval. The intersection is underlain by sulfidized, biotite-sericite-quartz ±garnet ±staurolite-altered rhyodacite (unit 5.2b). The ore zone consists of semi-massive pyrite-chalcopyrite ±sphalerite with traces of tellurides and electrum in a strongly silicified and aluminous host rock (quartz-

staurolite-kyanite-andalusite ±sericite). The ore zone also contains massive sulphides (pyrite-chalcopyrite-sphalerite with traces of galena and pyrrhotite). The immediate hanging-wall rocks consist of sulfidized and sericitized intermediate to felsic volcanic rocks that are biotite and garnet (porphyroblasts)-altered away from the ore zone (rhyodacite, unit 5.5).

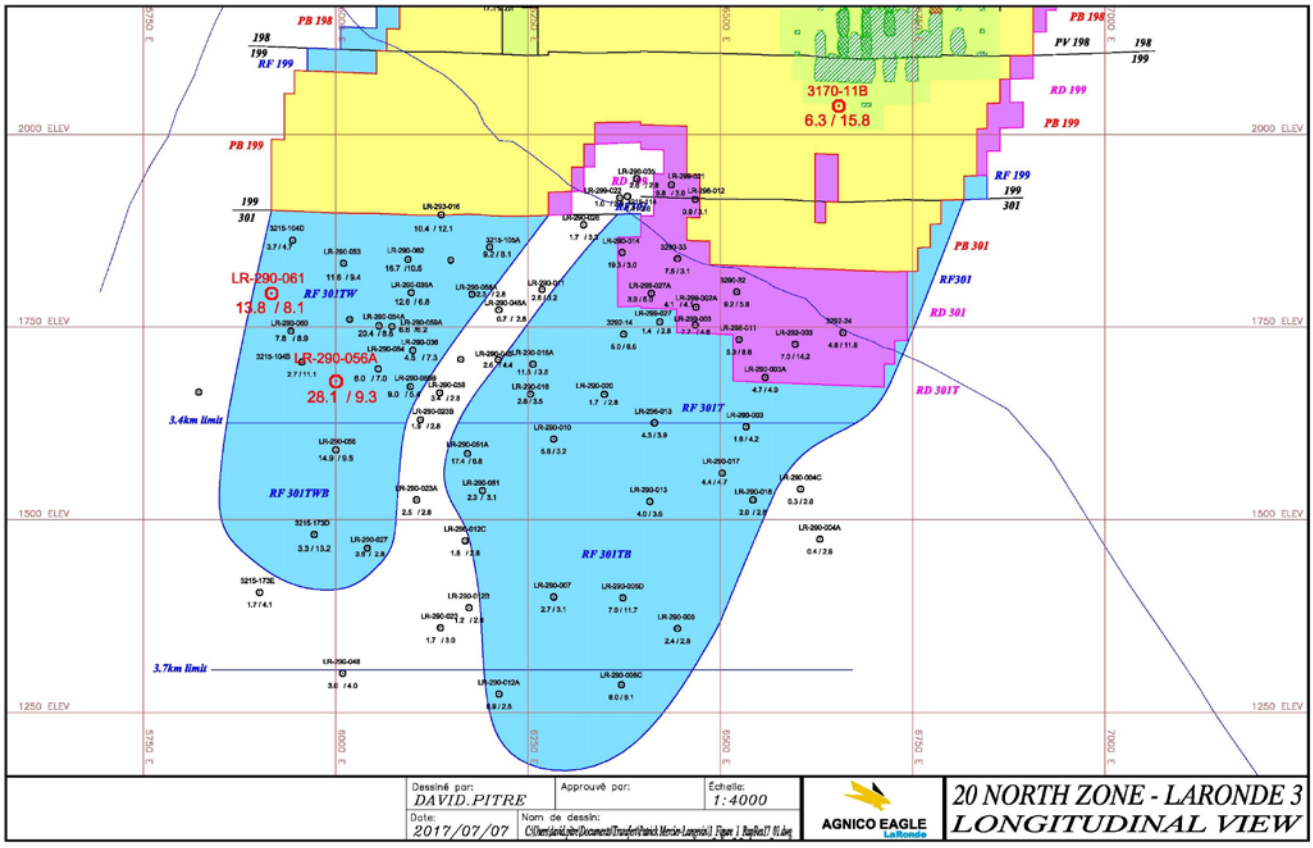

Figure 7.4. Longitudinal view (looking north, of the 20 North lens at depth in the mine (between 2750 m and 3800m below surface).

Stops 13 and 14: Facies relationships of the rhyolite dome/cryptodomes forming the footwall to the 20 North Lens: Lobate and brecciated rhyolite (WGS84, zone 17U, 690700 mE, 5347270 mN) and coherent facies (WGS84, zone 17U, 690838 mE, 5347283 mN). The volcanic architecture of the immediate stratigraphic footwall to the 20 North lens, which is the principal orebody (80%) at LaRonde Penna, can be studied in two surface outcrops. Both stops are located just south of the LaRonde Penna headframe and are only a few hundred meters apart (see Mercier-Langevin et al. 2017). In the footwall of the deposits, feldspar-phyric rhyodacite flow-breccia (Unit 5.2b; Mercier-Langevin et al., 2007b) has been intruded by feldspar-phyric rhyolite. Stop 13 shows a carapace breccia of the feldspar-phyric rhyolite that is cut by flow-banded lobes and overlain by a flow breccia (see Mercier-Langevin et al. 2017 – Supplement E). Perlitic fractures are present in some clasts, suggesting that the lava was initially glassy. The outcrop at Stop 2 shows coherent and flow-banded, feldspar-phyric rhyolites of the upper part of the massive dome. The volcanic facies relationships characterizing the rhyolite domes/cryptodomes are typical of rhyolite flow-dome complexes (e.g., Gibson et al., 1999) and imply that the LaRonde Penna mine was formed close to a felsic volcanic vent, in a proximal environment, likely characterized by the presence of synvolcanic faults that may have acted as upflow zones for the hydrothermal fluids. The 20 North lens was formed, at least in part, by sub-seafloor replacement within the uppermost part of this flow-dome complex (Dubé et al., 2007; Mercier-Langevin et al., 2007a, b).

7.3 References

Dubé B, Mercier-Langevin P, Hannington M, Lafrance B, Gosselin G, Gosselin P (2007) The LaRonde Penna world-class Au-rich volcanogenic massive sulfide deposit, Abitibi, Québec: Mineralogy and geochemistry of alteration and implications for genesis and exploration: Econ Geol 102: 633–666

Gibson HL, Morton RL, Hudak GJ (1999) Submarine volcanic processes, deposits, and environments favorable for the location of volcanic-associated massive sulfide deposits: Reviews in Economic Geology 8: 13–51

Mercier-Langevin P, Dubé B, Lafrance B, Hannington M, Galley A, Moorhead J, Gosselin P (2007a) Metallogeny of the Doyon-Bousquet-LaRonde mining camp, Abitibi greenstone belt, Quebec, *in* Goodfellow, W.D., ed., Mineral deposits of Canada: A synthesis of major deposit-types, district metallogeny, the evolution of geological provinces, and exploration methods: Mineral Deposits Division, Geological Association of Canada, Special Publication no. 5, p. 673–701

Mercier-Langevin P, Dubé B, Hannington MD, Davis DW, Lafrance B, Gosselin G (2007b) The LaRonde Penna Au-rich volcanogenic massive sulfide deposit, Abitibi greenstone belt, Quebec: Part I. Geology and geochronology: Econ Geol 102: 585–609

Mercier-Langevin P, Dubé B, Hannington MD, Richer-Laflèche M, Gosselin G (2007c) The LaRonde Penna Au-rich volcanogenic massive sulfide deposit, Abitibi greenstone belt, Quebec: Part II. Lithogeochemistry and paleotectonic setting: Econ Geol 102: 611–631

Mercier-Langevin P, Dubé B, Lafrance B, Hannington MD, Galley A, Marquis R, Moorhead J, Davis DW (2007d) A group of papers devoted to the LaRonde Penna Au-rich volcanogenic massive sulphide deposit, eastern Blake River Group, Abitibi greenstone belt, Quebec: Preface: Econ Geol 102: 577–583

Mercier-Langevin P, Dubé B, Blanchet F, Pitre D, Laberge A (2017) The LaRonde Penna Au-rich volcanogenic massive sulfide deposit: Reviews in Economic Geology 19, In press.

Chapter 8: (Day 5 – Part I) Geology and disseminated-stockwork gold mineralization at the world-class Canadian Malartic mine, Abitibi greenstone belt, Canada

Stéphane De Souza
Université du Québec à Montréal

Benoît Dubé
Natural Resources Canada – Geological Survey of Canada

Vicki McNicoll
Natural Resources Canada – Geological Survey of Canada

Patrick Mercier-Langevin
Natural Resources Canada – Geological Survey of Canada

Robert A. Creaser
University of Alberta

Ingrid Kjarsgaard
Consultant

8.1 Introduction

The Canadian Malartic open pit gold mine is located in the Malartic district (Trudel and Sauvé, 1992 and references therein), within and immediately to the south of the Larder Lake-Cadillac Fault Zone in the southern Abitibi greentone belt (LLCFZ; Fig. 8.1). This deposit represents the largest of a suite of gold deposits spatially associated with Neoarchean alkaline to sub-alkaline porphyritic dikes, sills, and stocks intruded into sedimentary and/or metavolcanic strata, during an episode of fluvial/alluvial sedimentation, also known as the Timiskaming assemblage, at ~ <2679-<2669 Ma (Corfu 1993; Robert 2001; Thurston et al., 2008; Bleeker 2015). This contribution summarizes some of the key elements of the Canadian Malartic deposit, including information about observations that will be made during the tour. There is a detailed description of the deposit in Supplement F (De Souza et al. 2017).

8.2 History

The earliest discovery of gold-bearing veins in the Malartic district was made in 1923, as reported by O'Neil (1935), whereas continuous mining activities from 1935 to 1979 preceded intermittent mining and exploration operations up to May 2011, when the Canadian Malartic open pit mine was put into commercial production by the Osisko Mining Corporation. The mine is currently owned and operated by the Canadian Malartic Partnership, which is jointly owned by Agnico-Eagle Mines and Yamana Gold. The Canadian Malartic open pit mine is developed on the grounds of three past-producing underground mines that exploited the same ore deposit: the Canadian Malartic, Sladen-Barnat, and East Malartic mines, which produced 33.5 (1.08 Moz), 37.8 (1.22 Moz), and 88.7 t of Au (2.85 Moz), at an average grade of 3.37, 4.5, and 4.92 ppm Au, respectively (Trudel and Sauvé 1992). In the past-producing mines, ore zones mostly consisted of disseminated, stockwork, and breccia ore bodies and vein arrays hosted in graywacke, diorite, and porphyritic intrusions (Derry 1939; Trudel and Sauvé 1992). The distribution of these ore zones is, at least in part, controlled by the Sladen Fault, an east-trending, south-dipping fault that represents one of the main metallotects of the Malartic district (Derry 1939; Sansfaçon and Hubert 1990; Fallara et al. 2000; De Souza et al. 2015, 2017; Perrouty et al. 2017). At the beginning of commercial production in 2011, the Canadian Malartic open pit mine had proven and probable reserves of 10.7 Moz Au (332 t Au) contained in 343.7 Mt of ore grading an average of 0.97 ppm Au that was calculated using a cut-off grade of 0.30 ppm Au, and of 0.32 and 0.26 ppm Au for the Barnat and Gouldie zones, respectively (Belzile and Gignac 2011). Gold production in 2016 amounted to 16.7 t (537,000 oz), which makes it the Canadian mine with the largest gold production.

8.3 Geology of the Canadian Malartic mine

The Canadian Malartic open pit mine is mainly hosted by sedimentary rocks of the Pontiac Group (Fig. 8.2), which consist of turbiditic graywacke with interlayered mudstone (Fig. 8.3A-C) that are located to the south of the LLCFZ. Metamorphic grade increases southward from the biotite zone to the garnet and staurolite zones (Fig. 8.1B). The minimum depositional age of the Pontiac Group is constrained by the crosscutting 2682 ± 1 Ma Lac Fournière Pluton (Fallara et al. 2000; Davis 2002), whereas the maximum age is given by the youngest detrital zircons from graywacke, which are dated at 2685.3 ± 3.0 Ma (Davis 2002; De Souza et al. 2017) and 2682.7 ± 1.9 Ma (Mortensen and Card 1993).

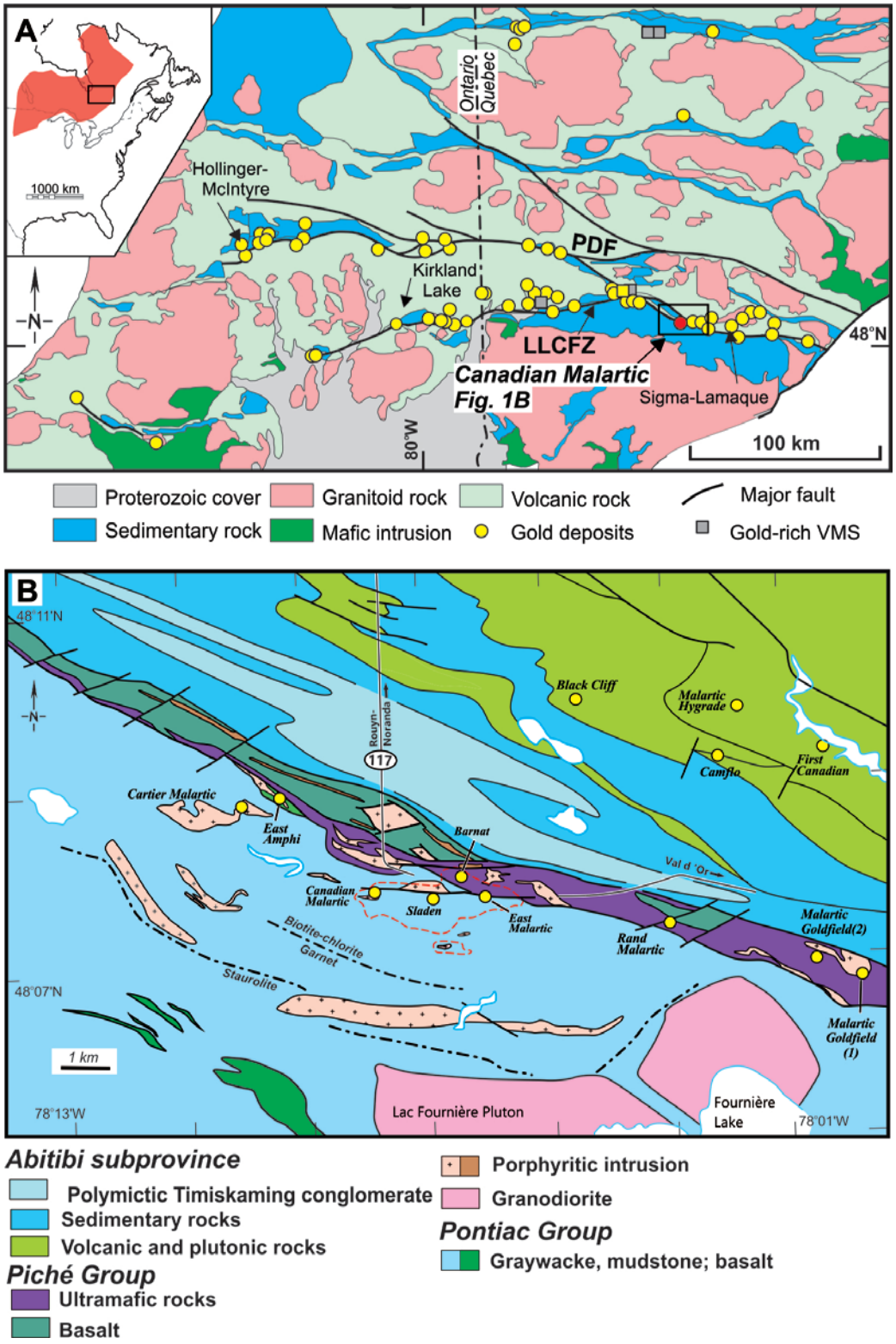

Figure 8.1. a Generalized geological map of the Abitibi greenstone belt showing the distribution of the main gold deposits and faults. Inset shows the distribution of the Superior Province. Modified from Dubé and Gosselin (2007). **b** Geological map of the Malartic district with the location of the main gold showings and past-producing gold mines. Geology is from this study and Sansfaçon and Hubert (1990), Fallara et al. (2005), and Pilote (2013). The final configuration of the Canadian Malartic open pit mine is outlined by the stippled red line. LLCFZ = Larder Lake - Cadillac Fault Zone, PDF = Porcupine-Destor fault zone.

The Pontiac Group is intruded by plutonic rocks of various compositions, all of which are known, at least locally, to show some evidence of hydrothermal alteration, and to host ore-grade zones. These intrusive rocks include porphyritic quartz monzodiorite and granodiorite stocks, and felsic and intermediate sills and dikes (Fig. 8.3D-G), and mafic-ultramafic lamprophyre dikes. Timiskaming-age magmatism in the Malartic district is constrained by U-Pb zircon geochronology of the porphyritic granodiorite, quartz monzodiorite, and a felsic sill, all from the site of the Canadian Malartic mine, and dated at 2678.4 ± 1.7 Ma, 2677.8 ± 1.5 Ma, and 2677.4 ± 0.9 Ma, respectively (De Souza et al. 2015, 2017).

In the Canadian Malartic mine area, structural studies have shown that the Pontiac Group has undergone polyphase deformation, including an early D_1 phase of tight to isoclinal folding characterized by overturned folds, and a folded bedding-parallel S_1 schistosity, that are overprinted by foliation, folds, and faults related to a D_2 phase of deformation (Sansfaçon and Hubert 1990; De Souza et al. 2015, 2017). The east-trending brittle-ductile Sladen Fault varies from a ~ 1 to 10-meter-wide planar deformation and alteration zone, to a ≤ 100 m wide fault zone comprising multiple subsidiary faults with evidence of both ductile and brittle strain increments (Fig. 8.3H-I). The fault cuts the Sladen zone quartz monzodiorite, and it locally marks the southern limit of the LLCFZ in the eastern part of the deposit (Fig. 8.2A; Cormie 1948; Sansfaçon and Hubert 1990; Fallara et al. 2000).

8.4 Distribution of the ore zones and hydrothermal alteration

The Canadian Malartic mine comprises east- and northwest-trending ore zones that are hosted in both the Pontiac and Piché groups (Fig. 8.2B). The main northwest-trending ore zones correspond to the P, A, Gilbert, and Gouldie zones in the Pontiac Group, and the Barnat zone in the Piché Group. The trace of these ore bodies is subparallel to the S_2 cleavage and F_2 faults and related fracture networks. They are discordant relative to bedding and to all intrusive rock types. The surface distribution of gold clearly illustrates the spatial and geometrical relationships between mineralized zones and D_2 faults, especially in the southern part of the deposit, where both northwest-trending faults, S_2 foliation and ore zones are sub-parallel to the LLCFZ and developed at high angle to the folded bedding, along the short limb and in the hinge zone of the faulted F_2 S-type fold formed in the mine pit area (Fig. 8.2A). Similar spatial relationships are documented at the scale of the orebody in the Gilbert and Gouldie zones, where alteration zones and mineralized veins are preferentially developed within D_2 structures that cut the folded bedding and sills and dikes at high-angle (Fig. 8.4). One of the best examples of these relationships are illustrated in the sample given in figure 8.3J, with veinlets filling fractures along the S_2 cleavage, a mineralized breccia cutting the folded bedding and proximal beige/tan alteration invading the biotitized and sericitized sedimentary rocks along stratification. Carbonates and hydrothermal phlogopite and phengitic sericite define foliation in the mineralized D_2 high-strain zones and faults, and overprint the metamorphic mineralogy, along with poikilitic carbonate grains overprinting S_2. Hydrothermal mineral assemblages were separated into distal K-mica-calcite and calcite-hematite assemblages in the sedimentary rocks and quartz monzodiorite, respectively, and a proximal carbonate-feldspar assemblage developed in both protoliths. The transition from the distal to the proximal alterations is used herein in the sense of Eilu et al. (1999) for upper greenschist facies metamorphic rocks, i.e. by the introduction of hydrothermal dolomite. Hence, although referred to as distal, the K-mica-calcite and calcite-hematite alterations are also subject to host ore-grade gold values and to form part of the ore (≥ 0.350 ppm Au).

The east-trending Sladen zone extends eastward more-or-less continuously along the Sladen Fault, from the western limit of the current open pit and merges with the East Malartic zone to the east, which is located at the contact between the Piché and Pontiac groups (Fig. 8.2B). The East Malartic and Sladen zones dip steeply toward the south (60-90°), and comprise east-plunging (~55°) geometrical ore shoots at the intersection of intrusions or dike swarms with the Sladen Fault. The ore zones are largely located along and within the footwall of the Sladen Fault. A set of late, en enchelon, shallow west-dipping barren quartz extension veins is well developed especially within competent layers of the Pontiac Group sedimentary rocks and crosscutting intermediate and felsic dykes and sills. They are extentional veins oriented at high-angle to the east-plunging stretching lineation (L_2). They share analogies with the typical extension quartz veins that host part of the ore at the Sigma-Lamaque deposit (Robert and Brown, 1986). At Canadian Malartic, they are only locally deformed and boudinaged and are here interpreted as representing a syn- to late-D_2 coaxial strain increment, and as late- to post-main stage mineralization (Fig. 8.3K).

Relationships between the mineralized zones, the Sladen Fault, and the main intrusion that hosts the ore are well illustrated along section 4790 and in drill hole CM08-1845 (Fig. 8.5A-B). Along this section, the sedimentary rocks of the Pontiac Group and the quartz monzodiorite both show evidence of distal to proximal hydrothermal alteration as defined in De Souza et al. (2017). Distal assemblage in the sedimentary rocks is dark grey to bluish green and consists of biotite, phengitic sericite, and albite, with calcite increasing toward the mains ore zones, whereas proximal assemblage is tan coloured and represented by calcite, dolomite, feldspar (albite and K-feldspar), phlogopite, and sericite (Fig. 8.6A). The fresh quartz monzodiorite is altered to a calcite-hematite assemblage defining a 50-m thick envelop in the intrusion (Fig. 8.6B), whereas the proximal assemblage consists of a light grey to pinkish alteration in the immediate footwall of the Sladen Fault (Fig. 8.6C).

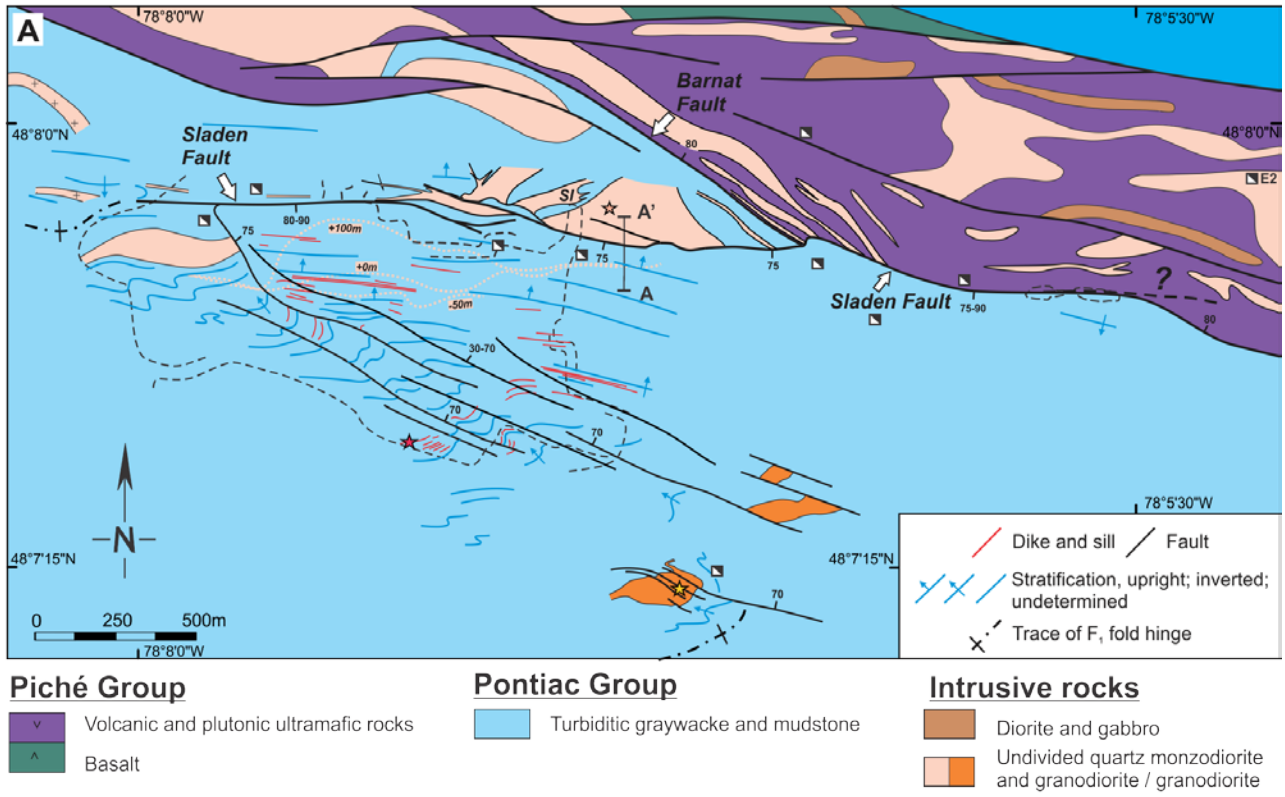

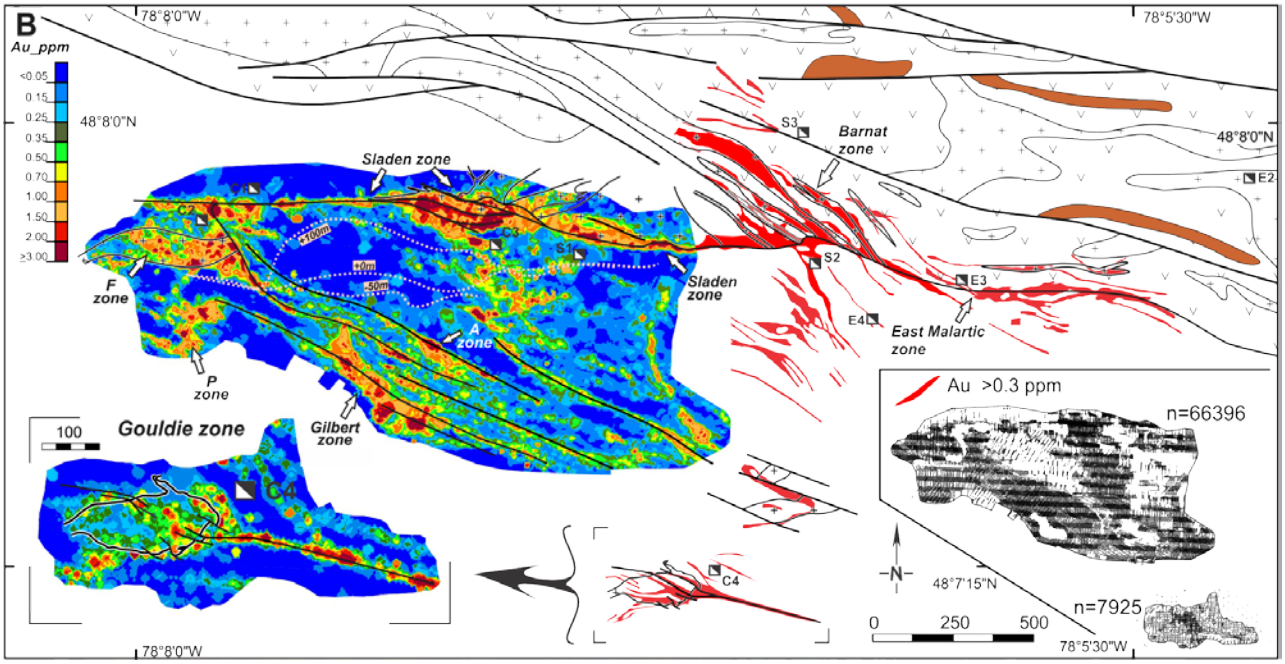

Figure 8.2. a Geological map of the Canadian Malartic Mine and surrounding area. The stippled pink lines represent the projection to surface of the quartz monzodiorite porphyry at + 100 m, + 0 m, and - 50 m relative to sea level. Filled stars indicate the location of samples collected for U-Pb zircon geochronology. **b** Surface distribution of gold. Shaded colors correspond to an interpolation of blast holes and RC drilling assay data. Red mineralized zones represent a compilation of exploration RC and diamond drill assays (Data from Canadian Malartic partnership). Inset shows the distribution of data points used for the interpolation.

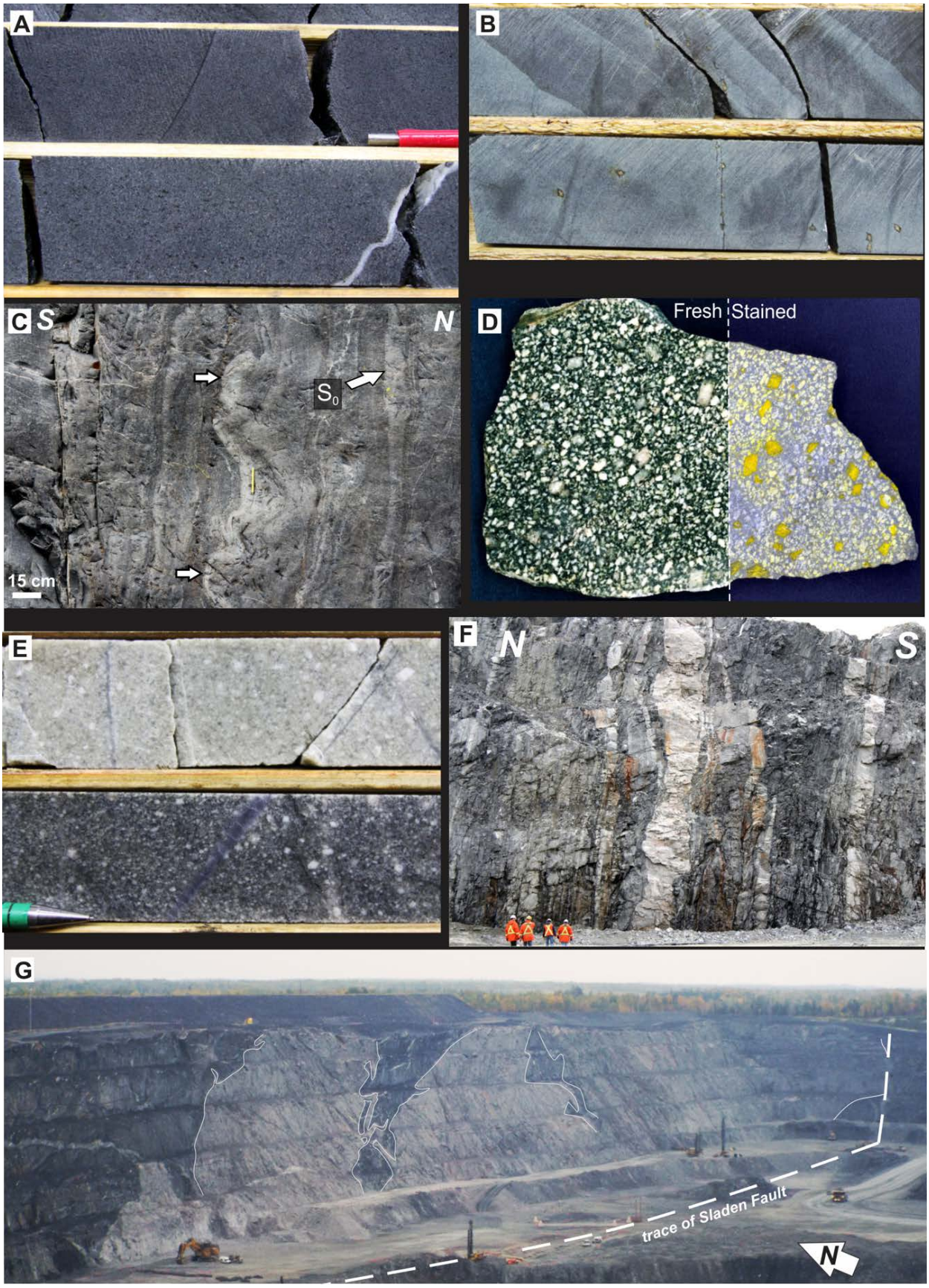
A
B
C
S
N
S_0
15 cm
D
Fresh
Stained
E
F
N
S
G
trace of Sladen Fault
N

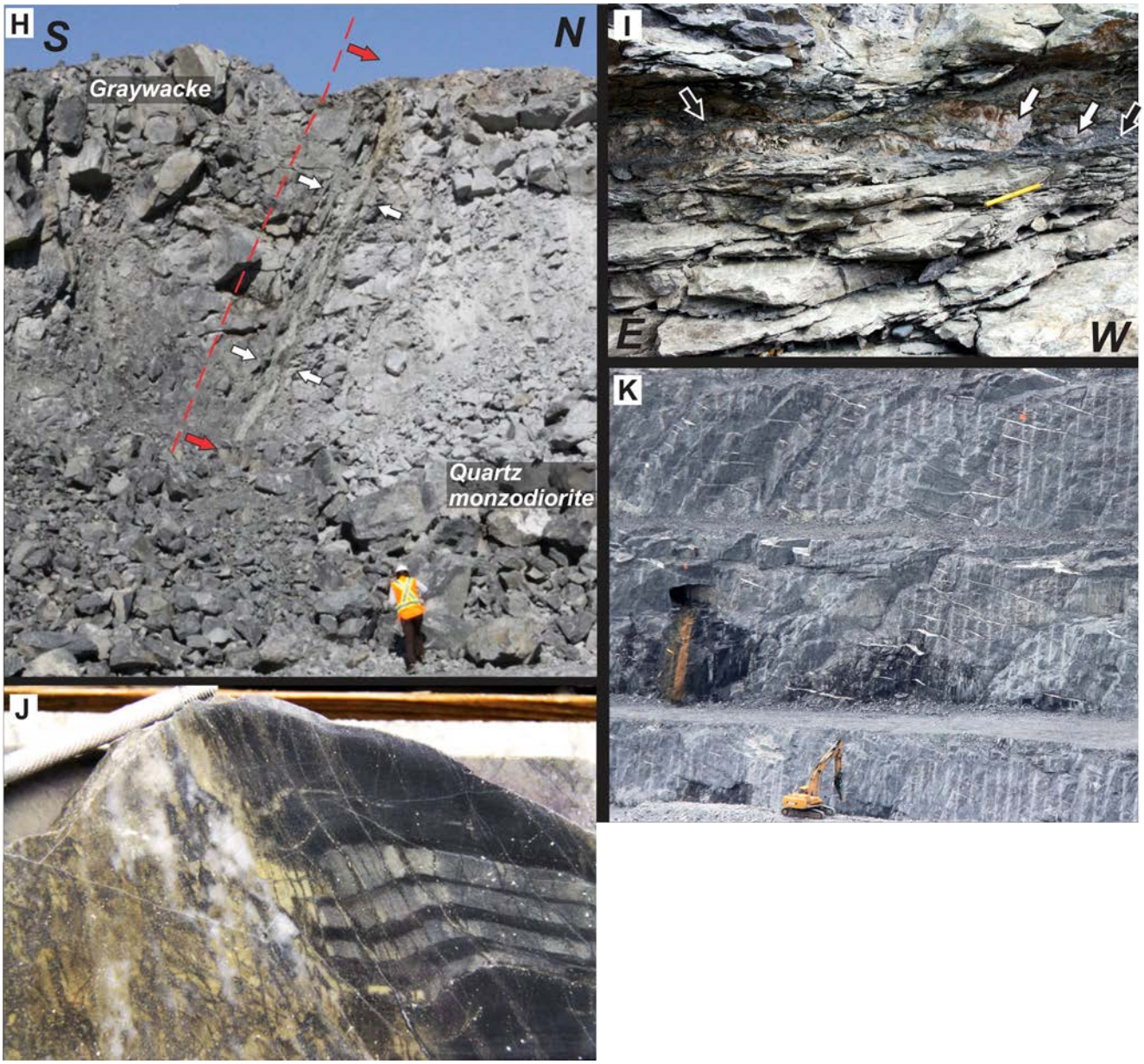

Figure 8.3. Host rocks of the Canadian Malartic gold Mine. **a** Pontiac Group graywacke. **b** Mudrock. **c** Graywacke with load structures indicating a north-younging sequence (white arrows). **d** Sladen zone quartz monzodiorite with cobaltinitrite staining of K-feldspar (yellow). **e** Gouldie zone granodiorite. **f** Swarm of felsic sills intruded into sedimentary rocks of the Pontiac Group. **g** Panoramic view looking northeast at the Sladen zone intrusion. **h** Looking west at Sladen Fault, showing altered quartz monzodiorite in the footwall and graywacke in the hanging wall. The main proximal alteration in the hanging wall is delimited by the red arrows and stippled line, whereas the main brittle deformation envelop is delimited by the white arrows. **i** Looking down at Sladen Fault, with altered graywacke in the hanging wall (upper half) and carbonate-feldspar-altered quartz monzodiorite with mylonitic foliation overprinted by thin gouge zones (black arrows) containing folded and dismembered quartz veins (white arrows). **j** Biotite- (black) and sericite-altered (greyish green) folded sedimentary rock with development of proximal (beige) alteration. Stratification is cut at high-angle by quartz-calcite veinlets with biotite selvages, and by a sub-parallel quartz-matrix breccia with related beige proximal alteration. Note the preferential replacement of mudstone over siltstone. **k** Section view showing en echelon barren extensional quartz veins preferentially hosted by competent greywacke, Pontiac Group sediment, south wall of the open pit.

Pyrite is the main sulfide mineral and reaches up to 5-7 modal percent. Tellurides are common and the main elements that define the chemical signature of the ore are Au-Te-W ± Ag-Bi-Mo-Pb. The Sladen Fault is marked by high strain zones distributed either along, or close to the contact between the quartz monzodiorite and the sedimentary rocks; a late brittle fault with unconsolidated breccia and/or gouge is also generally present.

8.5 Genetic model and conclusion

Based on our detailed observations and documented relationships between the ore zones, D_2 structures, and mineralized intrusions, we suggest that D_2 initiated with the formation of the penetrative S_2 foliation and folding of the Pontiac Group strata. Increasing strain and folding resulted in shearing along fold limbs and formation of faults and veinlets along S_2 cleavage planes, especially in the F_2 fold hinge zones. As a result, the bulk of the mineralization is interpreted to have occurred after development of the syn-D_2 metamorphic biotite. Hydrothermal alteration and mineralization were penecontemporaneous with the syn- to late- D_2 brittle and brittle-ductile deformation increments, but pre-barren shallow dipping extensional quartz veins. As synthesized by Poulsen et al. (2000), many genetic models have been proposed to explain the genesis of the Canadian Malartic mine, including a syngenetic model of gold deposition in silicified graywacke of the East Malartic mine (Kerrich 1983) and a gold porphyry deposit model (Issigonis 1980). More recently, Robert (2001) included Canadian Malartic in the syenite-associated disseminated gold deposit type. Helt et al. (2014) identified Canadian Malartic as a type-example of the oxidized intrusion-related gold deposit subclass of the more inclusive intrusion-related deposit clan (Sillitoe 1991; Goldfarb et al. 2005).

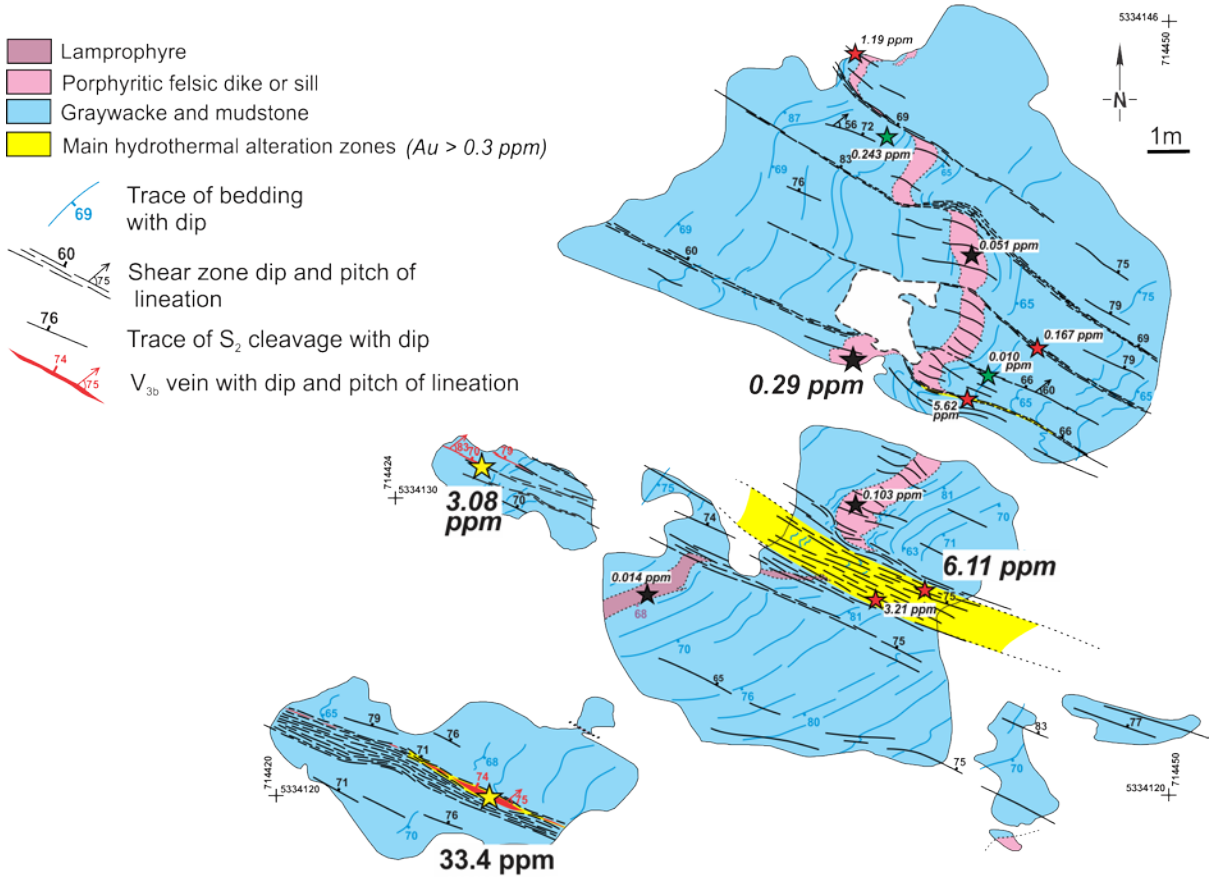

Figure 8.4. Detailed geological map of the SE extension of the mineralized Gilbert zone. Stars locate assayed samples with values in ppm Au; Black = intrusive rocks; green unaltered and distally altered sedimentary rocks; Red = proximally altered sedimentary rocks; Yellow = alteration zones and/or vein.

In light of the new field, geochemical, geochronological, and mineral chemistry data, additional comparisons can be made with gold deposits of the Abitibi greenstone belt and elsewhere. The presence of widespread potassic alteration, the Au-Te-W ± Ag-Bi-Mo-Pb metallic signature of the ore, and the spatial association of mineralization with porphyritic intrusions, are reminiscent of gold deposits associated with alkaline magmatism (Jensen and Barton 2000; Robert 2001) and reduced intrusion-related deposits (e.g., Goldfarb et al. 2005; Hart 2007), and are elements that are coherent with a magmatic-hydrothermal system, as proposed by Helt et al. (2014). Nevertheless, intrusions at Canadian Malartic are not reduced and a simple magmatic-hydrothermal model for the Canadian Malartic mine cannot entirely explain its timing, geometry, and geochemistry. In fact, the relationships and characteristics documented for the auriferous veins, stockworks, and disseminated ore bodies,

have also been described from clastic sedimentary rock-hosted Proterozoic and Phanerozoic orogenic gold deposits (e.g. Bierlein and Crowe 2000; Partington and Williams 2000). Aside from the absence of As, the combination of widespread carbonate alteration, the overall low Cu, Zn, and Pb contents, CO_2, K_2O, Na_2O, and S metasomatism, spatial association with brittle-ductile faults, shear zones and fold hinges, and the metallic signature of the ore are all common features of Archean orogenic gold deposits in metamorphic terranes (Groves et al. 1998; Hagemann and Cassidy 2000; Goldfarb et al. 2005). Most importantly, field evidence suggests that hydrothermal alteration, disseminated ore bodies and vein networks are associated with widespread brittle and brittle-ductile structures formed as a result of D_2 deformation, including F_2 folds in the Pontiac Group. There is thus a link between gold mineralization and the post-Timiskaming D_2 phase of deformation, and especially with faults and shear zones formed late during the evolution of F_2 folding, in the hinges and along short limbs of folds (De Souza et al. 2015, 2017). Overprinting of the metamorphic biotite, muscovite, chlorite, and oligoclase by hydrothermal carbonates, phlogopite, phengitic sericite, and feldspar, suggests that mineralization was syn- to late-dynamothermal metamorphism. The absolute age of gold mineralization is estimated at 2664 ±11 Ma by Re-Os dating of ore-related molybdenite (De Souza et al. 2015, 2017), and corresponds to the age bracket attributed to metamorphism in the Pontiac Group following Timiskaming sedimentation (2670-2660 Ma; Powell et al. 1995; Easton 2000).

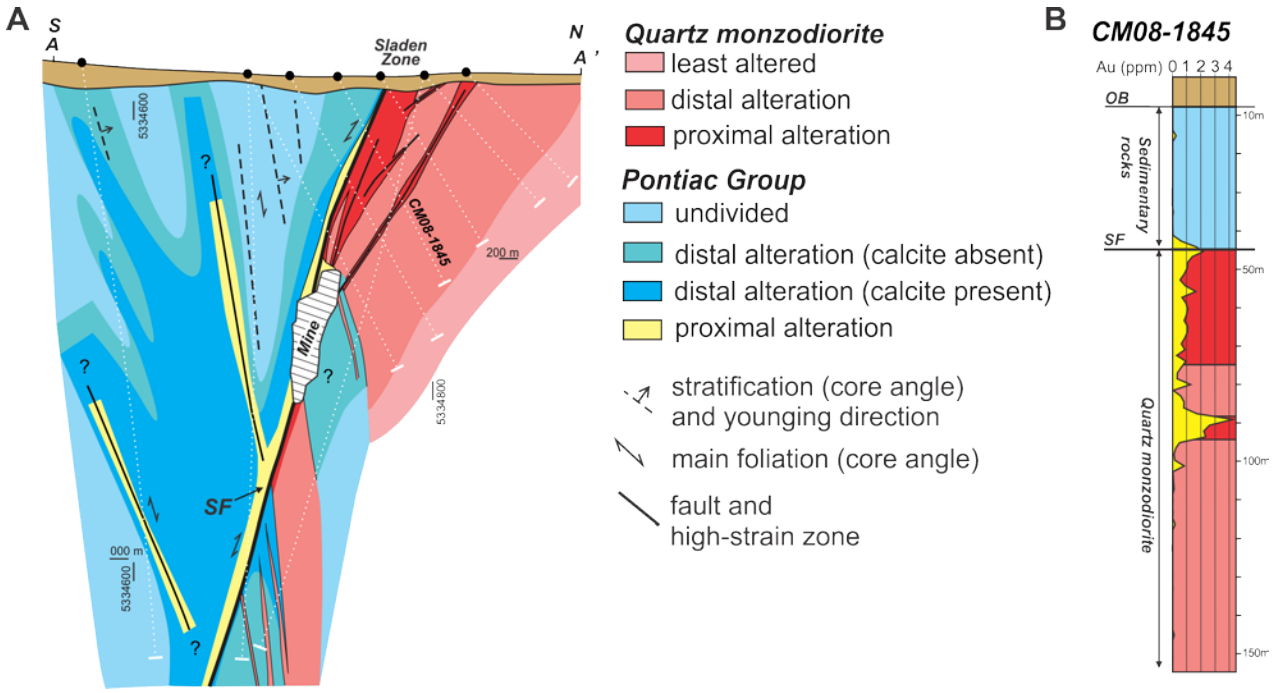

Figure 8.5. a Geological section across the Sladen zone (section 4790; see Figure 8.2a for location of section). **b** Simplified geological log and gold assays for drill core CM08-1845. SF – Sladen Fault; OB – over burden. Assays provided by Canadian Malartic Partnership.

Widespread devolatization of the Pontiac Group sedimentary rocks, during this episode of metamorphism, provides the needed conditions for the generation of large volumes of S-, CO_2-, K-, and potentially Au-rich hydrothermal fluids in amphibolite-grade rocks, and focusing of these fluids into upper greenschist facies rocks along the LLCFZ, the Sladen Fault and other D_2 structures. Beaudoin and Raskevicius (2014) obtained $\delta^{18}O$ and δD values of 6.3 to 10.9 ‰ and of -4 to -11‰ for hydrothermal minerals, respectively. These isotopic values correspond to metamorphic rather than magmatic-hydrothermal waters, which is consistent with a syn-D_2 episode of hydrothermal alteration. Perrouty et al. (2017) propose a similar scenario, but in which auriferous magmatic-hydrothermal fluids were derived from the ca. 2668-2663 Ma Decelles batholith (Mortensen and Card 1993) or similar granitoid rocks in the Pontiac Group. Disequilibrium between the hydrothermal fluid and the host sedimentary and intrusive rocks resulted in chemical gradients necessary for widespread carbonatization and potassic alteration (calcite-sericite-biotite), followed by intense feldspathic and carbonate (calcite and dolomite) replacement zones, sulfidation, and gold deposition along the main structures. Contribution to the total gold endowment of the Canadian Malartic Mine by an early, syn-Timiskaming magmatic-hydrothermal phase of mineralization, as proposed by Helt et al. (2014) and De Souza et al. (2015) cannot be excluded. As such, the main characteristics of the Canadian Malartic deposit can also be explained by syn-D_2 deformation gold (ca. 2670–2660 Ma)

superimposed onto, or in part remobilized from, a gold-bearing magmatic/hydrothermal system related to Timiskaming-age porphyritic intrusions emplaced along the LLCFZ.

As illustrated by the underground workings of the past-producing mines and the distribution of the ore bodies, and not unlike the Main Break at Kirkland Lake (Ispolatov et al., 2008), the Sladen Fault zone hosts much of the higher-grade ore at Canadian Malartic and represents one of the main hydrothermal fluid conduits for the upflow of the Au-bearing hydrothermal fluids. The variable geometry, rheology, and composition of the various intrusive and sedimentary rocks, have provided strain heterogeneities and chemical gradients for the formation of structural and chemical traps that host the gold. This is well illustrated where large mineralized envelops are preferentially developed in intrusive rocks, at the intersection with mineralized northwest-trending D_2 faults in the Gouldie and F zones, and in the footwall of the Sladen Fault. Moreover, D_1 shortening at ~ 2682-2680 Ma, and formation F_1 folds in the Pontiac Group, prior to the deposition of the Timiskaming conglomerate and to the flare-up of alkaline magmatism that characterizes the Timiskaming episode (Bleeker 2015), may have contributed to control the emplacement of the quartz monzodiorite and other dikes and sills along verticalized bedding, and as proposed by Perrouty et al. (2017), to the emplacement of some of the intrusions in F_1 fold hinge zones.

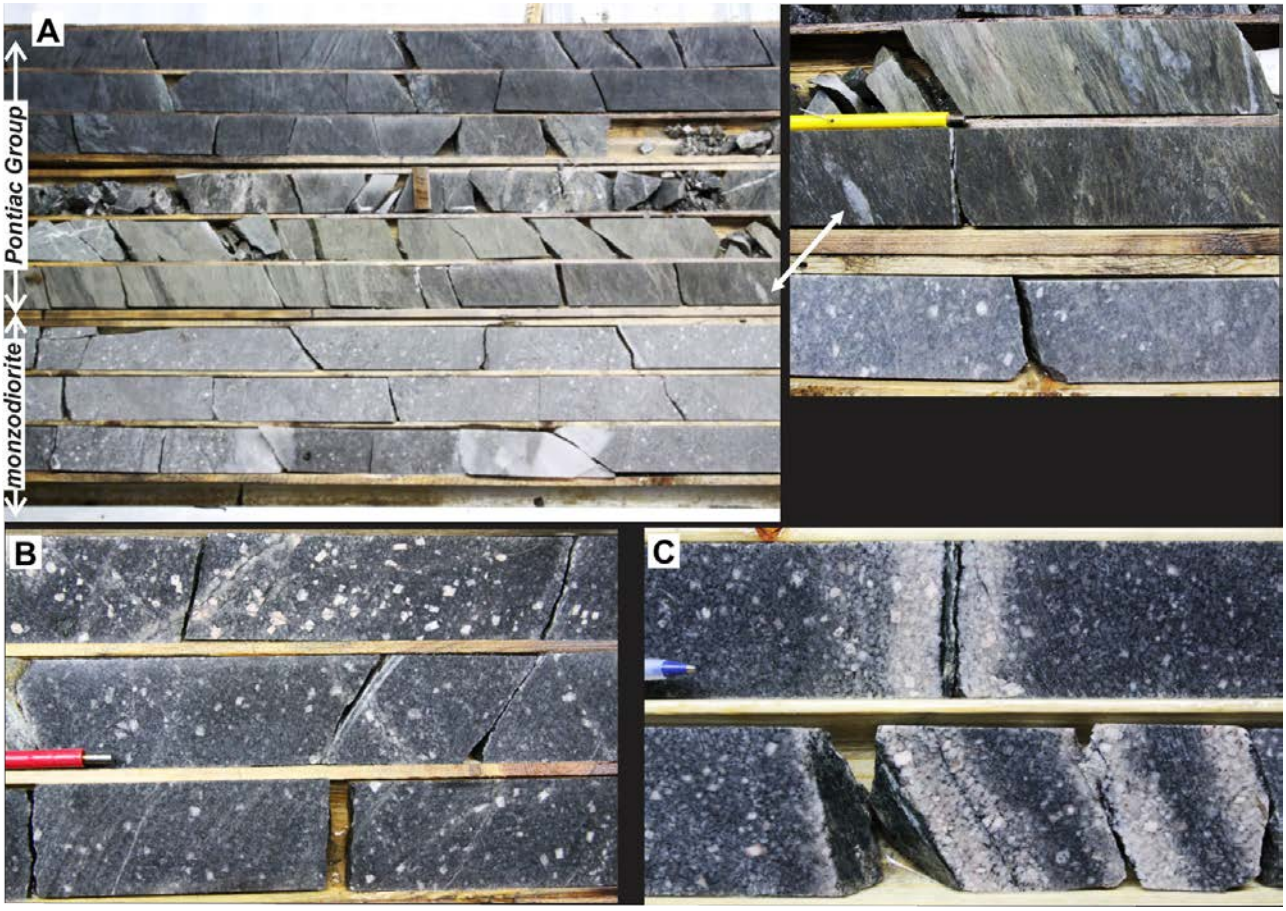

Figure 8.6. Mineralized and hydrothermally altered sedimentary rocks and quartz monzodiorite along section 4790. **a** Deformation zone along Sladen Fault with altered sedimentary rocks (grey to tan) in the hanging wall and quartz monzodiorite in the footwall (grey). **b** Distal calcite-hematite alteration in the quartz monzodiorite. **c** Quartz-carbonate-biotite-pyrite veinlet with proximal feldspar-carbonate pink alteration halo in quartz monzoriotite.

8.6 Acknowledgements

The Canadian Malartic Mine exploration and geology teams are acknowledged for giving access to their operations, and for their ongoing support during research, especially Donald Gervais, Gregory Poirier, Marie-Claude Brunet-Ladrie, and François Bouchard for organizing and leading part of the field visit.

8.7 References

Beaudoin G, Raskevicius T (2014) Constraints on the genesis of the Archean oxidized, intrusion-related Canadian Malartic gold deposit, Quebec, Canada - A discussion: Econ Geol 109: 2067–2068

Belzile E, Gignac LP (2011) Updated resource and reserve estimates for the Canadian Malartic project Malartic, Quebec: NI 43-101 Report, 261 p.

Bierlein FP, Crowe DE (2000) Phanerozoic orogenic lode gold deposits. Reviews in Economic Geology 13: 103–139

Bleeker W (2015) Synorogenic gold mineralization in granite-greenstone terranes: the deep connection between extension, major faults, synorogenic clastic basins, magmatism, thrust inversion, and long-term preservation, *In:* Targeted Geoscience Initiative 4: Contributions to the Understanding of Precambrian Lode Gold Deposits and Implications for Exploration, (ed.) B. Dubé and P. Mercier-Langevin; Geological Survey of Canada, Open File 7852: 25–47

Corfu F (1993) The evolution of the southern Abitibi greenstone belt in light of precise U-Pb geochronology, Econ Geol 88: 1323-1340

Cormie JM (1948) East Malartic Mine: Structural Geology of Canadian Ore Deposits, A Symposium Arranged by a Committee of the Geology Division, Canadian Institute of Mining and Metallurgy: 865–867

Davis DW (2002) U-Pb geochronology of Archean metasedimentary rocks in the Pontiac and Abitibi Subprovinces, Quebec, constraints on timing, provenance and regional tectonics: Precambrian Res 115: 97–117

Derry DR (1939) The geology of the Canadian Malartic gold mine, N. Quebec: Econ Geol 34: 495–523

De Souza S, Dubé B, McNicoll VJ, Dupuis C, Mercier-Langevin P, Creaser RA, Kjarsgaard IM (2015) Geology, hydrothermal alteration, and genesis of the world-class Canadian Malartic stockwork-disseminated Archean gold deposit, Abitibi, Quebec, *In:* Targeted Geoscience Initiative 4: Contributions to the Understanding of Precambrian Lode Gold Deposits and Implications for Exploration, (ed.) B. Dubé and P. Mercier-Langevin; Geological Survey of Canada, Open File 7852: 113–126

De Souza S, Dubé B, McNicoll VJ, Dupuis C, Mercier-Langevin P, Creaser RA, Kjarsgaard IM (2017) Geology and hydrothermal alteration of the world-class Canadian Malartic gold deposit: genesis of an Archean stockwork-disseminated gold deposit in the Abitibi Greenstone Belt, Québec: Reviews in Economic Geology 19: in-press.

Dubé B, Gosselin P (2007) Greenstone-hosted quartz-carbonate vein deposits, in Goodfellow, W.D., ed., Mineral deposits of Canada: A synthesis of major deposit-types, district metallogeny, the evolution of geological provinces, and exploration methods: Mineral Deposits Division, Geol Assoc Canada, Special Publication 5: 49–73

Easton RM (2000) Metamorphism in the Canadian Shield, Ontario, Canada. I. The Superior Province: Can Miner 38: 287-317

Eilu PK, Mathison CI, Groves DI, Allardyce WJ (1999) Atlas of Alteration assemblages, styles and zoning in orogenic lode-gold deposits in a variety of host rock and metamorphic settings: The University of Western Australia, Publication 30, 50 p.

Fallara F, Ross PS, Sansfaçon R (2000) Caractérisation géochimique, pétrographique et structurale: Nouveau modèle métallogénique du camp minier de Malartic: Ministère des Ressources Naturelles du Québec, report MB 2000-15, 161 p.

Fallara F, Ross PS, Sansfaçon R, Grant M (2005) Lac Fournière: Ministère des Ressources Naturelles du Québec, Geological compilation map 32D01-200-0102, 1:20,000.

Goldfarb RJ, Baker T, Dubé B, Groves DI, Hart CJR, Gosselin P (2005) Distribution, character, and genesis of gold deposits in metamorphic terranes: Econ Geol 100th anniversary vol: 407–450

Groves DI, Goldfarb RJ, Gebre-Mariam M, Hagemann SG, Robert F (1998) Orogenic gold deposits: A proposed classification in the context of their crustal distribution and relationship to other gold deposit types: Ore Geology Rev 13: 7-27

Hagemann SG, Cassidy KF (2000) Archean orogenic lode gold deposits: Reviews in Economic Geology 13: 9–68

Hart CJR (2007) Reduced intrusion-related gold systems, in Goodfellow, W.D., ed., Mineral deposits of Canada: A synthesis of major deposit-types, district metallogeny, the evolution of geological provinces, and exploration methods: Mineral Deposits Division, Geol Assoc Canada, Special Publication 5: 95–112

Helt KM, Williams-Jones AE, Clark JR, Wing BA, Wares RP (2014) Constraints on the genesis of the Archean oxidized, intrusion-related Canadian Malartic gold deposit, Quebec, Canada: Econ Geol 109: 713–735

Ispolatov V, Lafrance B, Dubé B, Creaser R, Hamilton M (2008) Geologic and structural setting of gold mineralization in the Kirkland Lake-Larder Lake gold belt, Ontario: Econ Geol 103: 1309–1340

Issigonis MJ (1980) Occurrence of disseminated gold deposits in porphyries in Archean Abitibi belt, northwest Quebec, Canada: Institution of Mining and Metallurgy London, Transactions, Section B: Applied Earth Sciences 89: 157–158

Kerrich R (1983) Geochemistry of gold deposits in the Abitibi greenstone belt: Canadian Institute of Mining and Metallurgy, Special Volume 27, 75 p.

Jensen EP, Barton MD (2000) Gold deposits related to alkaline magmatism: Reviews in Economic Geology 13: 279–314

Mortensen JK, Card KD (1993) U-Pb age constraints for the magmatic and tectonic evolution of the Pontiac Subprovince, Quebec: Canadian Journal of Earth Sciences 30: 1970–1980

O'Neil JJ (1935) La mine d'or Canadian Malartic, Comté d'Abitibi: Service des Mines de Québec, rapport annuel, Partie B : 69–99

Partington GA, Williams PJ (2000) Proterozoic lode gold and (iron)-copper-gold deposits: A comparison of Australian and global examples: Reviews in Economic Geology 13: 69–101

Perrouty S, Gaillard N, Piette-Lauzière N, Mir R, Bardoux M, Olivo GR, Linnen RL, Bérubé CL, Lypaczewski P, Guilmette C, Feltrin L, Morris WA (2017) Structural setting for Canadian Malartic style of gold mineralization in the Pontiac Subprovince, south of the Cadillac Larder Lake Deformation Zone, Québec, Canada: Ore Geology Rev 84: 185-201

Pilote P (2013) Géologie – Malartic: Ministère des Ressources Naturelles du Québec, map CG-32D01D-2013-01, 1:20,000.

Poulsen KH, Robert F, Dubé B (2000) Geological classification of Canadian gold deposits: Geological Survey of Canada Bulletin 540, 106 p.

Powell WG, Hodgson CJ, Hanes JA, Carmichael DM, McBride S, Farrar E (1995) $^{40}Ar/^{39}Ar$ geochronological evidence for multiple postmetamorphic hydrothermal events focused along faults in the southern Abitibi greenstone belt: Canadian J Earth Sci 32: 768-786

Robert F (2001) Syenite-associated disseminated gold deposits in the Abitibi greenstone belt, Canada: Miner Dep 36: 503–516

Robert F, Brown AC (1986) Archean gold-quartz veins at the Sigma mine, Abitibi greenstone belt, Quebec. Part 1: Geologic relations and formation of the vein system: Econ Geol 81: 578-592

Sansfaçon R, Hubert C (1990) The Malartic gold district, Abitibi greenstone belt, Québec: Geological setting, structure and timing of gold emplacement at Malartic Gold Fields, Barnat, East-Malartic, Canadian Malartic and Sladen Mines, in Rive M, Verpaelst P, Gagnon Y, Lulin JM, Riverin G, Simard A, eds., The northwestern Quebec polymetallic belt: A summary of 60 years of mining exploration: The Canadian Institute of Mining and Metallurgy, Special Volume 43: 221–235

Sillitoe RH (1991) Intrusion-related gold deposits. *In* Gold Metallogeny and Exploration, Blackie, Glasgow and London: 165-209

Trudel P, Sauvé P (1992) Synthèse des caractéristiques géologiques des gisements d'or du district de Malartic: Ministère de l'Énergie et des Ressources du Québec, report MM 89-04, 113 p.

Thurston PC, Ayer JA, Goutier J, Hamilton MA (2008) Depositional gaps in Abitibi greenstone belt stratigraphy: A key to exploration for syngenetic mineralization: Econ Geol 103: 1097–1134

Chapter 9: (Day 5 – Part II) The “Malartic Lake Shore” gold showing and the Rivière-Héva Fault Zone, Abitibi, Québec, Canada

Francis Guay
Université du Québec à Chicoutimi

Pierre Pilote
Ministère de l'Énergie et des Ressources naturelles du Québec

Réal Daigneault
Université du Québec à Chicoutimi

Vicki McNicoll
Natural Resources Canada – Geological Survey of Canada

9.1 Introduction

The Archean Abitibi Subprovince is well-known for its gold endowment especially along major fault zones or breaks such as the Cadillac Fault Zone (CFZ) (e.g., Robert 1989; Dubé and Gosselin 2007; Bedeaux et al. 2017). Major fault zones are considered as preferential conduits for magmatic intrusion and hydrothermal activity (Robert 1996). Typical orogenic gold quartz veins are well defined in the Val-d'Or area that is a type locality with the Sigma-Lamaque world-class deposits (Robert and Brown 1986). In these deposits, gold-quartz-tourmaline-carbonate veins occupy subvertical to moderately dipping shear zones associated with subhorizontal extensional veins that are particularly well developed in competent intrusive bodies. The association between gold endowment and vein-type deposits within or in proximity to major fault or shear zones is therefore quite a common feature. However, early “pre-regional deformation” or pre-main shortening gold systems have been well documented in the Val-d'Or area in a number of deposits such as the Norlartic mine (Couture et al. 1994), the Siscoe mine (Backman 1936; Sauvé et al. 1993; Rober, 1994), and the Orion no. 8 deposit (Bertrand-Blanchette 2016). Such early vein-type deposits, considered as synvolcanic in many cases, also occur elsewhere in the Québec side of the Abitibi and are considered as equivalents to submarine magmatic-hydrothermal systems, with examples such as the Géant Dormant (Gaboury and Daigneault 1999) and Chevrier deposits (Legault and Daigneault 2006). When those early vein-type gold deposits occur in major deformation zones, their synvolcanic origin is difficult to determine with confidence.

The Malartic Lake shore showing, which is currently the subject of an ongoing MSc project by the senior author, is a vein-type gold prospect (Bousquet and Carrier 2008; Guay et al. 2016) located directly within the Rivière-Héva Fault Zone (RHFZ) in the southern Abitibi greenstone belt (Fig. 9.1). This major fault zone separates felsic units belonging to the 2702-2700 Ma Héva Formation from the 2708 Ma mafic-ultramafic sequences belonging to the Dubuisson Formation. The occurrence of several narrow cm-thick quartz veins rich in gold, silver, galena, and other metals that are subparallel with the main fabric, their association with intermediate and lamprophyric dike swarms, and the potassic alteration represent the main characteristics of this showing. We propose that the Malartic Lake Shore gold showing represents a good example of a pre-main regional deformation ore deposit type.

9.2 Geological setting

This Malartic Lake gold showing, or the study area (Figs. 9.1 and 9.2), is located in the Southern part of the Archean Abitibi Subprovince, at the interface between two major group units, the Malartic and the Louvicourt groups.

The 2714-2706 Ma Malartic Group (Imreh 1984; Pilote et al. 1999; Pilote 2000) consists of an intercalation of ultramafic and mafic flows of tholeiitic affinity. This group is subdivided into the La Motte-Vassan, Dubuisson, and Jacola formations to the top and globally seen as a deep oceanic floor volcanic environment (Pilote 2000; Scott et al. 2002). The 2705-2700 Ma Louvicourt Group (Pilote 2000; Scott et al. 2002), conformable on the Malartic Group, is divided into the Val-d'Or Formation and Héva Formation at the top. Intermediate to felsic flows and volcaniclastic rocks of the Val-d'Or Formation display a transitional to calc-alkaline affinity and are interpreted to have been formed in an arc-type environment (Scott et al. 2002). The 2702-2700 Ma Héva Formation contains mafic flows of tholeiitic affinity and minor felsic volcaniclastite of transitional to calc-alkaline affinity (Scott et al. 2002).

The showing area consists of two large stripped outcrops adjacent one another (Fig. 9.2). The western outcrop is 150 x 40 m-wide while the eastern one is 90 x 65 m-wide. The western outcrop is dominated by an

assemblage of mafic pillowed volcanic rocks associated with komatiitic basalt. Pilote et al. (2014) interpreted this sequence as part of the 2708 Ma Dubuisson Formation (Malartic Group). The eastern outcrop displays the contact between the previous assemblages with felsic volcaniclastic rocks belonging to the 2702 Ma Héva Formation (Louvicourt Group). The area is metamorphosed to the upper greenschist facies (Pilote et al. 2014) and display the effect of a strong ductile deformation associated with the RHFZ. The subvertical regional or "main schistosity" (Sp) within the deformation zone is roughly NW-trending but described a flexion from NNW to NW trending from west to east within the two outcrops.

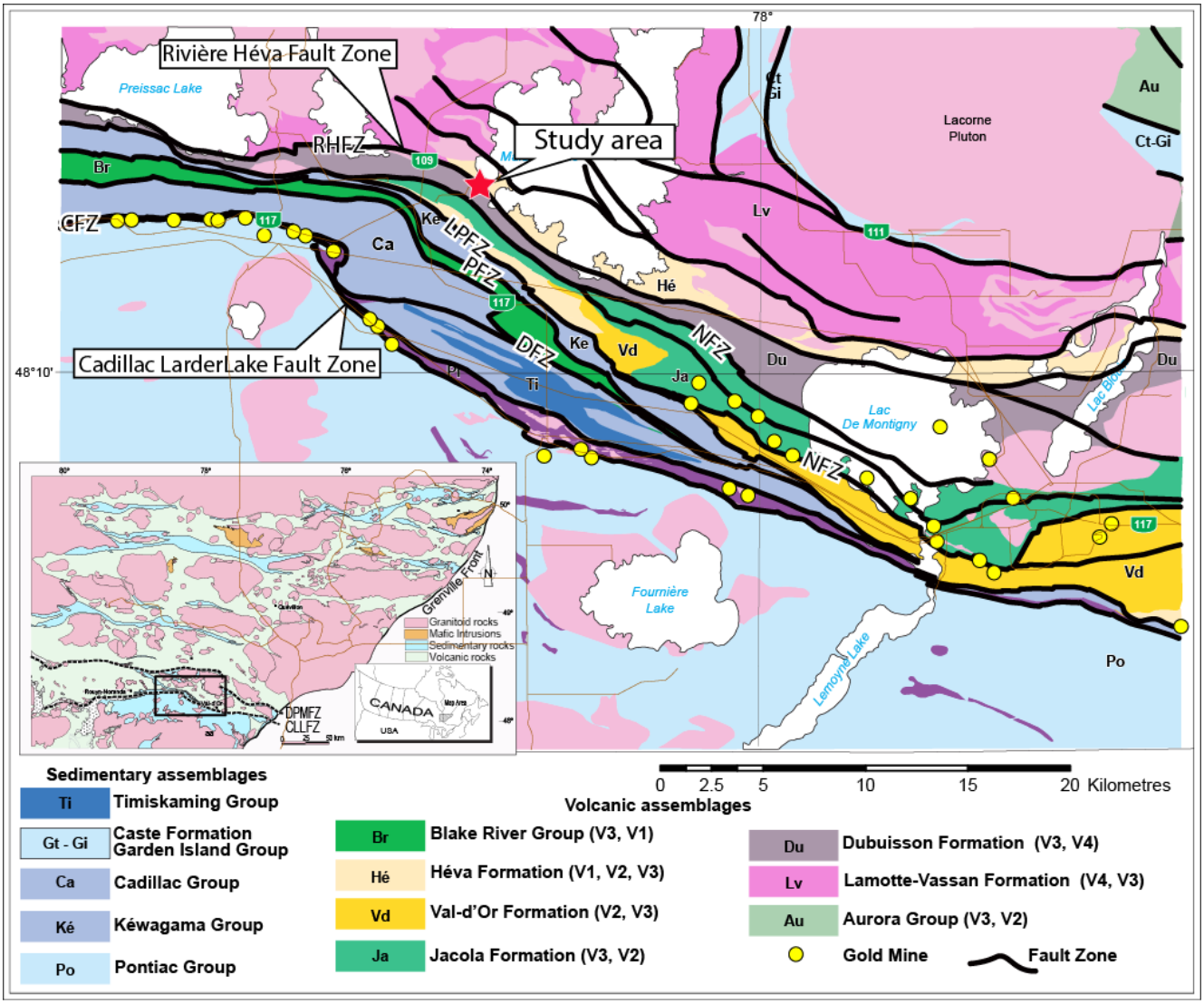

Figure 9.1. Simplified geology of the Val-d'Or – Malartic area (Daigneault 1996; Pilote 2013; Pilote et al. 2014; Sigeom-MERN database). DFZ = Destor faul zone, LPFZ = La Pause fault zone, NFZ = Norlartic fault zone, PFZ = Parfouru fault zone, RHFZ = Rivière-Héva fault zone.

These outcrops (Fig. 9.2) expose a series of intermediate to mafic dikes. These dikes are usually 5 to 30 cm in thickness and follow the attitude of the principal schistosity. A number of those dikes are described as lamprophyres (Bousquet and Carrier 2008; Guay et al. 2016).

Numerous auriferous quartz veins are present; they are mainly located on the western outcrop. These veins contain pyrite, chalcopyrite, and galena. They are strongly affected by the deformation (boudinage, folding, and transposition) and are systematically truncated by all dike families, which implies an early origin for the auriferous vein system.

This showing is located directly along the RHFZ (Fig. 9.1). The fault corresponds to the contact between the felsic units belonging to 2702 Ma Héva Formation to the northeast with the mafic-ultramafic unit belonging to the 2708 ma Dubuisson Formation to the southwest. The fault is associated with a km-scale ductile deformation corridor characterized by a strongly developed Sp fabric. The fault zone, which in fact consists of a series of parallel, discrete

faults and their associated high-strain envelope, can be followed for more than 100 km from west to east (Pilote et al. 2014). Detailed mapping in this area (Pilote 2013; Pilote et al. 2014) has established that all units are vertical to subvertical and are facing south.

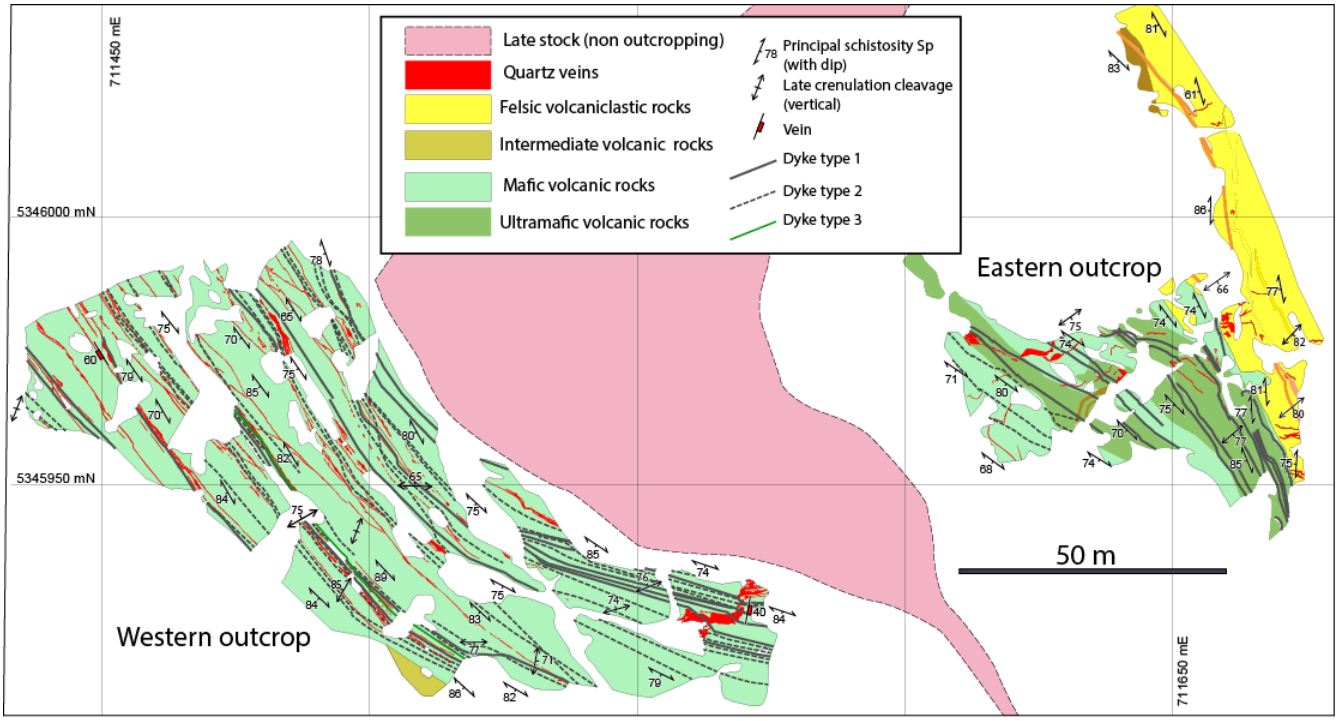

Figure 9.2. Simplified geology of the western and eastern outcrops, adapted from Guay et al. (2016) and modified from Bousquet and Carrier (2008, 2009a, and 2009b).

9.3 Main observations

The western and eastern outcrops of the Malartic Lakeshore showing are characterized by the development of strong planar and linear fabrics. The main regional, schistosity (Sp, or S1) strikes SE with a regular strong dip to the SW. This schistosity bends slightly near the southern end of the Western outcrop, where the strike varies from N160° to N105°.

Strain partitioning is observed with respect of the Sp intensity. To visualize the variation of this intensity, a field anisotropy index (AI) is used to qualify the degree of planar fabric development (Daigneault 1996). This index, based on visual inspection of the rock, varies from 0 (no fabric) to 5 (strong mylonitic fabric) and helps estimate the degree of structural anisotropy at various scales. An AI lower than 3 represents rocks with preserved primary volcanic or sedimentary features while an AI over 3 is attributed to rocks dominated by secondary structural features (fabrics). The purpose of this index is not to make a direct assessment of strain intensity since strain markers are relatively rare in this volcanic context. But the index is quite useful to describe strain variability especially within the same rock type. The AI was attributed to a homogeneous surface of 1 to 5 square meters where structural measurements were performed (Fig. 9.3). The resulting map shows several anastomosed corridors of much higher strain. Several of these corridors are centred on ubiquitous quartz veins which will be discussed further below. Structural anisotropy culminates to the east at the contact between mafic volcanic units and a felsic volcaniclastic unit, the latter displaying a strong mylonitic fabric.

The stretching lineation (Ls) is expressed by the preferential elongation of minerals and crystals in the deformed rocks. Most of the Ls plunge through the SE with slight variations from moderate to shallow plunges (Fig. 9.4). Dip-slip lineations are present in rocks with moderate anisotropy index while strike-slip lineations become prevalent in high anisotropic deformation corridors and especially along the mafic-felsic contact on the eastern outcrop (Fig. 9.4).

The synthesis of the individual Sp fabric measurements (mean plane = N132°/79°) favors a southwest dip in general for the RHFZ. Stretching lineations are dip-slip in moderately deformed rocks while it becomes shallowly southeast plunging in higher-strain zones. This variation in attitude of the stretching lineations is interpreted as a transition from a regime dominated by shortening to a regime dominated by a lateral component of movement along the RHFZ even if no clear shear sense indicators were recognized in the two outcrop zones for this potential

late deformation increment. But the shortening event can be associated with a reverse movement along the RHFZ. The presence of the younger Héva Formation underneath the older Dubuisson Formation represents a stratigraphic inversion which can be explained by a reverse component of motion on the RHFZ. The implication(s) of this reverse component of motion will be discussed in the field.

Two main sets of crenulation cleavages are present in the study area, with a principal one being ENE-trending (075°/90°) (Fig. 9.4). The main ENE-trending family is locally associated with chevron folds mostly in the high strain zone present at the interface between the mafic-felsic group units. A north-south more discrete cleavage is also locally recognized without any folds association.

9.3.1 Veins

Two distinct sets of quartz veins are present. Type 1 includes the main set of gold-bearing veins which are present only in the mafic volcanic unit present on the western outcrop, and locally on the eastern outcrop. Type 2 consists of barren quartz veins with minor tourmaline and is present mostly in the felsic unit on the eastern outcrop. Only Type 1 will be discussed in more details below.

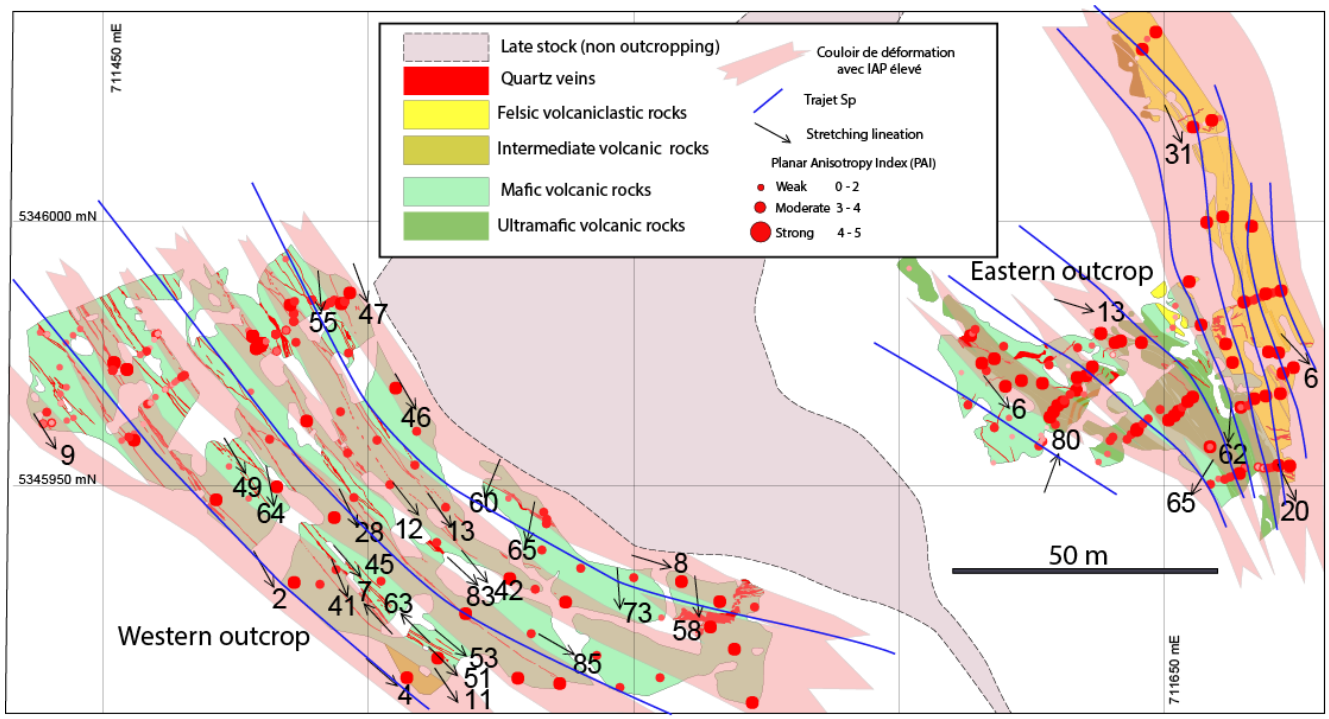

Figure 9.3. Distribution of stations, anisotropy index and trajectory of the main schistosity Sp.

9.3.3.1 Gold bearing quartz veins (Type 1)

Multiple Type 1 gold bearing quartz veins are present in the study area. The vein array is made off a series of subparallel veins displaying a mean spacing of 5 to 10 m. The 30 to 70 cm-thick veins are, for most of the western outcrop, subparallel in plan view with the main Sp fabric. They can be followed for more than 100-150 m each, but the array seems to have a wider extent exceeding the size of the outcrops. However, they display a shallower dip (60°) to the SW with respect to the Sp dip (75-80°). Pinch and swell veins are common and 30- to 50 cm-long boudins isolated from one another display a lenticular shape. Boudins axes are commonly subvertical.

The veins geometry change from the eastern to the western outcrop. Veins become folded, locally transposed and crosscut by the axial planar Sp fabric. Folds are open to locally tight with axes plunging at 40 degrees to the SE. The overall vein fold geometry forms an S-shape pattern that terminates at the contact with the felsic unit (Fig. 9.2).

9.3.2 Vein paragenesis

Veins consist of quartz (70-90%), with minor calcite (10-20%), barite (1-10%), and locally biotite, chlorite, and albite. The presence of barite in the veins was confirmed by µXRF analysis. It is relevant here to point out that this mineral was previously confused with albite, a mistake that could be quite common, in the absence of appropriate analyses.

Veins are banded, and their margins commonly consist of milky quartz while their centre presents a smokey quartz associated with sulfides, barite, and gold (Fig. 9.6). In thin section, quartz is generally granoblastic with triple junctions. But despite the deformation affecting all veins, some thicker ones display bands with preserved primary features such as intergrowth of idiomorphic centimetric quartz crystals interpreted as comb textures, well-formed

bipyramidal quartz crystals, open cavities, features collectively representing textures produced in an extensional regime.

Sulfide phases may represent 1-15% of the vein content, including pyrite, chalcopyrite, galena, and minor sphalerite. Some visible gold grains are present locally. Microprobe analysis of a selection of mineralized samples (Guay et al. 2016) revealed the presence of silver telluride and bismuth telluride spatially associated with visible gold. Gold concentration of 1300 ppm was measured within bismuth telluride and 42 800 ppm with silver telluride. Gold grains were analysed and contain systematically between 21 and 36% of silver, consisting of electrum (Guay et al. 2016).

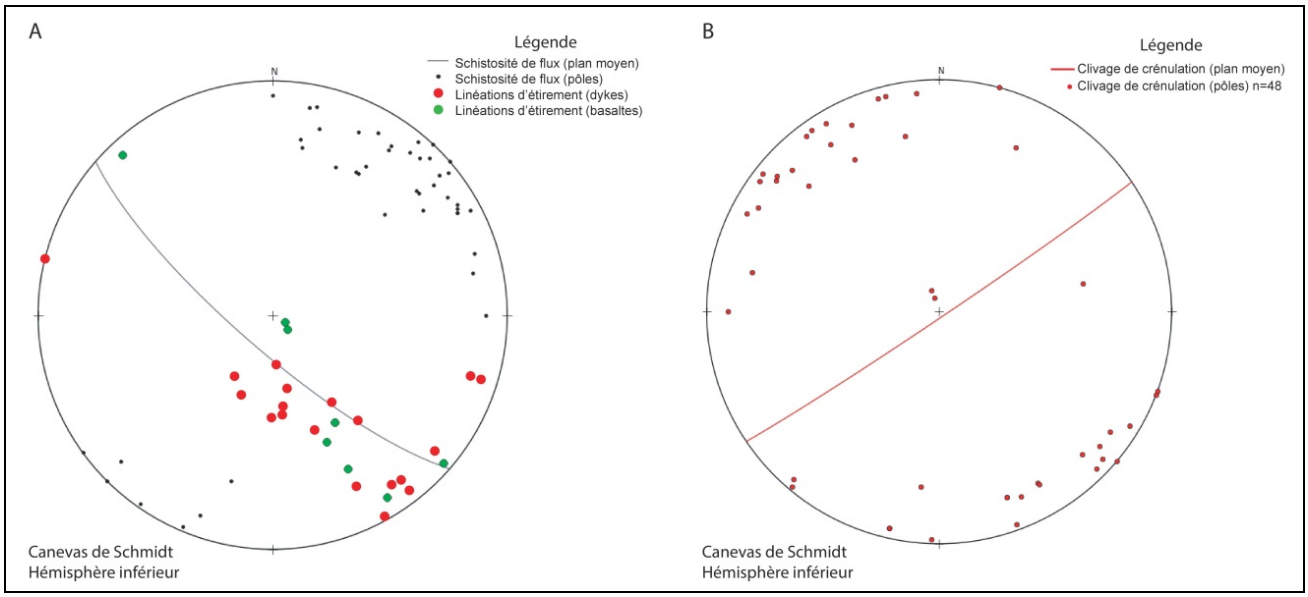

Figure 9.4. Schmidt stereographic projections. **a** Main schistosity Sp and stretching linations. **b** Crenulation cleavages.

9.4 Stop descriptions

The selected stops will allow participants to observe the auriferous quartz vein system and some features related to the evolution of the regional deformation in this area.

9.4.1 Stop 1 – Western outcrop

This outcrop is dominated by mafic volcanic flows (basalts) which are commonly pillowed. The pillows are strongly deformed (elongation ratio 1: 7) and face to the SW, which would correspond to the regional polarity reported in Pilote et al. (2014). Epidotized pillow cores are locally present. The intensity of the deformation is commonly high. The main schistosity is penetrative in the mafic units and a crenulation cleavage is commonly present in the most altered and deformed zones.

This outcrop is crosscut by a multitude of cm to dm-wide intermediate to mafic dikes, which can be separated into distinct mineralogical compositions: gabbro, quartz diorite, and lamprophyre.

Several auriferous veins are present on this stop (Fig 9.5). Two sets of veins are are particularly prominent depending on whether they are subparallel or at angle with the main schistosity. The veins that are at angle with the schistosity are thinner (5-10 cm) and are generally barren. The veins subparallel to the main schistosity are thicker (20-40 cm) and are longer, commonly up to tens of meters long. They are composed of quartz, calcite, barite, and albite. They are mineralized in pyrite, chalcopyrite, and galena and have gold contents of up to 178 g/t over 0.6 m in a selected sample (Bousquet and Carrier 2009a and b). Gold grains are visible locally. The veins have a composite (ribboned) texture, show open space filling textures which suggest several opening episodes. A dm-wide (up to 50 cm wide) black chlorite alteration is developed in the vein selvages. These veins are overprinted by the main fabric and strongly deformed (boudinaged, folded, and transposed). Quartz veins are cut by all dike sets, except the synvolcanic gabbro dikes. As the dikes themselves are schistose and therefore deformed, this suggests that these veins must have an early origin.

9.4.2 Stop 2 – Eastern outcrop

The eastern outcrop shows the faulted contact between mafic volcanic rocks and felsic volcaniclastic rocks (Fig. 9.2). The felsic volcaniclastic rocks consist of lapilli tuffs according to Fisher (1961) classification. That outcrop shows strongly altered and sulfide-rich rocks in its central part. These altered zones vary in width from a few cm up to a few m, and can be traced for over 25 meters. This zone is subparallel to the presumed stratification of the rock and to the main schistosity. It may correspond to a more porous level preferentially infiltrated by early hydrothermal fluids

related to a potential VMS-style activity.

Figure 9.5. Mineralized veins. **a** to **d** show the early, main mineralized veins (Type 1). **e** and **f** show late, syn-main deformation veins (Type 2). **a** Main mineralized veins, boudinaged and disrupted, hosted in mafic volcanic rock, western outcrop. **b** Intense boudinage of a mineralized vein, western outcrop. **c** Boudinaged vein with development of a large hydrothermal biotite-chlorite alteration front hosted in mafic volcanic rocks, western outcrop. **d** Quartz vein with Py-Cp-Gn mineralization, western outcrop. **e** Qz-Ca-Tl vein hosted in felsic volcanoclastic rocks crosscutting the main schistosity and partly folded by this schistosity, eastern outcrop. **f** Qz-Ca-Tl veins hosted in felsic volcanoclastic rocks and crosscut by the Rivière-Héva fault. This fault is located at the contact of the mafic-felsic rocks, eastern outcrop.

Figure 9.6. Mineralized banded quartz vein showing a well preserved mineralogical zonation with quartz (Qz) at the outer margin, quartz-calcite-feldspath (Qz+Ca+Fp) toward the centre of the vein, and barite-quartz-calcite (Ba+Qz+Ca) directly at the core. Barite is the white mineral.

9.5 References

Backmann OL (1936) Geology of Siscoe gold mine. Can Mining Jour 57: 467-475

Bedeaux P, Pilote P, Daigneault R, Rafini S (2017) Synthesis of the structural evolution and associated gold mineralization of the Cadillac Fault, Abitibi, Canada. Ore Geol Rev 82: 49-69

Bertrand-Blanchette S (2016) Géologie et minéralisations aurifères de la Zone no. 8 Orion, secteur Malartic Hygrade, région de Malartic. Unpub. M.Sc. thesis, Université du Québec à Montréal, Montréal, Québec, Canada.

Bousquet D, Carrier A (2008) Travaux de décapage sur l'indice « RLM », propriété Malartic Lake Shore, Corporation Minière Golden Share. Ministère de l'Énergie et des Ressources naturelles du Québec, filière des travaux statutaires, GM 64349, 69 p., 5 maps

Bousquet D, Carrier A (2009a) Programme de forage 2008 sur l'indice aurifère « RLM », propriété Malartic Lake Shore, Corporation Minière Golden Share. Ministère de l'Énergie et des Ressources naturelles du Québec, filière des travaux statutaires, GM 64938, 932 p., 20 map.

Bousquet D, Carrier A (2009b) Programme de forage 2009 sur l'indice aurifère « RLM », propriété Malartic Lake Shore, Corporation Minière Golden Share. Ministère de l'Énergie et des Ressources naturelles du Québec, filière des travaux statutaires, GM 64939, 376 p., 19 maps

Couture JF, Pilote P, Machado N, Desrochers JP (1994) Timing of gold mineralization in the Val-d'Or district, southern Abitibi belt: evidence for two distinct mineralizing events. Econ Geol 89: 1542-1551

Daigneault R (1996) Couloirs de déformation de la Sous-province de l'Abitibi. Ministère des Ressources naturelles, Québec : MB 96-33, 132 p.

Dubé B, Gosselin P (2007) Greenstone-hosted quartz-carbonate vein deposits. *In:* Mineral Deposits of Canada: A Synthesis of Major Deposit-Types, District Metallogeny, the Evolution of Geological Provinces, and Exploration Methods, Goodfellow WD (ed), Geological Association of Canada, Mineral Deposit Division, Special Publication 5: 49-73

Fisher RV (1961) Proposed classification of volcaniclastic sediments and rocks. Geol Soc of Am Bull 72: 1409-1414

Gaboury D, Daigneault R (1999) Evolution from sea floor-related to sulfide-rich quartz vein-type Gold mineralization during deep submarine volcanic construction: The Géant Dormant Gold Mine, Archean Abitibi Belt, Canada. Econ Geol 94: 3-22

Guay F, Pilote P, Daigneault R (2016) Minéralisation aurifère filonienne et déformation de l'indice « Rive du lac Malartic », Sous-province de l'Abitibi, Québec. Ministère de l'Énergie et des Ressources naturelles du Québec : MB 2017-03, 78 p.

Imreh L (1984) Sillon de La Motte-Vassan et son avant-pays méridional: synthèse volcanologique, lithostratigraphique et gîtologique. Ministère de l'Énergie et des Ressources Naturelles du Québec: MM 82-04, 72 p.

Legault M, Daigneault R (2006) Synvolcanic gold mineralization within a deformation zone: the Chevrier deposit, Chibougamau, Abitibi Subprovince, Canada. Miner Dep 41: 203-228.

Pilote P (2000) Géologie de la région de Val-d'Or, Sous-province de l'Abitibi: volcanologie physique et évolution métallogénique. Ministère de l'Énergie et des Ressources, Québec: MB 2000-09, 110 p.

Pilote P (2013) Géologie Malartic, 32D01-NE. Ministère de l'Énergie et des Ressources naturelles du Québec: map CG-32D01D-2013-01.

Pilote P, Scott C, Mueller W, Lavoie S, Riopel P (1999) Géologie des Formations Val-d'Or, Héva et Jacola - nouvelle interprétations du Groupe de Malartic. Ministère des Ressources naturelles, Québec: DV 99-03, p 19.

Pilote P, Daigneault R, David J, McNicoll V (2014) Architecture des Groupes de Malartic, de Piché et de Cadillac et de la Faille de Cadillac, Abitibi. Révision géologique, nouvelles datations et interprétations. Ministère de l'Énergie et des Ressources naturelles, Québec; DV 2015-03, page 37.

Robert F (1989) Internal structure of the Cadillac tectonic zone southeast of Val-d'Or, Abitibi greenstone belt, Quebec. Can Jour of Earth Sci 26: 2661-2675

Robert F (1994) Vein fields in gold districts: the example of Val-d'Or, southeastern Abitibi Subprovince, Québec. *In:* Current Research 1994-C; Geological Survey of Canada, pp 295-302

Robert F (1996) Filons de quartz-carbonates aurifères. *In:* Géologie des types de gîtes minéraux du Canada; Eckstrand OR, Sinclair WD, Thorpe RI (eds). Geological Survey of Canada - Geological Society of America; Géologie du Canada 8: 387-405

Robert F, Brown AC (1986) Archean gold-bearing quartz veins at the Sigma Mine, Abitibi greenstone belt, Quebec; Part I, Geologic relations et formation of the vein system. Econ Geol 81: 578-592

Sauvé P, Imreh L, Trudel P (1993) Description des gîtes d'or de la région de Val-d'Or. Ministère de l'Énergie et des Ressources, Québec: MM 91-03, 178 p.

Scott CR, Mueller WU, Pilote P (2002) Physical volcanology, stratigraphy and lithogeochemistry of an Archean volcanic arc: evolution from plume-related volcanism to arc rifting of SE Abitibi Greenstone Belt. Val-d'Or, Canada. Prec Res 115: 223-260

Chapter 10: (Day 5 – Part III) Spinifex Ridge area – komatiitic flows and physical volcanology

Pierre Pilote
Ministère de l'Énergie et des Ressources naturelles du Québec

Wulf Mueller
Université du Québec à Chicoutimi

Christine Champagne
Université du Québec à Chicoutimi

Réal Daigneault
Université du Québec à Chicoutimi

Note from the author: This text is modified and adapted from numerous field trips given and led by Prof. W. Mueller (deceased) and coworkers in this area in the period 2004-2008.

10.1 Introduction and historical considerations

In an historical perspective, ultramafic lava flows, named komatiites after the type-locality in South Africa (Viljoen and Viljoen 1969a, b), are observed worldwide in numerous Archean greenstone belts: in Canada (Pyke et al. 1973; Imreh 1974a, b; Arndt et al. 1979; Barnes et al. 1983; Houlé et al. 2017 – Supplement B), in Zimbabwe (Bickle et Nisbet 1993), in Australia (e.g., Lesher et al. 1981; Hill et al. 1987; Barnes et al. 1988), in Brazil (Arndt et al. 1989), and in Finland (Blais et al. 1986).

Komatiites are subaqueous lava flows and associated sills-dikes that have more than 18 wt % MgO (Arndt and Nisbet 1982; Arndt 1994), display elevated Ni and Cr contents, and have very low TiO_2, Na_2O, K_2O, and incompatible trace elements (see Supplement B for further details on Archean komatiites: Houlé et al., 2017 – in press). This ultramafic rock with few exceptions, is restricted to the Archean and Paleoproterozoic. Most of the chemical variation can be accounted for by crystallization and accumulation of olivine. Olivine-rich cumulate rocks at the base of flows contain 30-40% MgO, whereas the spinifex-textured upper parts have 20-28% MgO (Arndt et al. 1997). Aphyric flows and chilled margins of komatiitic flows with a minor amount of olivine phenocrysts (Fo_{94}) contain ca. 28-30 wt% MgO (Barnes et al. 1983; Arndt 1986), suggesting this composition represents the composition of a magmatic liquid. An almost two-fold increase in TiO2, Al_2O_3, and CaO from komatiites with 20 to 35 wt % MgO can be accounted for by 30-50% crystallization of olivine (Smith and Erlank 1982).

Komatiites constitute small proportions of most greenstone belts (e.g., <5 % Abitibi belt) and are associated with tholeiitic and komatiitic basalts (12-18 wt%; Arndt and Nisbet 1982). Major and trace element geochemistry permits the distinction into Al-depleted or Barberton-type and Al-undepleted or Munro-type varieties (Nesbitt et al. 1979; Smith and Erlank 1982; Jahn et al. 1982). Several subtypes of komatiites have since been identified, but these appear to be subordinate, and essentially represent variations of a plume theme (e.g., Sproule et al. 2002 and quoted references).

A theoretical cross section of a complete komatiite flow (Fig. 10.1; Pyke et al. 1973; Arndt et al. 1977) contains a cooling segment (A-division) and an accumulation segment (B-division). Divisions within flows have distinct textural zones, and are called A1 - A3 and B1 - B4 zones. The A-division contains polygonal joints, indicative of thermal contraction (A1 - zone), and skeletal sheaths/blades or needles of olivine or pyroxene, referred to as spinifex (A2-3 - zones; Viljoen and Viljoen 1969a, b). In contrast, the B-zone is characterized by an accumulation of olivine or pyroxene phenocrysts, via crystal settling, and has been interpreted to reflect the crystallization history (Renner et al. 1994). Although the B-zone shows the effects of crystal accumulation, in both thick and thin flows this zone must be responsible for flow inflation, or at least represent a strong component of ballooning. The low viscosity of komatiites requires inflation to thicken flows significantly. For example, only hours were required to inflate subaerial pahoehoe flows (Hon et al. 1994). Such time-scales would be appropriate for komatiites.

Spinifex growth occurs from the roof downwards and in sheet flows thermal contraction fractures are generally restricted to the initial 10 cm of the roof. Once the crust is formed, an efficient insulation barrier is achieved, and komatiite underflow may continue, stagnate or cause flow inflation. Barnes (1985) noted that A- and B-divisions formed during quiescent periods with subsequent pulses causing continued flow. Although not expressed, the notion of flow inflation is inferred. Rip-

ups of A-3 zone spinifex in the cm-thick B-1 zone is suggestive of flow turbulence, erosion, and early A-zone cooling conditions. Tube-shaped komatiites have less pronounced spinifex growth because a thick glassy zone with polygonal fractures forms not only at the tops, but also at the bases and sides, restricting spinifex growth to the central segment.

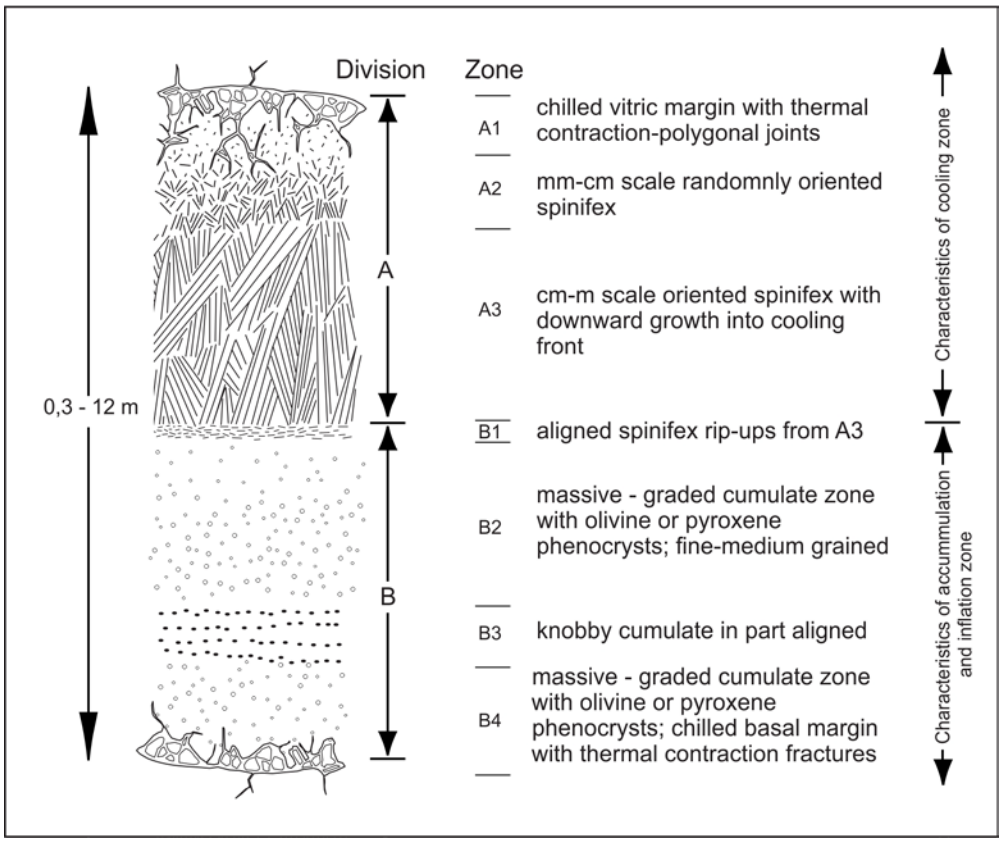

Figure 10.1. Subdivisions of a typical ultramafic flow (Pyke et al. 1973; Champagne 2004). A- and B- divisions reflect both the cooling and accumulation history of komatiites flows. The B-division may also indicate a significant stage of flow inflation (Pyke et al. 1973; Champagne 2004).

10.2 The Spinifex Ridge area

The Spinifex Ridge area is part of the 1.7 to 3 km-thick La Motte-Vassan Formation of the Malartic Group (Imreh 1984). Ultramafic flows constitute approximately up to 95% of this formation (Imreh 1980), whereas felsic tuffaceous and volcaniclastic units are minor. Dimroth et al. (1982) and Imreh (1984) referred to this region as the La Motte-Vassan plain, as it represents an Archean ocean floor or possibly plateau. The ca. 100 m-thick, north-facing, ultramafic flow units at Spinifex Ridge are located on the northern flank of the La Motte Anticline (Imreh 1980; Dimroth et al. 1982). This locality represents one of many kilometric ultramafic volcanic curved enclaves hosted in the Harricana monzonitic Pluton (Fig. 10.2; Pilote 2014). This sector is characterized by major shallow north-dipping structures, the Manneville fault zone, located north and south of Spinifex Ridge (Daigneault et al. 2002, 2004; Pilote 2014). The Spinifex Ridge area has been map in detail by Champagne et al. (2002) and Champagne (2004). Many of the following descriptions are based on this work.

Ultramafic flows from the Val-d'Or - Malartic area were initially interpreted by Gunning and Ambrose (1940) as intrusive bodies. On the Québec side of the Abitibi greenstrone belt, Imreh (1974a, b) was historically the first to have recognized the volcanic and effusive nature of these ultramafic units. This finding led to a major geological mapping program at various scales in this region, supervised by Imreh and his coworkers (Imreh 1978, 1980, 1984). Other significant contributions were made at that time by Gélinas et al. (1976) and Lajoie and Gélinas (1978).

10.3 Physical volcanology of Spinifex Ridge komatiitic flows

Two prominent komatiite effusive flow forms are observed at Spinifex Ridge: 1) master tubes and tube-shaped flows, and 2) flat sheet-like flows. Local tuff or volcaniclastic horizons are associated with these flows. The salient characteristics of the both flow forms are presented in Table 10.1. One of the primary conclusions is that A- and B-zones correlate with flow geometry at Spinifex Ridge (Table 10.1). Sheetflows contain a

prevalent A-zone, whereas tube-shaped flows and master tubes display a dominant B-zone or a massive zone without spinifex. The A/B-zone ratios help distinguish flow types with tube-shaped flows having low A/B-zone ratios <1 (average 0.38), and sheet flows having high A/B-zone ratios >1 (average 1.20). Similarly, aspect ratios of width and thickness (height) are strikingly different, as the average for small tubes is <10, for master tubes is <15 and for sheetflows is >20. In comparison, Archean pillowed flows have aspect ratios of <2 (Dimroth et al. 1978; Sanschagrin 1981). Although well developed at Spinifex Ridge, komatiites generally lack A2-A3 spinifex zones and well-defined B-zones and this is a function of flow morphology, lava flow velocity, effusion rate, water access into the flow (hence cooling rate), and possibly insulating over-riding flow. Thermal quenching is far more efficient around tube-shaped komatiites than sheetflows, as their smaller width permits seawater access into the flow via thermal contraction fractures.

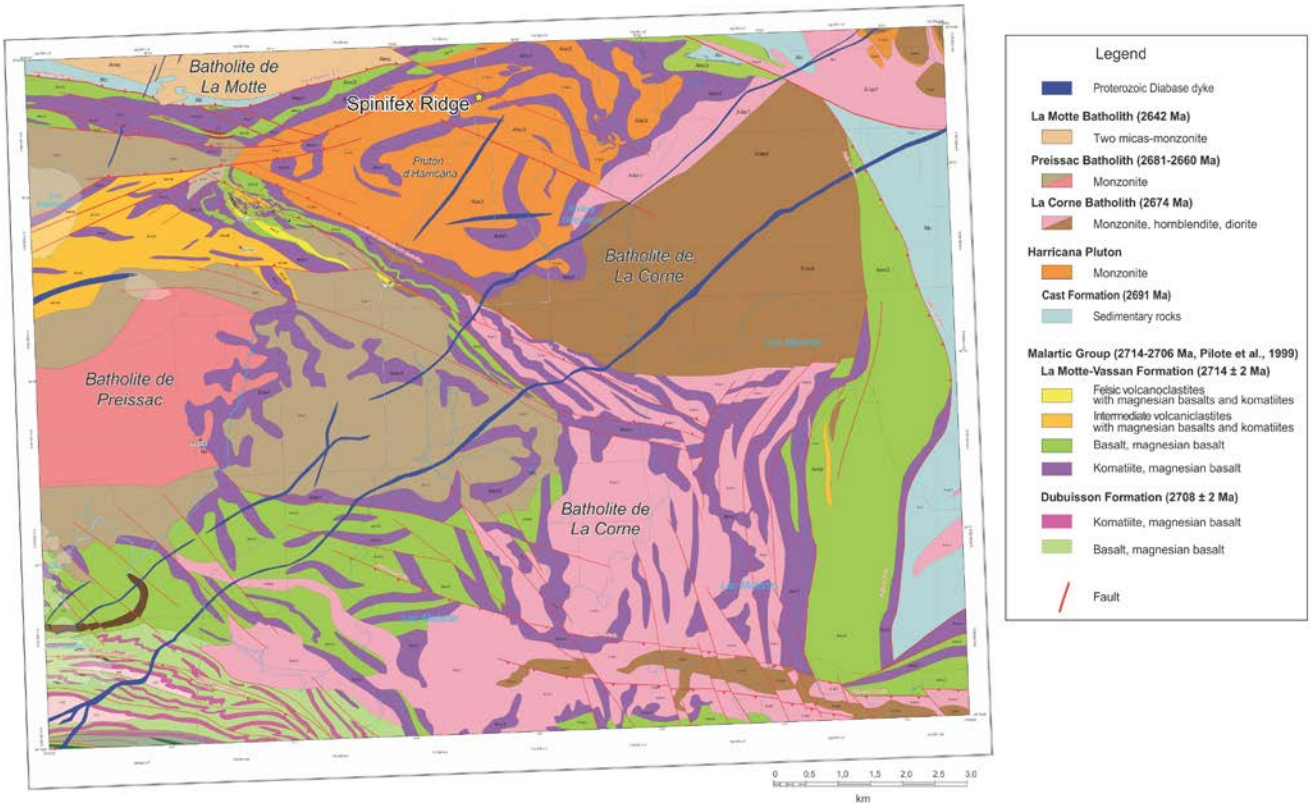

Figure 10.2. Geology of the La Motte area (Pilote 2014). The position of the Spinifex Ridge area is indicated by the yellow star.

A bedding-parallel vertically dipping schistosity is omnipresent and readily recognized in the B-division of komatiite flows, which display a variation in strike/dip of 060-080/78-90. Flows may be locally overturned. Deformation is best developed in the B-divisions and is poorly developed in the resistant A-divisions. The metamorphic grade is amphibolite facies. The outcrop zone at Spinifex Ridge is one of the best exposures for the physical volcanology of high-MgO komatiite flows (25-40% MgO) in the world. Two outcrops zones are considered: (1) *Outcrop West* next to the principal road (route 109) and (2) the 40 x 80 m^2 *Outcrop East*, 325 m east from the road outcrop (Fig. 10.3).

In addition, a well-defined thermal (mechanical?) erosion surface was proposed by Champagne (2004). A possible thin chilled band at the erosive contact may be due to reheating (remelting) from the overlying flow (e.g., Burkhard 2003). Erosion channels can down cut into the substrate up 10 cm per day (over several months) and hence remelt the substrate in sustained pahoehoe flows - channels (Kauahikaua et al. 2003). Thermal erosion in komatiite flows is an intriguing subject, as numerous magmatic Ni-Cu deposits (Lesher et al. 1984; Cowden 1988; Lesher and Campbell 1993; Beresford et al. 2005) are inferred to be associated with such channels (Australia, Québec Far North).

10.3.1 Stop 1 - Spinifex Ridge Outcrop West (Nad83 UTM17 713176 5361523)

This road cut is the classical expression of an Abitibi outcrop: excellent textural characteristics but insufficient in size to conduct major interpretations. *Outcrop West* displays nine discrete units with sharp basal and upper contacts (Fig. 10.4). The striking feature is that the 37.50-144.20 cm-thick A-divisions with the well-developed A1, A2-, and A3-zones are consistently thicker than the B-

cumulate zones (Table 10.1). The A/B ratio average at this outcrop is 1.54 and larger than that of *Outcrop East* (average 1.04; Champagne 2004). The A-division thickness is used to infer that these should be sheetflows when compared to the flow features and A-division thicknesses at *Outcrop East*. The A1-zone displays cm-thick chilled margins with local related thermal fractures (commonly referred to as polygonal joints) that do not penetrate deep into the flows. The A2-zone with random cm-mm-scale spinifex is thin and thermal fractures penetrate into this segment but rarely further down. The A3-zone that is exceptionally well developed with individual spinifex fans attaining almost 1 m in length. We assume that these thick A3-zones result from the insulation effect of A1-, A2-zones and the absence of any synvolcanic fractures that penetrated deep into the flow. Deep-penetrating cooling fractures would probably have inhibited significant spinifex growth. In contrast, thermal fractures were far more efficient at the base (see single flow units 4 and 6; Fig. 10.4). In order to produce thick A-divisions, stagnation or ponding of flow occur. An explanation to accommodate over-thick A-divisions is flow draining of the magma channel via the underlying B-division. This is a deflation structure similar to flows on Lonquimay volcano (Naranjo et al. 1992). Under subaerial conditions, viscous channeled a'a flows with levees develop, but not in the subaqueous realm where closed tubes form. In open channels, drainage cavities do not form because the roof sinks progressively as magma drains to distal flow field segments (Fig. 10.4). In the subaqueous realm, thick A-divisions remain, and B-divisions record the inflation-deflation history.

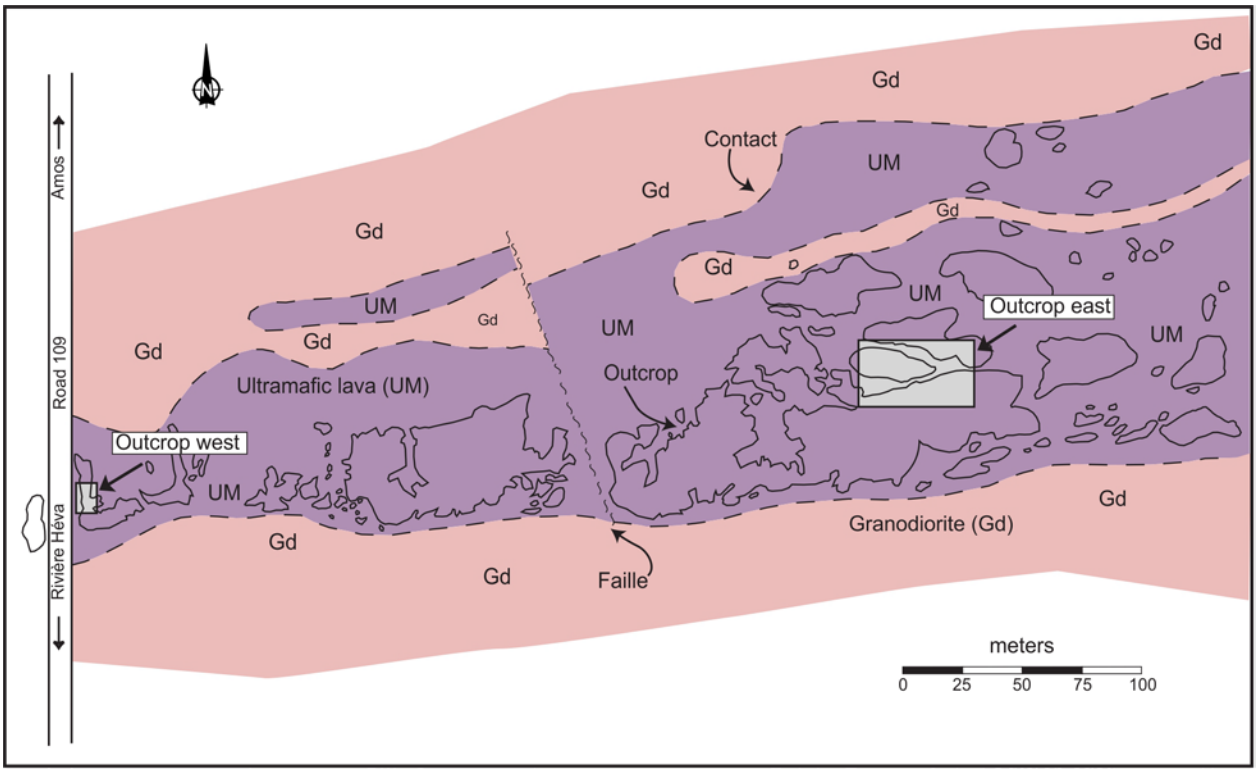

Figure 10.3. Detailed location of Spinifex Ridge in the La Motte-Vassan Formation (Road 109 north) showing Outcrop west and Outcrop east (modified from Champagne 2004).

The 36.85-80.05 cm-thick B- (cumulate) division contains B1, B2, B3, and B4-zones. The contact to the A-division is sharp and usually defined by a 1-4 cm-thick foliated B1-zone with rip-ups of spinifex from the A3-zone. The spinifex rip-ups suggest an underflow (similar to an undertoe with water currents in tidal regimes) or that magma current has some erosive power and during spinifex growth down into hotter medium, platy spinifex becomes dislodged and is entrained into the underflow. Contacts between zones are distinct and B2- and B4-zones are massive or graded due to settling of cumulates in the lava. The knobby cumulate B3-zone is restricted flow units 5-7 (Fig. 10.4). Clearly the A- and B-divisions reflect two distinct flow dynamic regimes. Several B-zones suggest ballooning and possibly the analogue to the stratified vesicular-non-vesicular horizons in pahoehoe flows (Self et al. 1998). The olivine cumulate B-zones need not be purely a product of vertical gravity settling from the roof of the flow, but could also be a product of a replenished magma underflow.

10.3.2 Stop 2 - Spinifex Ridge Outcrop East

The 40 x 80 m-large zone at Spinifex Ridge, referred to as *Outcrop East*, displays sheetflows and tube-shaped flows with the latter including two master tubes (Table 10.1). The volcanic flow architecture displays a basal sheetflow and an upper tube-shaped flow organization

whereby three 10-30 m-thick (?) effusive cycles were observed (Fig. 10.5). The relative change from unconfined to confined flow is a function of viscosity and flow volume. *In situ* brecciation is restricted to the tube-shaped flows. It is envisaged that the sheetflows grade laterally into tubeshaped counterparts as documented by Dimroth et al. (1978) for the mafic flows.

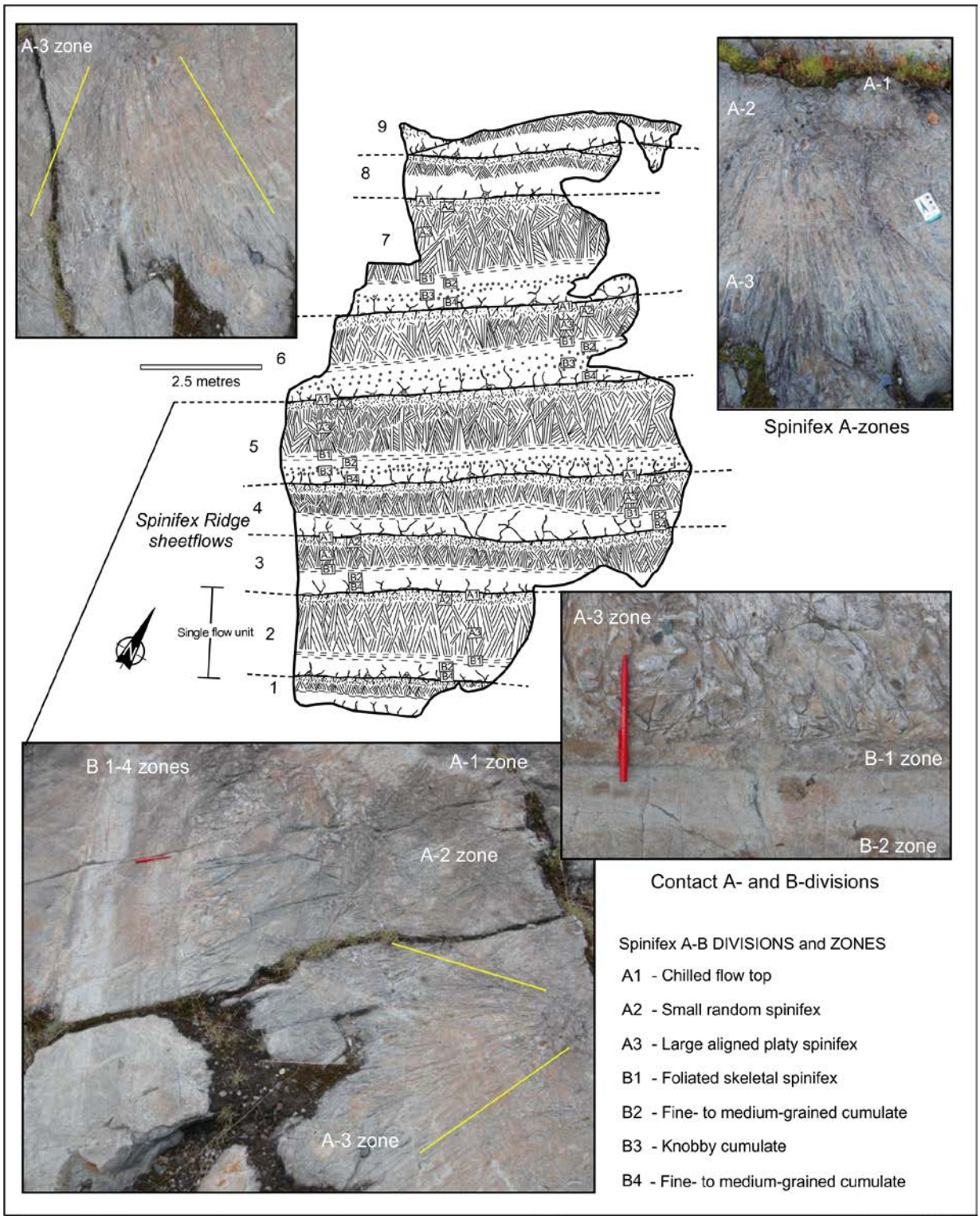

Figure 10.4. Spinifex Ridge road cut Outcrop west with A- and B-divisions (modified from Champagne 2004; Mueller 2004).

10.3.2.1 Sheetflows

The 8-80 m long and 0.5-2 m-thick sheetflows (Fig. 10.6) at *Outcrop East* represent the base of the effusive cycles. The A-division in comparison with B-divisions is thicker. Both the lateral extent of sheetflows and low-angle lateral flow terminations are indicative of a low viscosity. The A/B ratio of 1.04 for 20 sheetflows permitted us to interpret *Outcrop West* komatiites as sheeflows (A/B-ratio of 1.54; average of both outcrop zones 1.20, see Table 10.1). A3-zones are well developed and two types of contacts with the B-division are recorded: (1) A3-zones grow as radiating fans with a concave lower part indicating an apparent "growth" into the B-divisions and (2) a straight contact along sheetflow strike with local B1-zones. The over-thick A-divisions with respect to B-divisions argue for underflow runoff, and hence deflation. An important thermal or thermal-mechanical erosion surface was mapped in detail by Champagne (2004; Fig. 10.6). The observed along strike change from 1.52 to 0.20 m-thick flow with complete erosion of the A-division due to channel incision (Fig. 10.7) supports an erosive process. It is attributed to the overlying massive composite flow. An apparent fine cm-thick chilled margin with the overlying flow may be the effect of recrystallization from flow reheating. Another important observation is not only the vertical but also the lateral change of internal flow textures (Fig. 10.8). The common vertical A-B architecture in sheetflows is developed laterally towards the low-angle flow terminations, but is rarely observed because flows generally exceed outcrop exposure.

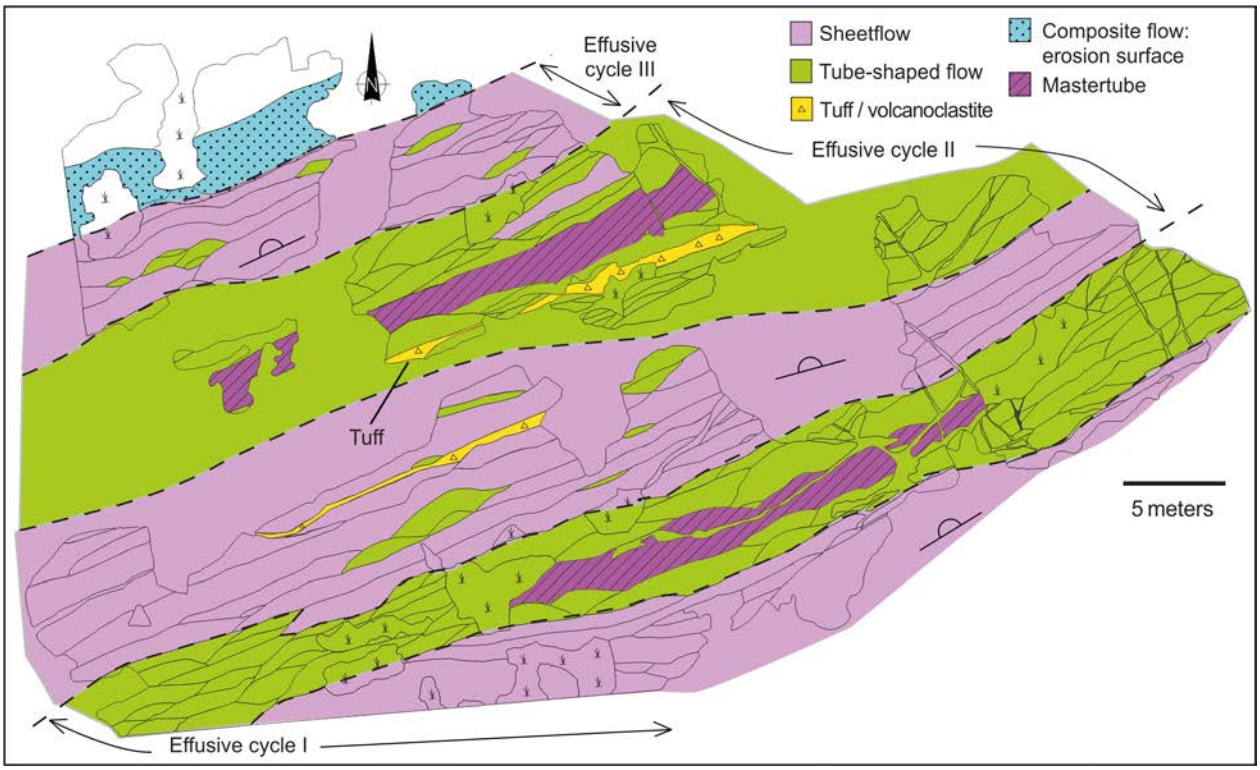

Figure 10.5. Outcrop east sheetflows at the base of effusive cycles overlain by tube-shaped flows. Note the presence of a large master tube in the central portion of tube-shaped flow segment (modified from Champagne 2004).

10.3.2.2 Tube-shaped flows

The 1.55-10.20 m-wide, tube-shaped flows (Fig. 10.8) constitute the upper portion of effusive flow cycles (Fig. 10.5). The A-divisions are poorly developed and are missing in half the measured flows. The lack of A-divisions is attributed to abundant fractures facilitating water ingestion and hence rapid cooling. Local *in-situ* brecciation is developed both at the margins and the interior of flows, and suggests selective flow movement after consolidation. Drainage cavities are locally developed, and the flat bottom contacts of these drainage cavities are indicators of the stratification in the flow field (Sawyer et al. 1983). Furthermore, they are indirect indicators of inflation, because multiple flow pulses and drainage are required. Drainage cavities commonly are at the same height as the low-angle flow terminations. The tube-shaped flows display lateral A1-A2-A3 variations. In contrast to bulbous basaltic pillow margins, low-angle (< 5-30°; Fig. 10.9) flow terminations are observed at Spinifex Ridge. This is a first order physical volcanological indication of the low viscosity and high temperature of high MgO-komatiites.

10.3.2.3 Komatiite tuffs

Thin laminated, graded bedded and rarely crossbedded 1-

10 cm thick tuffs in 5-100 cm-thick units are interstratified with the komatiites (Fig. 10.5). The deposits are composed of olivine crystals, komatiite fragments as well as vitric (hyaloclastite) shards that have a cuspate shape, an amoeboid shard shape, and a bent lazy L-shape (Fig. 10.10A). The tuff beds may have originated either through thermal granulation processes on the flow surface, implosion of pillow tubes, or local explosive hydroclastic fragmentation. Although these deposits are locally reworked, the combination of olivine crystals, volcanic fragments, and shards as primary constituents argue for a common pyroclastic heritage. Rare crossbeds suggest reworking, but the presence of delicate shard shapes favours limited re-sedimentation (Fig. 10.10B). The deposits were emplaced via low-concentration (Tb-beds) and locally high-concentration turbidites (Ta or S3-bed of Lowe 1982) with bedload transport as suggested by the crossbeds. The laminated fine-grained tuffs are considered suspension sedimentation with shards settling through the water column (Mueller 2003) that have settling velocities of hours-minutes. Two possible mechanisms can explain the tuff beds: (1) eruption-fed density currents from (very) small-scale, subaqueous, Surtseyan-type eruptions (Mueller, 2003), or (2) an Archean version of Limu-O-Pele, whereby the plastic shards in sheet hyaloclastites are derived through water entrapment by rapidly moving flows, which in turn cause explosive steam expansion (Maicher and White 2001). The crystal- and fragment-rich beds favour eruption-fed density currents, whereas the interpretation of shard-dominated sheet hyaloclastites from an explosion due to water entrapment is appealing.

Figure 10.6. Thin komatiite sheetflows with a thermal erosion surface in centre of photograph. Base of photograph is approximatively 3 m.

10.3.2.4 Further outcrop features

In addition to flow erosion surfaces, spinifex veins (dikelets) with symmetric spinifex growth on dyke margins intruded locally. These intrusive phases indicate ongoing magmatic activity and are further indicators of how komatiite flow fields inflate. Additionally, contemporaneous degasification (or segregation) pipes with abundant water vapor and low-temperature hydrothermal fluids (silica?) percolated throughout the flow field system. The inferred pipes transect the flows or developed along flow margins. Considering the high emplacement temperature of komatiites, it should not be surprising to have abundant heated sea-water and hydrothermal fluids seeping along flow boundary interfaces and thermal contraction fractures. The observed breccias in proximity to the pipes may in part be related to this fracturing. Another local characteristic are entrained blocks into the flow. These irregular komatiite blocks are suggestive of flow disruption up-flow with subsequent entrainment.

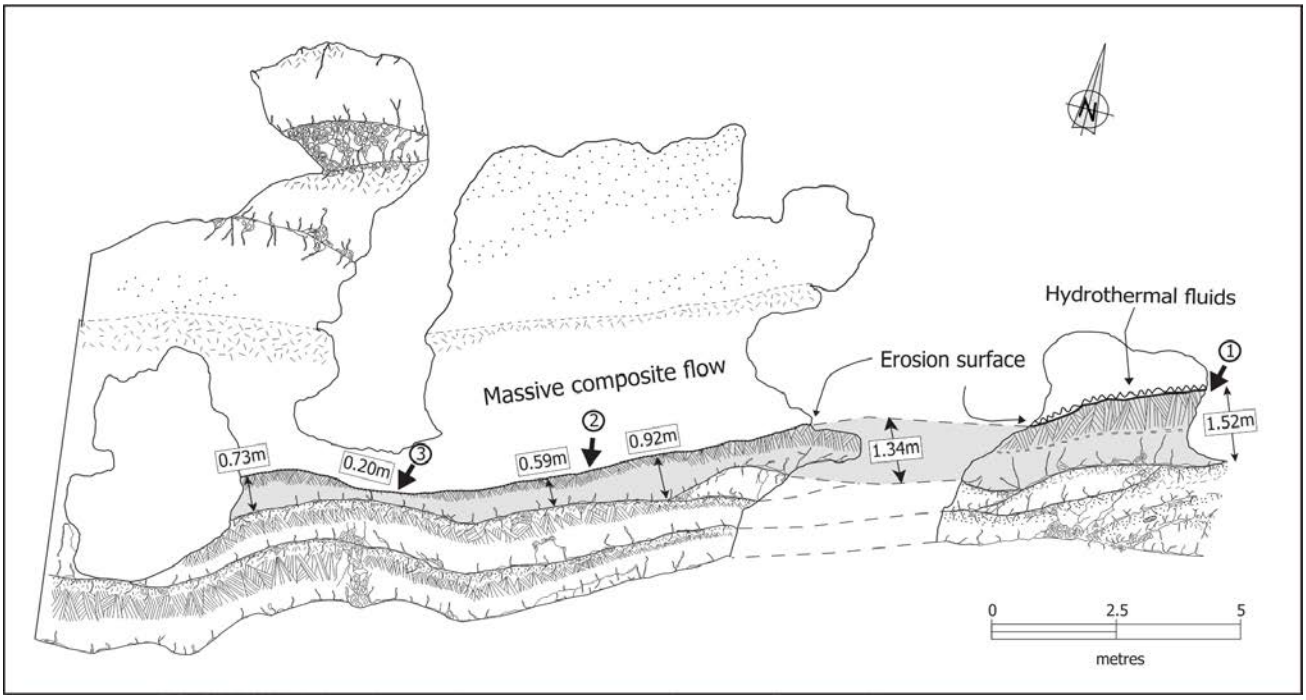

Figure 10.7. Spinifex-textured sheetflow eroded by a massive composite flow. Note the down-cutting of the A-division until it is completely eroded (Champagne 2004). See figure 10.5 for outcrop exposure.

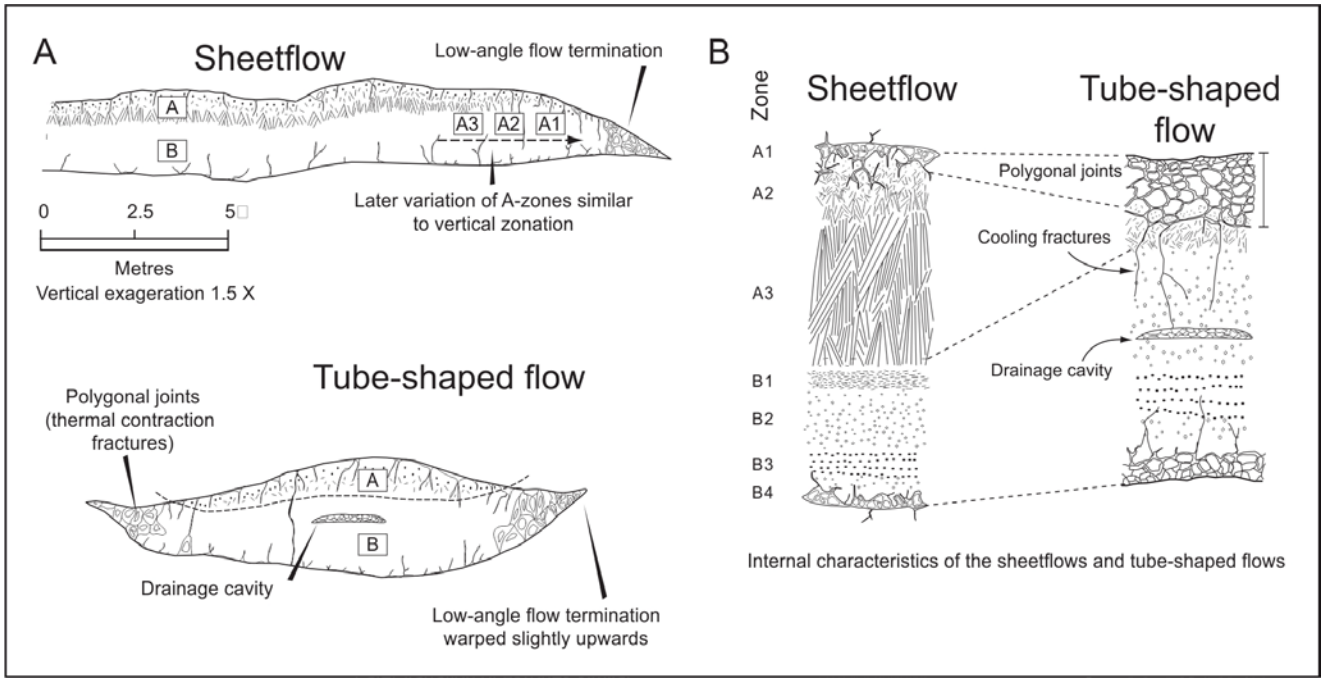

Figure 10.8. Vertical and lateral changes of internal flow textures in sheetflows and tube-shaped flows (Champagne 2004).

Figure 10.9. Low-angle tube flow termination with omnipresent polygonal jointing. Pen 13 cm.

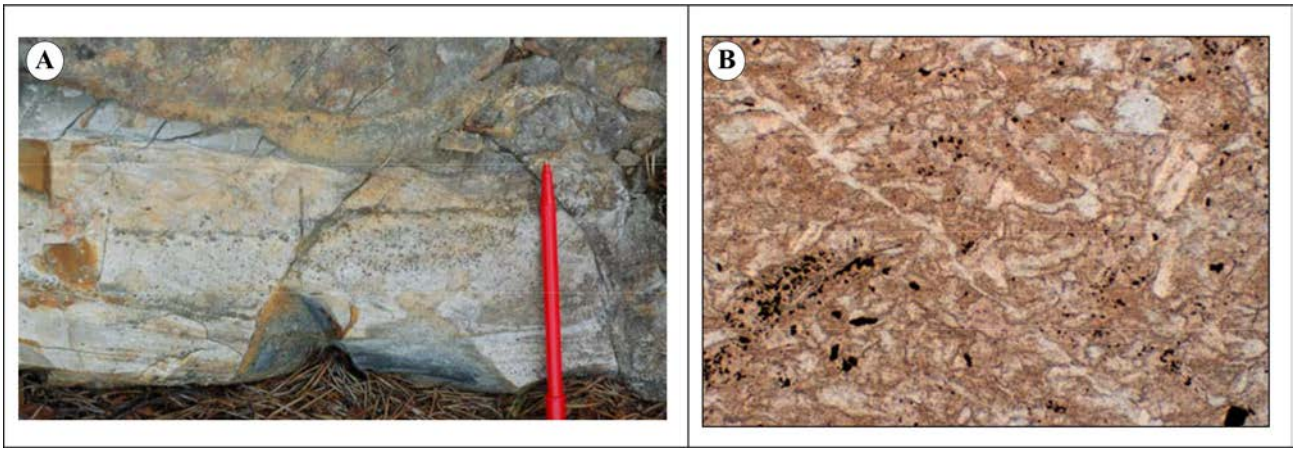

Figure 10.10. Grade bedded, laminated and cross-bedded komatiitic tuffs. **a** Cross-bedded komatiite tuff between komatiite flows. **b** Vermicular-shaped komatiite shards in a very-fined grained tuff matrix. Length of photo is 2.5 mm.

Table 10.1. Dimensions and characteristics of Spinifex Ridge komatiite flows (modified from Champagne 2004; Mueller 2004). Note the striking difference between sheetflow and tube-shaped flows.

Komatiite flow & characteristics	Size	Average (m)	Maximum (m)	Minimum (m)
Sheetflow	Width (W)	27.90	81.14	8.12
(n=29)	Thickness (T)	1.15	2.24	0.59
Aspect ratio	W/T.	23.20	36.18	10.79
Tube-shaped flow	Width (W)	4.90	10.20	1.55
(n=45)	Thickness (T)	0.78	1.50	0.30
Aspect ratio	W/T.	6.34	13.56	3.48
Mastertube flow	Width (W)	27.65	32.14	29.89
(n=2)	Thickness (T)	2.04	2.13	2.09
Aspect ratio	W/T.	12.98	15.74	14.36
Sheetflow features	**A-Zone (T)**	**B-zone (T)**	**A/B-zone ratio**	**Cavities & Joints**
Prominent A1, A2, A3, B2, B3, B4 zones; tabular flows with low-angle lateral terminations	61.30 cm (average)	53.27 cm (average)	1.20 (average)	Drainage cavities absent; polygonal joints prominent at roof & flow margin
Tube-shaped features	**A-Zone (T)**	**B-zone (T)**	**A/B-zone ratio**	**Cavities & Joints**
Prominent A1, A3, B2, B4 zones; flat to arched tubes with low-angle lateral terminations	21.96 cm (average; n=22)	54.61 cm (average; n=22)	0.38 (average; n=22)	Drainage cavities locally present; polygonal joints prominent in flow

10.4 References

Arndt NT (1986) Differentiation of komatiite flows. J Petrol 27: 279-301

Arndt NT (1994) Archean Komatiites. In: Condie KC (ed) Archean crustal evolution. Developments in Precambrian Geology 11, pp. 11-44

Arndt NT, Nisbet EG eds (1982) Komatiites. George Allen and Unwin, London, 526p

Arndt NT, Naldrett AJ, Pyke DR (1977) Komatiitic and Fe-rich tholeiitic lavas of Munro Township, northeastern Ontario. J Petrol 18: 319-369

Arndt NT, Francis D, Hynes AJ (1979) The field characteristics and petrology of Archean and Proterozoic Komatiites. Can Mineral 17:147-163

Arndt NT, Teixeira NA, White WM (1989) Bizarre geochemistry of komatiites from Crixas greenstone belt, Brazil. Contrib Mineral Petrol 101: 187-197

Arndt NT, Albarede F, Nisbet EG (1997) Mafic and ultramafic magmatism. In: de Wit MJ, Ashwal LD (eds) Greenstone belts. Oxford University Press, London, pp 233-254Barnes S-J (1985) The petrography and geochemistry of komatiite flows from the Abitibi greenstone belt and a model for their formation. Lithos 18: 241-270

Barnes SJ, Gorton MP, Naldrett AJ (1983) A comparative study of olivine and clinopyroxene flows from Alexo, Abitibi greenstone belt, Ontario, Canada. Contrib Mineral Petrol 83: 293-308

Barnes SJ, Hill RET, Gole MJ (1988) The Perserverance Ultramafic Complex, Western Australia: the product of komatiite lava river. J Petrol 29: 305-331

Beresford S, Stone WE, Cas R, Lahaye Y, Jane M (2005) Volcanological controls on the localization of the komatiite-hosted Ni-Cu-(PGE) Coronet deposit, Kambalda, western Australia. Econ Geol 100: 1457-1467

Bickle MJ, Nisbet EG eds (1993) The geology of the Belingwe greenstone belt, Zimbabwe: a study of the evolution of Archean continental crust. Geological Society of Zimbabwe, Special Publication 2: 239p

Blais S, Auvray B, Jahn B, Taipale K (1986) Processus de fractionnement dans les coulées komatiitiques archéennes: cas de laves à spinifex de la ceinture

de roches vertes de Tipasjârvi (Finlande oriental). Can J Earth Sci 24: 953-966

Burkhard DJM (2003) Thermal interaction between lava lobes. Bull Volcanol 65: 136-143

Champagne C (2004) Volcanologie physique et géochimie des komatiites de Spinifex Ridge, Formation de La Motte-Vassan, Abitibi. MSc thesis, Université du Québec à Chicoutimi.

Champagne C, Pilote P, Mueller W (2002) Volcanologie physique et géochimie des komatiites archéennes: Groupe de Malartic, Abitibi, Québec. Ministère des Ressources naturelles, Québec, MB 2002-04: 69p (with map).

Cowden A (1988) Emplacement of komatiite lava flows and associated nickel sulfides at Kambalda, western Australia. Econ Geol 83: 436-442

Daigneault R, Mueller WU, Chown EH (2002) Oblique Archean subduction; accretion and exhumation of an oceanic arc during dextral transpression, Southern volcanic zone, Abitibi Subprovince, Canada. Precambrian Res 115: 261-290

Daigneault R, Mueller WU, Chown EH (2004) Abitibi greenstone belt plate tectonics: the diachronous history of arc development, accretion and collision. In: Eriksson P, Altermann W, Nelson D, Mueller WU, Catuneanu O (eds) The Precambrian Earth: tempos and events. Developments in Precambrian Geology 12, pp. 88-103

Dimroth E, Cousineau P, Leduc M, Sanschagrin Y (1978) Structure and organization of Archean subaqueous basalt flows, Rouyn-Noranda area, Quebec, Canada. Can J Earth Sci 15: 902-918

Dimroth E, Imreh L, Rocheleau M, Goulet N (1982) Evolution of the south-central part of the Archean Abitibi Belt, Quebec; Part I, Stratigraphy and paleogeographic model. Can J Earth Sci 19: 1729-1758

Gélinas L, Lajoie J, Brooks C (1976) Origin and significance of Archean ultramafic volcaniclastics from Spinifex Ridge, La Motte Township, Québec. Ministère des Richesses naturelles, Québec, DPV-428: 17p

Gunning HC, Ambrose JW (1940) Malartic area, Quebec. Geological Survey of Canada, Memoir 222: 142p

Hill RET, Gole MJ, Barnes SJ (1987) Physical volcanology of komatiites: a field guide to the komatiites between Kalgoorlie and Wiluna, Eastern Goldfields Province, Yilgarn Block, Western Australia. Geological Society of Australia, Excursion guide book 1: 74p

Hon K, Kauahikaua J, Denlinger R, Mackay K (1994) Emplacement and inflation of pahoehoe sheet flows; observations and measurements of active lava flows on Kilauea Volcano, Hawaii. Geol Soc Am Bull 106: 351-370

Imreh L (1974a) Esquisse géologique du sillon serpentinitique archéen de La Motte-Vassan. Ministère des Richesses Naturelles, Québec, DP-232: 8p

Imreh L (1974b) L'utilisation des coulées ultrabasiques dans la recherche minière: esquisse structurale et lithostratigraphique de La Motte-Vassan. Bull Volcanol 38: 291-314

Imreh L (1978) Album photographique de coulées méta-ultramafiques sous-marines archéennes dans le sillon de La Motte-Vassan. Ministère des Richesses naturelles, Québec, V-6: 131p

Imreh L (1980) Variations morphologiques des coulées méta-ultramafiques komatiitiques du sillon archéen de La Motte-Vassan, Abitibi-Est, Québec. Precambrian Res 12: 3-30

Imreh L (1984) Sillon de La Motte-Vassan et son avant-pays méridional: synthèse volcanologique, lithostratigraphique et gîtologique. Ministère de l'Énergie et des Ressources, Québec, MM 82-04: 72p

Jahn BM, Gruau G, Glickson AY (1982) Komatiites of the Onverwacht Group, South Africa: REE chemistry, Sm-Nd age and mantle evolution. Contrib Mineral Petrol 80: 25-40

Kauahikaua J et al. (2003) Chapter 4: Hawaiian lava-flow dynamics during the Pu'u O'o-Kupaianaha eruption: a tale of two decades. In: Heliker C, Swanson DA, Takahashi TJ (eds) The Pu'u O'o-Kupaianaha eruption of Kilauea volcano, Hawaii: The first 20 years. US Geological Survey, Professional paper 1676, pp. 63-88

Lajoie J, Gélinas L (1978) Emplacement of Archean peridotitic komatiites in La Motte Township, Quebec. Can J Earth Sci 15: 672-677

Lesher CM, Campbell IH (1993) Geochemical and fluid dynamic modeling of compositional variations in Archean komatiite-hosted nickel sulfide ores in Western Australia. Econ Geol 88: 804-816

Lesher CM, Lee RF, Groves DI, Bickle MJ, Donaldson MJ (1981) Geochemistry of komatiites from Kambalda, western Australia; I, Chalcophile element depletion, a consequence of sulfide liquid separation from komatiitic magmas. Econ Geol 76: 1714-1728

Lesher CM, Arndt NT, Groves DI (1984) Genesis of komatiite-associated nickel sulphide deposits at Kambalda, Western Australia: A distal volcanic model. In: Buchanan DL, Jones MJ (eds) Sulphide deposits in mafic and ultramafic rocks. Institution of Mining and Metallurgy, London, pp. 70-80

Lowe DR (1982) Sediment gravity flows: II. Depositional models with special reference to the deposits of high density turbidity currents. J Sediment Petrol 52: 279-297

Maicher D, White JDL (2001) The formation of deep-sea Limu o Pele. Bull Volcanol 63: 482-496

Mueller WU (2003) A subaqueous eruption model for shallow-water, small volume eruptions: evidence from two Precambrian examples. In: White J,

Smellie J, Clague D (eds) Explosive subaqueous volcanism. Geophysical Monograph Series 140, pp. 189-203

Mueller WU (2004) Physical volcanology of komatiites. In: Eriksson P, Altermann W, Nelson D, Mueller WU, Catuneanu O (eds) The Precambrian Earth: tempos and events. Developments in Precambrian Geology 12, pp. 277-290

Naranjo JA, Sparks RS, Stasiuk MV, Moreno H, Ablay GJ (1992) Morphological, structural and textural variations in the 1988-1990 andesites lava of Lonquimay Volcano, Chile. Geol Mag 29: 657-678

Nesbitt RW, Sun SS, Purvis AC (1979) Komatiites: geochemistry and genesis. Can Mineral 17: 165-186

Pilote P (2014) Géologie - La Motte. Ministère de l'Énergie et des Ressources naturelles, Québec, carte CG-32D08B-2014-01

Pyke DR, Naldrett AJ, Eckstrand AP (1973) Archean ultramafic flows in Munro Township, Ontario. Geol Soc Am Bull 84: 955-978

Renner R, Nisbet EG, Cheadle MJ, Arndt NT, Bickle MJ, Cameron WE (1994) Komatiite flows from the Reliance Formation, Belingwe Belt, Zimbabwe; I, Petrography and mineralogy. J Petrol 35: 361-400

Sanschagrin Y (1981) Étude des variations latérales et verticales des faciès dans les coulées de basaltes tholéiitiques du Groupe de Kinojévis, canton d'Aiguebelle, Abitibi. MSc thesis, Université du Québec à Chicoutimi

Sawyer EW, Barnes SJ, Buck M (1983) Pillow shelves: determination of bedding direction and structural facing direction from shelves in deformed pillows. Can J Earth Sci 20: 1483-1487

Self S, Keszthelyi L, Thordarson T (1998) The importance of pahoehoe. Ann Rev Earth Planet Sci 26: 81-110

Smith HS, Erlank AJ (1982) Geochemistry and petrogenesis of komatiites from the Barberton greenstone belt, South Africa. In: Arndt NT, Nisbet EG (eds) Komatiites. George Allen and Unwin, London, pp. 347-398

Sproule RA, Lesher CM, Ayer JA, Thurston PC, Herzberg CT (2002) Spatial and temporal variations in the geochemistry of komatiites and komatiitic basalts in the Abitibi greenstone belt. Precambrian Res 115: 153-186

Viljoen MJ, Viljoen RP (1969a) The geology and geochemistry of the lower ultramafic unit of the Onverwacht Group and a proposed new class of igneous rocks. Geological Society of South Africa, Special Publication 2: pp. 55-86

Viljoen MJ, Viljoen RP (1969b) Evidence for the existence of a mobile extrusive peridotitic magma from the Komati Formation of the Onverwacht Group. Geological Society of South Africa, Special Publication 2: pp. 87-112

Native gold in a quartz±carbonate vein hosted in strongly iron-carbonatized mafic volcanic rocks from the Lac Fortune area west of Rouyn-Noranda